UNIVERSITÀ
DEGLI STUDI
DI PADOVA

Sede Amministrativa: Università degli Studi di Padova

Dipartimento di Biologia

SCUOLA DI DOTTORATO DI RICERCA IN: BIOSCIENZE E BIOTECNOLOGIE
INDIRIZZO: NEUROBIOLOGIA
CICLO: XXVII

INVESTIGATION OF THE PATHOPHYSIOLOGY OF MIGRAINE USING FAMILIAL HEMIPLEGIC MIGRAINE MOUSE MODELS

Direttore della Scuola: Ch.mo Prof. Giuseppe Zanotti
Coordinatore d'indirizzo: Ch.mo Prof. Daniela Pietrobon
Supervisore: Ch.mo Prof. Daniela Pietrobon

Dottorando: Clizia Capuani

INDEX

RIASSUNTO 5

SUMMARY 9

1. INTRODUCTION 13

1.1. Migraine 13
1.1.1. Neurobiology of migraine 13
1.1.2. CSD phenomenology 15
1.1.3. Mechanisms of experimental CSD 16
1.1.4. CSD and migraine 19

1.2. Familial Hemiplegic Migraine 21
1.2.1. The α2 Na,K-ATPase and its functional roles 23
1.2.2. Functional consequences of FHM mutations 24

1.3. Cortex and its organization 26
1.3.1. Cellular populations in the cortex 27
1.3.2. Astrocyte-neuron communication 29
1.3.2.1. Astrocytic glutamate uptake 30
1.3.2.2. Astrocytic potassium uptake 32
1.3.2.3. Synaptically-activated transporter-mediated current and K^+ current evoked in astrocytes by extracellular stimulation 33
1.3.3. Excitation/inhibition balance in the cortex 34

1.4. Cortical network electrical activity 36
1.4.1. Slow oscillations and their neuronal counterparts, up- and down-states 36
1.4.2. Initiation, propagation and termination of up-states 37

2. AIM OF WORK (I) 41

3. RESULTS (I) 43

4. DISCUSSION (I) 55

5. AIM OF WORK (II) 59

6. RESULTS (II) 61

6.1. Does W887R FHM2 mutation facilitate the induction and the propagation of experimental cortical spreading depression (CSD) induced in cortical slices by high KCl pulses? 61

6.2. Does the loss-of-function of α2 Na,K-ATPase result in an impaired astrocyte-mediated clearance of glutamate from the synaptic cleft during cortical neuronal activity? 64

6.3. Is the clearance of K^+ by astrocytes during cortical neuronal activity impaired as a consequence of the loss-of-function of α2 Na,K-ATPase? 72

6.4. Is Ca^{2+} content in the intracellular Ca^{2+} stores of astrocytes in FHM2 KI mice increased and does Ca^{2+} release from stores contribute to the facilitation of experimental CSD in FHM2 KI mice? 73

7. DISCUSSION (II) 77

8. MATERIALS AND METHODS 83

8.1. Animals 83

8.2. Coronal cortical slices preparation 83
8.2.1. Solutions 83
8.2.2. Slices preparation 84

8.3. Patch clamp technique 84
8.3.1. Patch clamp mode 86

8.4. Patch clamp setup and recordings 86
8.4.1. Microscope 87
8.4.2. Electrophysiological setup 87
8.4.3. Cell identification 88
8.4.3.1. Pyramidal cells identification 88
8.4.3.2. Astrocytes identification 89
8.4.4. Solutions 90
8.4.4.1. Extracellular solutions 90
8.4.4.2. Intracellular solutions 90
8.4.4.3. Drugs and toxins 91
8.4.5. Electrodes 91

8.4.5.1. Recording electrode 91
8.4.5.2. Stimulating electrode 91
8.4.6. Data acquisition and analysis 91
8.4.6.1. Recordings and analysis of spontaneous recurrent cortical activity 92
8.4.6.2. Recordings and analysis of STC and K^+ currents from astrocytes 93

8.5. Experimental CSD 94

8.6. Measurements of Ca^{2+} transients in astrocytic primary cultures 95

8.7. Statistical analysis 95

ABBREVIATIONS 97

REFERENCES 99

RIASSUNTO

L'emicrania è un disturbo neurologico comune e altamente invalidante, che colpisce più del 10% della popolazione, dovuto ad una disfunzione primaria del cervello che porta all'attivazione e alla sensibilizzazione episodica delle vie nocicettive trigeminovascolari.

L'emicrania emiplegica familiare (FHM) è un rara forma di emicrania con aura considerata un buon modello per lo studio dell'emicrania; infatti gli attacchi tipici di FHM sono simili a quelli della normale emicrania con aura, eccetto per il sintomo dell'emiparesi (Pietrobon and Moskowitz, 2013). Mutazioni missenso con guadagno di funzione nel gene *CACNA1A*, codificante la subunità formante il poro dei canali del Ca^{2+} voltaggio dipendenti $Ca_V2.1$ (denominati anche canali del Ca^{2+} di tipo P/Q), causano FHM di tipo 1 (FHM1) e mutazioni con perdita di funzione nel gene *ATP1A2*, codificante la subunità astrocitaria α2 della Na,K-ATPasi, causano FHM di tipo 2 (FHM2) (Ophoff *et al.*, 1996; De Fusco *et al.*, 2003).

Topi knock-in (KI) per le mutazioni che causano FHM1 e FHM2 presentano una facilitazione nell'induzione e nella propagazione della *cortical spreading depression* (CSD) (van den Maagdenberg *et al.*, 2004, 2010; Leo *et al.*, 2011), il fenomeno neurologico alla base dell'aura emicranica e un evento chiave innescante l'attivazione del sistema trigeminovascolare.

Topi FHM1 KI per la mutazione R192Q, mostrano un aumentato influsso di Ca^{2+} attraverso i canali del Ca^{2+} di tipo P/Q e un aumento nella probabilità di rilascio di glutammato alle sinapsi piramidali della corteccia (Pietrobon, 2010; Tottene *et al.*, 2009), che potrebbe spiegare la facilitazione della CSD sperimentale osservata in questi topi. Recentemente, nel nostro laboratorio, è stato dimostrato che la frequenza degli *up-state* registrati in fettine acute di corteccia, simili alle oscillazioni lente riportate *in vivo* (Steriade *et al.*, 1993), è maggiore nel topo FHM1 KI che nel WT. Questo dato suggerisce che il guadagno di funzione dei canali del Ca^{2+} di tipo P/Q faciliti i meccanismi di generazione degli *up-state* e/o riduca il periodo refrattario dopo un *up-state* (Fabbro, Sessolo, Vecchia and Pietrobon, dati non pubblicati).

Lo scopo della prima parte del mio lavoro è stato quello di approfondire il ruolo dei canali del Ca^{2+} di tipo P/Q nell'attività ricorrente di circuito alla base degli *up-state* nei topi WT. Ho studiato l'effetto dell'inibizione farmacologica dei canali del Ca^{2+} di tipo P/Q sulla attività ad *up-state* registrata da neuroni piramidali dello strato 2/3 in fettine acute di corteccia somatosensoriale di topo. Per questo scopo ho eseguito esperimenti di singolo e doppio patch clamp. Ho trovato che il blocco di questi canali del Ca^{2+} trasforma gli *up-state* in eventi che ricordano le scariche epilettiformi interictali. Ho analizzato le conduttanze medie eccitatorie ed inibitorie (G_e and G_i) durante gli *up-state* in controllo, durante gli eventi epilettiformi simil-interictali dopo il blocco dei canali del Ca^{2+} di tipo P/Q e nel periodo iniziale di applicazione

dell'inibitore di questi canali, ovvero quando solo una parte dei canali era stata bloccata. Ho trovato che 1) i canali del Ca^{2+} di tipo P/Q svolgono un ruolo fondamentale nel controllare sia la trasmissione sinaptica eccitatoria sia quella inibitoria sulle cellule piramidali durante l'attività ricorrente di circuito sottostante gli *up-state*. Tuttavia, il blocco di questi canali riduce maggiormente l'inibizione ricorrente rispetto all'eccitazione, spostando di conseguenza l'equilibrio eccitazione-inibizione a favore dell'eccitazione. 2) Quando, come risultato del blocco dei canali del Ca^{2+} di tipo P/Q, il rapporto G_e/G_i supera un valore critico, l'attività spontanea di circuito cambia e gli *up-state* vengono trasformati in eventi simili alle scariche epilettiformi interictali. Questi dati suggeriscono che, nella corteccia cerebrale, i canali del Ca^{2+} di tipo P/Q svolgono un ruolo predominante nel controllo della trasmissione sinaptica inibitoria rispetto a quella eccitatoria.

Dal momento che in molte sinapsi corticali, i canali del Ca^{2+} di tipo P/Q e di tipo N (denominati anche $Ca_V2.2$) cooperano nel controllare la trasmissione sinaptica, ho studiato anche l'effetto del blocco dei canali del Ca^{2+} di tipo N sull'attività ad *up-state*. L'inibizione farmacologica di questi canali causa una riduzione della frequenza degli *up-state*, suggerendo che i canali del Ca^{2+} di tipo N sono coinvolti nel regolarne la frequenza. Dopo il blocco dei canali del Ca^{2+} di tipo N, il rapporto G_e/G_i aumenta ma non sufficientemente a trasformare gli *up-state* in eventi epilettiformi simil-interictali.

L'obiettivo della seconda parte del mio progetto è stato quello di studiare i meccanismi, ancora non noti, alla base della facilitazione della CSD sperimentale nel topo FHM2 KI. Dopo aver determinato le condizioni sperimentali in cui poter osservare la facilitazione della CSD *in vitro*, ho indagato tre possibili meccanismi che potrebbero spiegare la facilitazione della CSD nel topo eterozigote FHM2 KI, in fettine acute di corteccia somatosensoriale di topo.

Dato lo specifico accoppiamento sia funzionale che strutturale negli astrociti tra la α2 Na,K-ATPasi e i trasportatori del glutammato a livello delle sinapsi corticali glutammatergiche (Cholet *et al.*, 2002), ho verificato se la perdita di funzione della α2 Na,K-ATPasi compromettesse la rimozione, mediata dagli astrociti, del glutammato dalla fessura sinaptica durante l'attività neuronale. Ho pertanto valutato il tasso di rimozione del glutammato misurando elettrofisiologicamente la corrente attivata sinapticamente mediata dai trasportatori del glutammato (STC), indotta negli astrociti dello strato 1 attraverso la stimolazione extracellulare delle afferenze neuronali nello stesso strato sia con singoli impulsi che con treni di impulsi ad alta frequenza (50 and 100 Hz). Ho isolato farmacologicamente la STC, al fine di misurarne il tempo di decadimento che fornisce una misura relativa della rimozione del glutammato mediata dagli astrociti (Bergles and Jahr, 1997; Diamond and Jahr, 2000). Ho trovato che la rimozione del glutammato rilasciato è effettivamente più lenta nei topi FHM2 KI rispetto ai topi WT. Il rallentamento della rimozione del glutammato era più pronunciato dopo un treno di impulsi rispetto a dopo un singolo stimolo e aumentava

all'aumentare della frequenza del treno. I miei dati dimostrano che la perdita di funzione della α2 Na,K-ATPasi compromette la rimozione del glutammato e suggeriscono che la rimozione del glutammato diventa più inefficiente all'aumentare della frequenza dell'attività corticale.

Sorprendentemente, l'ampiezza della STC dopo un singolo stimolo era più grande nel topo FHM2 KI che nel topo WT. Dal momento che l'ampiezza della STC è proporzionale al rilascio di glutammato evocato alle sinapsi dalla stimolazione extracellulare (Bergles and Jahr, 1997; Diamond and Jahr, 2000), questo risultato potrebbe suggerire che la stimolazione extracellulare provoca un rilascio di glutammato maggiore nel topo FHM2 KI che nel topo WT. Infatti, durante stimolazioni ripetute, la STC deprime di più nel topo FHM2 KI che nel topo WT, come previsto nel caso di probabilità di rilascio di glutammato aumentata nel topo FHM2 KI.

Considerato il ruolo chiave dei recettori NMDA nel ciclo di feedback positivo che innesca la CSD (Tottene *et al.*, 2011; Pietrobon and Moskowitz, 2014), sia la ridotta rimozione del glutammato sia l'aumentato rilascio del neurotrasmettitore potrebbero essere implicati nella facilitazione osservata nel topo FHM2 KI.

Visto che molti modelli della CSD includono un aumento della concentrazione extracellulare di K^+ al di sopra di un valore critico, come un evento innescante la CSD (Pietrobon and Moskowitz, 2014), e alla luce delle evidenze farmacologiche che indicano che l'α2 e/o l'α3 Na,K-ATPasi partecipano alla rimozione del K^+ dallo spazio extracellulare durante l'attività neuronale intensa (D'Ambrosio *et al.*, 2002; Kofuji and Newman, 2004), ho indagato se la rimozione del K^+ mediata dagli astrociti fosse compromessa nel topo FHM2 KI. Ho registrato elettrofisiologicamente la corrente sostenuta indotta negli astrociti dello strato 1 da stimolazione extracellulare; questa corrente è per lo più dovuta all'influsso di K^+ attraverso i canali Kir e il suo tempo di decadimento fornisce una misura indiretta della velocità di rimozione del K^+ mediata dagli astrociti. Questi esperimenti preliminari evidenziano che il tempo di decadimento della corrente di K^+ evocata da treni di impulsi è simile nel topo FHM2 KI e nel topo WT. Se tale risultato venisse confermato, indicherebbe che non ci sono variazioni nel tasso di rimozione del K^+ nel topo FHM2 KI rispetto al topo WT.

Dal momento che l'α2 Na,K-ATPasi è strettamente accoppiata allo scambiatore Na^+/Ca^{2+} a livello di microdomini di membrana sovrapposti al reticolo endoplasmatico (Lencesova *et al.*, 2004; Golovina *et al.*, 2003), abbiamo valutato se il contenuto di Ca^{2+} nei depositi intracellulari degli astrociti nel topo FHM2 KI fosse aumentata. Abbiamo ottenuto una misura indiretta della quantità di Ca^{2+} nei depositi andando a misurare negli astrociti corticali in coltura i transienti di Ca^{2+} indotti da ionomicina in un mezzo senza Ca^{2+}. Il transiente di Ca^{2+} nel topo FHM2 KI era maggiore che nel topo WT, indicando un aumentato contenuto di Ca^{2+} nei depositi degli astrociti del topo FHM2 KI.

Misurando la soglia e la velocita della CSD dopo aver svuotato i depositi di Ca^{2+} usando acido ciclopiazonico (CPA), un inibitore della SERCA, ho osservato che lo svuotamento delle riserve di Ca^{2+} riduce la facilitazione della CSD nel topo FHM2 KI, senza influenzare la CSD nel topo WT. Questo risultato suggerisce che l'aumentata concentrazione di Ca^{2+} all'interno dei depositi degli astrociti è coinvolta nella facilitazione della CSD sperimentale nel topo FHM2 KI.

SUMMARY

Migraine is a common, highly disabling episodic neurological disorder affecting more than 10% of the population and arises from a primary brain dysfunction that leads to episodic activation and sensitization of the trigeminovascular pain pathway.

Familial hemiplegic migraine (FHM) is a rare and very severe monogenic autosomal dominant subtype of migraine with aura. Apart from the motor aura and the possible longer duration of the aura, typical FHM attacks resemble migraine with aura attacks (Pietrobon and Moskowitz, 2013); thus, FHM can be considered as a model of the common forms of migraine. Gain-of-function missense mutations in *CACNA1A* gene, encoding the pore-forming subunit of the neuronal voltage-gated Ca^{2+} channel $Ca_V2.1$ (also known as P/Q-type Ca^{2+} channel), cause FHM type 1 (FHM1) and loss-of-function mutations in *ATP1A2*, the gene encoding the astrocytic Na,K-ATPase α2 subunit, cause FHM type 2 (FHM2) (Ophoff *et al.*, 1996; De Fusco *et al.*, 2003). FHM knock-in (KI) mice carrying mutations causing either FHM1 or FHM2 show facilitation of induction and propagation of experimental CSD (van den Maagdenberg *et al.*, 2004, 2010; Leo *et al.*, 2011), the phenomenon underlying migraine aura and a key triggering event for trigeminovascular activation.

FHM1 KI mice, carrying the R192Q mutation, show an increased influx of Ca^{2+} through P/Q-type Ca^{2+} channels in neurons, including cortical pyramidal cells, and an increased probability of glutamate release at cortical pyramidal cells synapses (Pietrobon, 2010; Tottene *et al.*, 2009), that may explain the facilitation of experimental CSD. Recent findings in our laboratory (Fabbro, Sessolo, Vecchia and Pietrobon, manuscript in preparation) show that the frequency of the up-states recorded in acute cortical slices, that resemble slow oscillation *in vivo* (Steriade *et al.*, 1993), is larger in FHM1 KI than WT mice, suggesting that the gain-of-function of P/Q-type Ca^{2+} channels facilitates the mechanisms of up-states generation and/or decreases the refractory period after an up-state.

The first aim of my work was to further investigate the role of P/Q-type Ca^{2+} channels in the recurrent network activity underlying the up-states in WT mice. I studied the effect of pharmacological inhibition of P/Q-type Ca^{2+} channels on the up-state activity recorded from layer 2/3 pyramidal neurons in acute slices of mouse somatosensory cortex, by performing single and double patch clamp experiments. I found that the block of P/Q-type Ca^{2+} channels transforms the up-states into events resembling interictal epileptiform discharges. I evaluated the mean excitatory and inhibitory synaptic conductances (G_e and G_i) during the control up-states, during the simil-interictal epileptiform events after P/Q-type Ca^{2+} channels block as well as immediately after the application of the P/Q-type Ca^{2+} channels blocker when the channels were not completely blocked. I showed that 1) P/Q-type Ca^{2+} channels have

a dominant role in controlling both excitatory and inhibitory synaptic transmission onto pyramidal cells during the spontaneous recurrent network activity that underlies the up-states. However, the block of P/Q-type Ca^{2+} channels reduces recurrent inhibition more than recurrent excitation and shifts the cortical excitation-inhibition balance towards excitation. 2) When, as a consequence of the block of P/Q-type Ca^{2+} channels, G_e/G_i increases above a critical value, the spontaneous network activity changes and the up-states are transformed into events resembling simil-interictal epileptiform discharges. These data suggest that, in the cerebral cortex, P/Q-type Ca^{2+} channels play a more prominent role in controlling inhibitory compared to excitatory synaptic transmission.

Given that at many cortical synapses P/Q- and N-type (also known as $Ca_V2.2$) Ca^{2+} channels cooperate in controlling synaptic transmission, I also investigated the effect of blocking N-type Ca^{2+} channels on up-state activity. Pharmacological inhibition of this channel strongly reduces the up-states frequency, indicating a role for N-type Ca^{2+} channel in controlling up-states frequency. After the block of N-type Ca^{2+} channels, G_e/G_i increases but not sufficiently to transform up-states in simil-interictal epileptiform events.

The aim of my second project was to investigate the unknown mechanisms underlying facilitation of experimental CSD in FHM2 KI mice. After setting the conditions in which facilitation of CSD was observed *in vitro*, I studied three possible mechanisms that may underlie the facilitation of CSD in heterozygous FHM2 KI mice, in acute slices of mouse somatosensory cortex.

Given the specific localization and functional coupling of the α2 Na,K-ATPase to glutamate transporters in astrocyte processes surrounding cortical glutamatergic synapses (Cholet *et al.*, 2002), I first investigated whether the loss-of-function of α2 Na,K-ATPase results in an impaired astrocyte-mediated clearance of glutamate from the synaptic cleft during cortical neuronal activity. I monitored the rate of glutamate clearance electrophysiologically, by measuring the synaptically-activated glutamate transporter-mediated current (STC) evoked in astrocytes of layer 1 by extracellular stimulation of neuronal afferents in the same layer. Either single pulse stimulation or trains of stimuli at high frequencies (50 and 100 Hz) were delivered. I isolated the STC pharmacologically in order to measure the STC decay time course that provides a relative measure of the glutamate clearance by astrocytes (Bergles and Jahr, 1997; Diamond and Jahr, 2000). I found that the clearance of glutamate release is slower in FHM2 KI compared to WT mice. The slowing of glutamate clearance was more pronounced after a train stimulation than a single stimulus and increased with increasing frequency of the train. My data show that the loss-of-function of α2 Na,K-ATPase results in an impairment of glutamate clearance and suggest that the impairment increases with increasing frequency of cortical activity.

Surprisingly, the STC amplitude after a single pulse stimulation was higher in FHM2 KI than in WT mice. Given that the STC amplitude is proportional to the glutamate

release evoked at the synapses by the extracellular stimulation (Bergles and Jahr, 1997; Diamond and Jahr, 2000), this result would suggest that the extracellular stimulation elicits a larger glutamate release in FHM2 KI than in WT mice. Indeed, during repetitive stimulation the STC depressed more in FHM2 KI than WT mice, as expected if the probability of glutamate release is increased in the mutant mice.
Given the key role of NMDA receptors in the positive feedback cycle, that ignites CSD (Tottene *et al.*, 2011; Pietrobon and Moskowitz, 2014), both the reduced clearance of glutamate and the increased glutamate release may be implicated in the facilitation of CSD in FHM2 KI mice.

Given that most models of CSD include local increase of extracellular K^+ concentration above a critical value, as a triggering event in the initiation of CSD (Pietrobon and Moskowitz, 2014), and that pharmacological evidence indicates that α2 and/or α3 Na,K-ATPase participate in the clearance of K^+ from the extracellular space during intense neuronal activity (D'Ambrosio *et al.*, 2002; Kofuji and Newman, 2004), I investigated whether K^+ clearance by astrocytes is impaired in FHM2 KI mice. I evaluated the rate of K^+ clearance from the interstitial space, by recording the slowly decaying current, which is mainly due to K^+ influx through Kir channels, evoked in layer 1 astrocytes by extracellular stimulation. I measured the decay time course of this current, which provides an indirect measure of the K^+ clearance rate by astrocytes. Preliminary experiments show that the decay time course of the K^+ current evoked by train stimulation is similar in WT and FHM2 KI mice. If confirmed, this result would indicate that there are no changes in the rate of K^+ clearance in FHM2 KI mice compared to WT.

Given that α2 Na,K-ATPase is tightly coupled to the Na^+/Ca^{2+} exchanger at plasma membrane microdomains that overlay the endoplasmic reticulum (Lencesova *et al.*, 2004; Golovina *et al.*, 2003) and hence its loss-of-function could influence Ca^{2+} homeostasis, we investigated whether the Ca^{2+} content in the intracellular Ca^{2+} stores of astrocytes in FHM2 KI mice is increased. We obtained an indirect measure of the amount of Ca^{2+} in the stores, by measuring in cultured cortical astrocytes the Ca^{2+} transient induced by ionomycin in Ca^{2+}-free medium. This transient was larger in FHM2 KI mice compared to WT mice, indicating that the Ca^{2+} content is increased in the intracellular Ca^{2+} stores of astrocytes in FHM2 KI mice.
I measured CSD threshold and velocity after depletion of intracellular Ca^{2+} stores by CPA, a SERCA inhibitor, and I observed that depletion of Ca^{2+} stores reduces the facilitation of CSD in FHM2 KI mice, without affecting CSD in WT mice. This result suggests a role of increased Ca^{2+} concentration within the astrocytes intracellular stores in the facilitation of experimental CSD in FHM2 KI mice.

1. INTRODUCTION

1.1. Migraine

Migraine is a common, highly disabling episodic brain disorder that affects more than 10% of the population in western countries with a higher prevalence in women (15-25%) than men (6-8%). Given its strong impact in the quality of life for individuals and society, migraine is classified by the World Health Organization as one of the 20 most disabling disorders (Pietrobon and Striessnig, 2003).

Migraine can be divided in two major subtypes: migraine with aura (MA) and without aura (MO). Migraine attacks are typically characterized by unilateral and throbbing, often severe headache lasting from 4 to 72 hours, often accompanied by nausea, phonophobia and photophobia (MO). In about one third of patients, the headache is preceded by transient neurological symptoms, called 'aura' (MA). Aura symptoms are most frequently visual, but may involve other senses or, rarely, can cause motor or speech deficits. Migraine aura can last up to 60 minutes and frequently consists in a scotoma (an area of lost vision) with a scintillating border, drifting slowly across the visual field (Pietrobon and Striessnig, 2003).

Migraine has a strong (up to 50%) genetic component, higher in MA than in MO, characterized by a multifactorial polygenic inheritance. External and internal factors (migraine triggers) can modulate the inherent migraine threshold. Several loci have been linked to migraine (both MA and MO) but the causative genes have not been identified yet, except for Familial Hemiplegic Migraine (FHM), a rare autosomal subtype of MA characterized by dominant inheritance (Vecchia and Pietrobon, 2012; Pietrobon and Moskowitz, 2013).

1.1.1. Neurobiology of migraine

Most migraine attacks start in the brain, as suggested by the premonitory symptoms (*e.g.*, difficulty with speech and reading, increased emotionality, sensory hypersensitivity) that in many patients may occur up to 12 hours before the attack and are highly predictive of the attack, and by the nature of typical migraine triggers (stress, sleep deprivation, oversleeping, hunger and prolonged sensory stimulation). Moreover, psychophysical and neurophysiological studies have provided clear evidence that in the period between attacks migraineurs show hypersensitivity to sensory stimuli and abnormal processing of sensory information (Vecchia and Pietrobon, 2012; Pietrobon and Moskowitz, 2013).

A large body of indirect evidence supports the prevailing view that the development of migraine headache depends on the activation and sensitization of the trigeminovascular system (Pietrobon and Moskowitz, 2013; Noseda *et al.*, 2013).

Indeed, within the skull, pain sensitivity is primarily restricted to the meningeal blood vessels, which are densely innervated by nociceptive sensory afferent fibers of the ophthalmic division of the trigeminal nerve (Vecchia and Pietrobon, 2012; Pietrobon and Moskowitz, 2013).

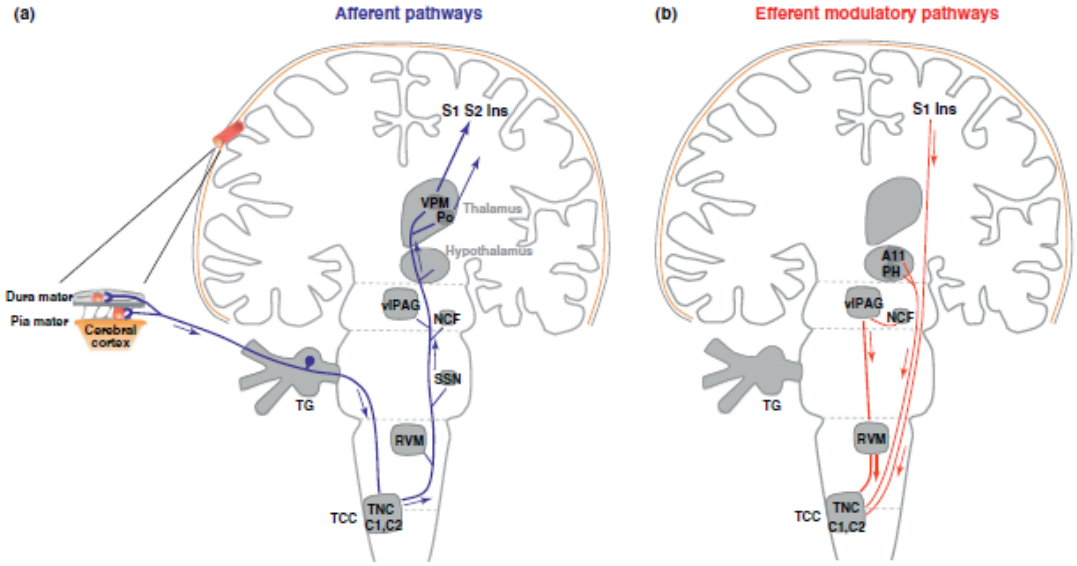

Figure 1.1. Neuronal structures and pathways involved in the trigeminovascular activation and modulation of cephalic pain (from Vecchia and Pietrobon, 2012).

Schematic illustration of important neuronal structures and connections in the trigeminovascular pathways involved in migraine headache. a) Afferent pathways. b) Efferent modulatory pathways.
TG, trigeminal ganglion; TCC, trigeminocervical complex; C1, C2, dorsal horns of the cervical spinal cord; TNC, caudal division of the spinal trigeminal nucleus; SSN, salivatory nucleus; vlPAG, ventrolateral periacqueductal grey; NCF, the nucleus cuneiformis; RVM, rostral ventromedial medulla; VPM, ventroposteriomedial thalamic nucleus; Po, posterior thalamic nucleus; S1, S2, somatosensory cortex; Ins, insular cortex; PH, posterior hypothalamus; A11, dopaminergic hypothalamic nucleus.

In several animal models, including non-human primates, activation of the meningeal trigeminovascular afferents leads to activation of the so-called trigeminocervical complex (TCC) comprising the C1 and C2 dorsal horns of the cervical spinal cord and the caudal division of the spinal trigeminal nucleus (TNC). The TCC makes direct ascending connections with different areas in the brainstem, including the superior salivatory nucleus, the ventrolateral periacqueductal grey (vlPAG), the nucleus cuneiformis and with higher structures, including several hypothalamic and thalamic nuclei, which in turn make ascending connections with the cortex (Fig. 1.1a). Dura-sensitive ventroposteriomedial thalamic neurons project mainly in the so-called ‘pain matrix’ areas, formed by the trigeminal primary and secondary somatosensory (S1, S2) and the insular (Ins) cortex and thus are likely to play a role in the perception of the headache. Trigeminovascular posterior thalamic neurons project into non-trigeminal S1, as well as auditory, visual, retrosplenial, ectorhinal, and parietal association cortices, thus likely contributing to disturbances in neurological functions

involved in vision, auditory, memory, motor and cognitive performance. The trigeminovascular projections to specific hypothalamic and brainstem nuclei are likely to contribute to other aspects of the complex migraine symptomatology, such as loss of appetite, sleepiness, irritability, stress, pursuit of solitude and autonomic symptoms (Vecchia and Pietrobon, 2012; Pietrobon and Moskowitz, 2013, and references therein). The TCC receives descending projections from brainstem and hypothalamic nociceptive modulatory nuclei that may mediate descending modulation of trigeminovascular nociceptive traffic (Fig. 1.1b). The TCC also receives descending cortical projections from layer 5 pyramidal cells of the contralateral S1 and caudal Ins cortex (Pietrobon and Moskowitz, 2013, and references therein).

The maintenance of the severe prolonged pain of migraine headache involves sensitization of meningeal nociceptors and self-sustained sensitization of central neurons of the trigeminovascular system (Vecchia and Pietrobon, 2012).

Nevertheless, the nature and the mechanisms underlying the episodic activation of the trigeminovascular system is still debated (Pietrobon, and Moskowitz, 2013). Several experimental and clinical observations show that vasodilation of meningeal and/or extracranial arteries is neither necessary nor sufficient to cause migraine pain (Pietrobon and Moskowitz, 2013 and references therein). Therefore, the 'vascular theory', according to which the symptoms of migraine aura are caused by transient ischemia induced by vasoconstriction and the headache arises from rebound abnormal vasodilatation of intracranial arteries and consequent mechanical activation of perivascular sensory fibers, is untenable (Charles and Brennan, 2009; Dodick, 2008; Pietrobon and Moskowitz, 2013). It is now generally accepted that the primary cause of migraine headache lies in the brain and, given the wide genetic and clinical heterogeneity of migraine, several primary mechanisms presumably exist (Pietrobon and Moskowitz, 2013). Recent findings point to cortical spreading depression (CSD) as a key player in the pathogenesis of migraine (Levy *et al.*, 2012; Vecchia and Pietrobon, 2012; Pietrobon and Moskowitz, 2013, 2014).

1.1.2. CSD phenomenology

CSD consists in a slowly propagating (2-6 mm/min) wave of strong neuronal and glial cells depolarization that progresses across the cerebral cortex, generating a transient neuronal intense spike activity, followed by long-lasting neuronal suppression (Charles and Brennan, 2009; Pietrobon and Moskowitz, 2014). CSD causes no cell death or long-lasting damage in a normally metabolizing brain but imposes a considerable bioenergetic burden on tissue (Pietrobon and Moskowitz, 2014).

CSD is a complex phenomenon that has different phases. Recent findings indicate that during the early phase, lasting a few seconds, CSD-related depolarization is initiated by the activation of channels located in apical dendrites of pyramidal

neurons. This is followed by the main phase, lasting 15-20 seconds, in which there is the subsequent activation of other ion channels along most of the somatodendritic membrane. After the main phase, there is a late phase, in which channels in the somatobasal zone close and a net inward current is restricted to a narrow band in the proximal apical dendrites (Pietrobon and Moskowitz, 2014 and references therein).

CSD is characterized by the collapse of ion homeostasis, profound disruption of transmembrane ionic gradients and the release of neurotransmitters and other molecules from cellular compartments.

The transient, strong near-complete neuronal depolarization is accompanied by a rapid increase in K^+ extracellular concentration, a rapid decrease in the extracellular concentration of Na^+, Cl^- and Ca^{2+}. The reduction in Na^+ extracellular concentration is greater than the increase in K^+ extracellular concentration and electroneutrality is probably maintained by efflux of organic anions; indeed, several amino acids, including glutamate and aspartate, are released during CSD (Pietrobon and Moskowitz, 2014).

CSD has also been associated with large increases in the intracellular concentration of Ca^{2+} in both neurons and astrocytes in the cerebral cortex; however, the Ca^{2+} intracellular concentration increase in neurons precedes that in astrocytes and the CSD-associated neuronal Ca^{2+} wave is unaffected by suppression of the Ca^{2+} concentration increase in astrocytes (Pietrobon and Moskowitz, 2014).

CSD onset is also associated with a transient increase in extracellular pH that is followed by a decrease during the sustained depolarization. The transient increase in extracellular pH reflects a transient proton influx into (and/or HCO_3^- efflux from) neurons, as it is accompanied by a transient decrease in intracellular pH in neurons (Pietrobon and Moskowitz, 2014).

Astrocyte depolarization during CSD seems to be largely passive, caused by an increase in K^+ extracellular concentration. Moreover, a fast mitochondrial depolarization coincident with CSD occurs in neurons but not astrocytes (Pietrobon and Moskowitz, 2014).

Upon the influx of Na^+, Cl^- and water, the interstitial space shrinks (by 40-70%) mainly as a consequence of neuronal swelling *in vivo* and *in vitro*; by contrast, astrocytes display only passive swelling in response to CSD-inducing solutions in cortical slices and do not swell *in vivo* (Pietrobon and Moskowitz, 2014).

1.1.3. Mechanisms of experimental CSD

In migraineurs CSD occurs spontaneously in response to specific triggers, which might coincide with known migraine triggers, such as stress or intense and repetitive long lasting sensory stimulation, and the mechanisms that make the brain of migraineurs susceptible to these episodic 'spontaneous' CSDs are still unknown.

CSD can be experimentally induced by focal mechanical (pinprick), electrical or chemical (high concentrations of K^+) stimulation of the cerebral cortex or by inhibition

of the Na^+/K^+ ATPase (Pietrobon and Moskowitz, 2014). The experimental stimuli that can produce CSD in healthy brain tissue induce an anomalous increase in local extracellular K^+ concentration ($[K^+]_{out}$) and the release of glutamate (and other neurotransmitters) owing to depolarization of presynaptic terminals accompanied by increase in neuronal firing and activation of voltage-gated Ca^{2+} (Ca_V) channels (Fig. 1.2-1.3; Pietrobon and Moskowitz, 2014).

Both experimental data and computational models support the idea that an increase in $[K^+]_{out}$ above a critical value is a CSD key initiating event (Pietrobon and Moskowitz, 2014). When stimuli sufficiently intense to ignite a CSD are applied, the regulatory mechanisms that normally keep the $[K^+]_{out}$ within the physiological range are overwhelmed by a positive feedback cycle that produces a self-regenerating increase of the $[K^+]_{out}$ and of neuronal depolarization. This positive feedback cycle initiates when a net self-sustaining inward current across the membrane is generated, making the initial gradual neuronal depolarization self-regenerative. This is achieved when a sufficient number of voltage-dependent and/or $[K^+]_{out}$-dependent cationic channels carrying an inward current are activated. The net sustained inward current leads to membrane depolarization and the release of K^+, which in turn leads to further activation of the cationic channels, further depolarization and an increase in local $[K^+]_{out}$. This results in complete neuronal depolarization if the removal of K^+ from the interstitium, mainly by glial reuptake mechanisms, does not keep pace with its release (Fig. 1.2; Pietrobon and Moskowitz, 2014).

Nevertheless, the nature of the cationic channels that are crucial for generating the initial net inward current and that mediate local K^+ release remains unclear and controversial. There is a strong pharmacological evidence supporting a key role of NMDA receptors, as NMDA receptors antagonists inhibit *in vivo* CSD induction and propagation in a dose-dependent manner (Pietrobon and Moskowitz, 2014 and references therein).

Pharmacological and functional analyses of mutant mice with an altered CSD threshold show that the NMDA receptors implicated in CSD initiation are activated by glutamate released from synaptic terminals after the opening of voltage-gated Ca^{2+} channels (Fig. 1.2; Pietrobon and Moskowitz, 2014). A recent evidence suggests that P/Q-type Ca^{2+} channels ($Ca_V2.1$) have a particularly important role because CSD is abolished after specific blockade of these channels, even when CSD is triggered by largely suprathreshold stimuli (Tottene *et al.*, 2011). Moreover, in mice, carrying mutations that produce a partial loss-of-function of the P/Q-type Ca^{2+} channel (Pietrobon, 2010), the threshold for CSD induction in the cerebral cortex *in vivo* is greatly increased and K^+-evoked glutamate release, measured by *in vivo* microdialysis, is reduced by more than twofold (Ayata *et al.*, 2000). Conversely, familial hemiplegic migraine type 1 (FHM1) knockin (KI) mice, which carry gain-of-function mutations in the gene encoding the P/Q-type Ca^{2+} channel, show increased action potential-evoked glutamate release at cortical synapses (Tottene e al., 2009) and have a lowered

threshold for CSD induction *in vivo* (van den Maagdenberg *et al.*, 2004; van den Maagdenberg *et al.*, 2010) and in cortical slices (Tottene e al., 2009). Indeed, in FHM1 knockin mice CSD threshold is restored to the wild-type (WT) value, by restoring evoked glutamate release to the WT value through partial inhibition of P/Q-type Ca^{2+} channels (Tottene e al., 2009; see below). This supports a crucial role of P/Q-type Ca^{2+} channels in CSD induction and a causative relationship between increased P/Q-type Ca^{2+} channels-dependent glutamate release and facilitation of CSD initiation.

Astrocytes are also implicated in CSD initiation (Fig. 1.2). In the adult brain, the α2 Na^+/K^+-ATPase is expressed almost exclusively in astrocytes (Cholet *et al.*, 2002) and heterozygous FHM type 2 (FHM2) KI mice, carrying a loss-function mutation in the gene encoding α2 Na^+/K^+-ATPase (Leo *et al.*, 2011; see below), exhibit a lowered electrical threshold for CSD *in vivo*. Furthermore, in mouse brain slices it has been shown that astrocyte-directed inactivation of the major astrocytic gap junction protein, connexin 43, lowers the threshold for CSD generation (Theis *et al.*, 2003), probably as a consequence of deficient K^+ spatial buffering by astrocytes (Kofuji and Newman, 2004).

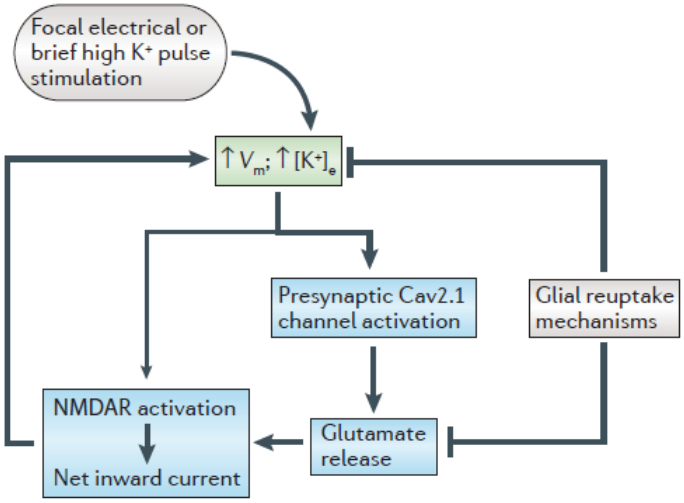

Figure 1.2. CSD initiation (adapted from Pietrobon and Moscowitz, 2014).
A schematic diagram of the initiation mechanism of CSD induced by a brief K^+ pulse or by electrical stimulation in which P/Q-type Ca^{2+} channel-dependent release of glutamate from cortical pyramidal cell synapses and activation of NMDA receptors (NMDARs) have a key role in the positive-feedback cycle that ignites CSD.
In this scheme, the glial reuptake mechanisms exert a dampening role by mediating both K^+ and glutamate reuptake. Although not illustrated, a relatively minor role of other ion channels (for example, postsynaptic Ca_V and/or voltage-gated Na^+ channels) in the initiation of the positive-feedback cycle cannot be excluded. Vm, membrane potential. $[K^+]_e$, K^+ extracellular concentration.

Taken together, these data support a model of CSD initiation, in which activation of presynaptic voltage-gated Ca^{2+} channels (in particular P/Q-type) with consequent release of glutamate from recurrent cortical pyramidal cell synapses and activation of NMDA receptors are key components of the positive feedback cycle that ignites CSD (Pietrobon and Moskowitz, 2014). The astrocytes limit CSD susceptibility, owing to their direct involvement in K^+ clearance and/or indirect role in glutamate clearance

(through functional coupling with glutamate transporters; Rose *et al.*, 2009; Pietrobon and Moskowitz, 2014; see below) during intense neuronal activity (Fig. 1.2).
The mechanism of CSD propagation is still unclear and four hypotheses have been proposed: two involve intercellular diffusion and opening of gap junctions in either glial cells or neurons and the other two are based on interstitial diffusion of a humoral agent, K^+ or glutamate (Pietrobon and Moskowitz, 2014 and references therein).

1.1.4. CSD and migraine

After the discovery of migraine visual aura in 1941 by Karl Lashley, Leão and Milner both pointed out the similarity between the velocity of CSD propagation and the propagation of visual aura reported by Lashley (Lashley, 1941; Leão, 1945; Milner, 1958): similarly to CSD in mammalian cortex, the speed of migraine aura spread is approximately 3 mm/min. Moreover, aura is characterized by negative symptoms (*e.g.* loss of sensation, visual scotoma) often preceded by positive symptoms (*e.g.* paresthesias, visual scintillations), that is reminiscent of the cessation of cortical neuronal activity preceded by a brief burst of action potentials at the CSD wave-front (Eikermann-Haerter and Ayata, 2010).

Accumulating evidences strongly implicate CSD in the genesis of visual aura and blood-oxygen-level-dependent (BOLD) magnetic resonance imaging (MRI) in humans has provided the most technically advanced demonstration of this (Pietrobon and Striessnig, 2003; Pietrobon and Moskowitz, 2014 and references therein).
Three additional lines of investigation reinforce the link between aura, CSD and migraine.
First, the discovery that certain genetic mutations cause FHM, increase the risk of migraine aura in humans and facilitate CSD in mouse models (Pietrobon and Moskowitz, 2013; Vecchia and Pietrobon, 2012). Indeed, two KI mice carrying human mutations causing FHM1 and one KI mice carrying human mutations causing FHM2 show a decreased threshold for CSD initiation and an increased velocity of CSD propagation (Eikermann-Haerter *et al.*, 2009; van den Maagdenberg *et al.*, 2004, 2010; Leo *et al.*, 2011).
Second, CSD activates the trigeminovascular system in animal models to cause head-ache. It was clearly demonstrated that CSD is able to directly activate the meningeal nociceptors and the second-order neurons in the TNC (Zhang *et al.*, 2010, 2011) and to elicit a long-lasting blood-flow increase within the middle meningeal artery and plasma protein leakage in the *dura mater* (Bolay *et al.*, 2002). CSD induces a large increase in the extracellular concentration of K^+ and hydrogen (H^+) ions, nitric oxide (NO), ATP, arachidonic acid and prostaglandins (Pietrobon 2005, 2007; Pietrobon and Moskowitz, 2013). It is hypothesized that these substances may activate the meningeal trigeminovascular afferents. Activation of the meningeal afferents leads to release of proinflammatory vasoactive neuropeptides that may promote neurogenic

inflammation in the dura and possibly sustain the activation of the trigeminovascular afferents and lead to their sensitization (Fig. 1.3; Charles and Brennan, 2009; Pietrobon and Moskowitz, 2013).

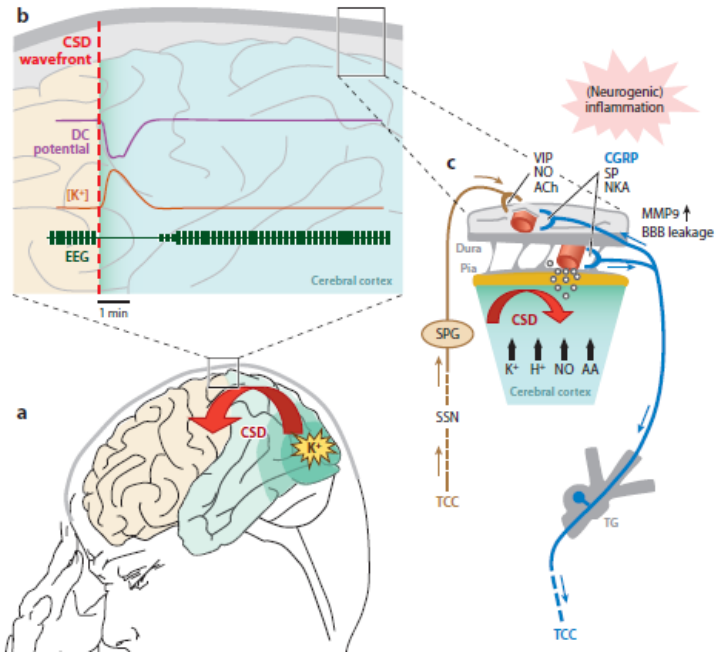

Figure 1.3. From cortical spreading depression (CSD) to trigeminovascular nociception (adapted from Pietrobon and Moskowitz, 2013).
a) CSD is believed to be ignited by local elevations of extracellular K^+ concentration above a critical level because of hyperactive neuronal circuits in the cerebral cortex. *b*) CSD is a slowly propagating wave of strong neuronal and glial depolarization accompanied by depression of spontaneous and evoked electroencephalographic (EEG) activity and by a large increase in extracellular K^+ concentration. *c*) Other noxious mediators (*open circles*), such as H^+, NO, arachidonic acid (AA) and serotonin, are released during CSD, in addition to glutamate and other neurotransmitters. The blue pathway represents the meningeal trigeminovascular afferents; also shown is a parasympathetic reflex involving activation of the superior salivatory nucleus (SSN) and the sphenopalatine ganglion (SPG) leading to release of vasoactive intestinal peptide (VIP), NO and acetylcholine (ACh) from the meningeal parasympathetic efferents. BBB, blood-brain barrier. TCC, trigeminocervical complex; TG: trigeminal ganglion; CGRP, calcitonin gene–related peptide; SP, substance P; NKA, neurokinin A; MMP9, matrix metalloproteinase.

Third, prophylactic drugs raise the electrical and KCl thresholds to evoke CSD, as a mechanism of prevention. At least five clinically used migraine prophylactic drugs, belonging to different pharmacological classes (valproate, topiramate, propanolol, amitriptyline and methysergide), which are effective in reducing the frequency of migraine attacks with or without aura, dose-dependently suppress CSD susceptibility in experimental animal models (Ayata *et al.*, 2006; Pietrobon and Moskowitz, 2014).

Evidences pointing to CSD as the electrical phenomenon underlying migraine aura symptoms are today widely accepted (Pietrobon and Moskowitz, 2014). Despite this, the question whether CSD may initiate the headache mechanisms in migraine is debated. In fact, most migraineurs do not experience aura, and even MA patients experience attacks without aura; the possibility that silent CSDs (i.e. CSDs involving areas of the brain that would not generate a perceived aura) may initiate the headache mechanisms in MO is neither proven nor disproven by current evidences. Moreover,

therapeutic intervention may abolish aura but not headache in some patients or on the contrary may help with headache without affecting aura in others (Pietrobon and Moskowitz, 2014).

1.2. Familial hemiplegic migraine

Familial hemiplegic migraine (FHM) is a rare and very severe monogenic autosomal dominant subtype of MA, whose aura symptoms include motor weakness and hemiparesis (often, but not always, unilateral) lasting for hours to days (Pietrobon, 2007; Pietrobon and Moskowitz, 2013).

FHM can be considered as a model of the common forms of migraine because the headache and aura features, apart from the hemiparesis, are identical (Thomsen *et al.*, 2002) and two-thirds of the FHM patients have, in addition to FHM attacks, also attacks of common non-hemiplegic migraine (Ferrari *et al.*, 2007); however, in FHM aura symptoms and also headache stay longer than in the common form of migraine.

In addition to typical FHM attacks, some FHM patients can suffer atypical more severe attacks with signs of diffuse encephalopathy, coma, confusion or impairment of consciousness, prolonged hemiplegia (lasting up to several days) and in few cases seizures (Thomsen *et al.*, 2002). Furthermore, about 20% of FHM families show permanent cerebellar symptoms of progressive cerebellar ataxia with or without nystagmus (Thomsen *et al.*, 2002). Emotional stress and minor head trauma are among the most common triggers of FHM attacks (Pietrobon, 2007).

FHM is a genetically heterogeneous pathology and three FHM causative genes, all encoding ion channels or transporters, have been identified. Mutations in the genes *CACNA1A* at chromosome 19p13 (Ophoff *et al.*, 1996), *ATP1A2* at chromosome 1q23 (De Fusco *et al.*, 2003) and *SCNA1A* at chromosome 2q24 (Dichgans *et al.*, 2005) are responsible for FHM1, FHM2 and FHM type3 (FHM3), respectively. From the clinical point of view, these three types of FHM display similar symptoms with the exception of FHM1 that is uniquely associated with cerebellar symptoms (Pietrobon, 2007).

The first gene identified is the *CACNA1A* (FHM1), which encodes the α1 subunit of neuronal voltage-dependent P/Q-type Ca^{2+} channels (Ophoff *et al.*, 1996). FHM1 shows an incomplete penetrance and other genetic or environmental factors could explain symptoms variability between subjects affected by the same FHM1 mutation. All the twenty-one FHM1 discovered mutations are missense mutations; some mutations are associated with a broad spectrum of clinical features besides hemiplegic migraine, such as cerebellar ataxia and epilepsy, both during severe FHM attacks or independent of FHM attacks (Pietrobon and Moskowitz, 2013).

The P/Q-type Ca^{2+} channels are widely expressed throughout the central nervous system (CNS) (Westenbroek *et al.*, 1995), including all brain regions implicated in the pathogenesis of migraine. P/Q-type Ca^{2+} channels play a dominant role in controlling neurotransmitter release, particularly at central synapses and their somatodendritic

localization points to additional postsynaptic roles, such as in neural excitability (Pietrobon, 2010, and references therein). In particular, P/Q-type Ca^{2+} channel play a predominant role in controlling the release of glutamate and GABA at both excitatory and inhibitory synapses between pyramidal cells and somatostatin (SOM) interneurons (Sessolo *et al.*, unpublished data). Likewise, the excitatory synaptic transmission between pyramidal cells and fast spiking (FS) interneurons in layer 2/3 somatosensory and layer 5 motor cortex, are controlled by P/Q-type Ca^{2+} channels (Pietrobon, 2010; Ali and Nelson, 2006; Tottene *et al.*, 2009; Zaitsev *et al.*, 2007; Rozov *et al.*, 2001). By contrast, synapses between layer 5 pyramidal cells and burst-firing bipolar interneurons of motor cortex, strongly depend on N-type Ca^{2+} channels ($Ca_V2.2$; Ali and Nelson, 2006). In different cortical areas, also inhibitory neurotransmission between FS interneurons and pyramidal cells are totally mediated by P/Q-type Ca^{2+} channels (Ali and Nelson, 2006, Zaitsev *et al.*, 2007), with the exception of layer 5 of the motor cortex, where it is exclusively dependent on N-type Ca^{2+} channels (Ali and Nelson, 2006).

FHM2 is caused by mutations in *ATP1A2*, the gene encoding the α2 Na^+/K^+-ATPase (De Fusco *et al.*, 2003). To date, more than 50 FHM2 mutations have been discovered; almost all are missense mutations that produce substitutions of conserved amino acids in important functional regions of the protein, but there are also small deletions and a single mutation affecting the stop codon, which causes an extension of the *ATP1A2* protein by 27 amino acid residues (Riant *et al.*, 2005; Jurkat-Rott *et al.*, 2004). Most of the *ATP1A2* mutations are associated with pure FHM; however, some are associated to complications like cerebellar ataxia, childhood convulsions, epilepsy and mental retardation. Interestingly, some *ATP1A2* mutations are associated with non-hemiplegic migraine phenotypes, such as basilar migraine and even common migraine (Russel and Ducros, 2011, and references therein). In the brain, α2 Na^+/K^+-ATPase is expressed almost exclusively in astrocytes in the adult (Moseley *et al.*, 2003) and its colocalization with glial glutamate transporters (Rose *et al.*, 2009) and with the Na^+/Ca^{2+} exchanger (Lencesova *et al.*, 2004; Golovina *et al.*, 2003) suggests specific roles in glutamate clearance and in the regulation of intracellular Ca^{2+} (see below for details).

FHM3 is caused by missense mutations in SCNA1A, the gene encoding the pore-forming α1 subunit of neuronal voltage-gated sodium (Na^+) channel $Na_V1.1$; the *SCN1A* gene was already known as an epilepsy gene previous to its identification as the FHM3 gene (Dichgans *et al.*, 2005). FHM3 can occur as pure hemiplegic migraine or in association with epileptic seizures or with elicited repetitive daily blindness attacks that are independent from the hemiplegic migraine attacks (Vecchia and Pietrobon, 2012 and references therein). $Na_V1.1$ channels are primarily expressed in the central nervous system (CNS) during late postnatal stages, more in caudal than rostral regions; in particular, they are highly expressed in certain inhibitory

interneurons, where they play an important role in sustaining high-frequency firing (Catterall *et al.*, 2010).

1.2.1. The α2 Na,K-ATPase and its functional roles

The Na,K-ATPase is a transmembrane P-type ion pump that utilizes the free energy of ATP hydrolysis to exchange Na^+ for K^+ and maintains gross cellular homeostasis. The stoichiometry of this transport consist of three Na^+ ions pumped out of and two K^+ ions pumped into the cells for each ATP molecule that is splitted. Na,K-ATPase is a heteromeric protein composed of a large α subunit, a smaller glycosylated β subunit and an auxiliary tissue-specific γ-subunit belonging to the FXYD protein family (Morth *et al.* 2007) (Fig. 1.4).

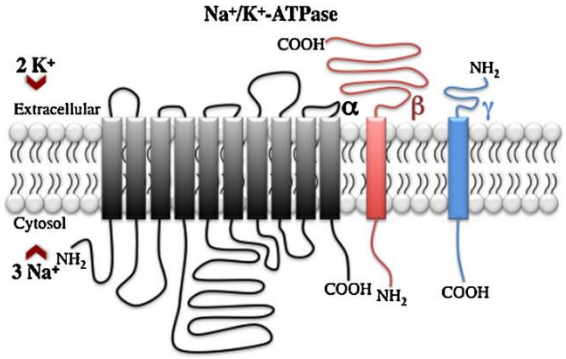

Figure 1.4. The Na,K-ATPase structure (from Doğanli *et al.*, 2013).
The Na,K-ATPase pump consists of a catalytic *α* subunit (grey), an ancillary β subunit (red) and a tissue-specific γ-subunits (FXYD protein, in blu). The *α*-subunit contains 10 transmembrane domains, whereas both the β- and the γ-subunits contain a single transmembrane region.

The α-subunit is the catalytic subunit and in mammals, it occurs in four isoforms (α1, α2, α3 and α4), that are non-uniformly expressed in a tissue- and development-dependent manner (Blanco, 2005). The α1 isoform, for instance, is the major isoform in the kidney and many other tissues, while the α2 isoform is the predominant in skeletal muscle. All the α1, α2 and α3 subunits are present in the adult brain: while the α1 isoform is equally distributed in both neurons and glial, α3 is neuron-specific. In the murine brain, the α2 Na,K-ATPase is primarily expressed in neurons during embryonic development and at time of birth and almost exclusively in astrocytes and some limited neuronal populations in the adult brain (Moseley *et al.*, 2003; Fink *et al.*, 1996). The α4 is testis specific and seems to be involved in the sperm motility (McDermott *et al.*, 2012).

The diverse cell-specific distributions of the α-subunits suggest distinct cellular functions in the cells in which they are expressed.

Studies in cell expression systems have shown that the α2 and α3 isoforms have a lower Na^+ affinity than α1, suggesting that those two isoforms are more suited to regulate large influxes of Na^+.

The colocalization of the α2 Na,K-ATPase with glutamate transporters in astrocyte suggests a functional specific role for this pump in the clearance of released glutamate

from the synaptic cleft during neuronal activity in the adult cortex (Pellerin and Magistretti, 1997; Rose *et al.*, 2009). At the ultrastructural level, α2 Na,K-ATPase appears preferentially localized in astrocytic processes around asymmetrical glutamatergic synaptic junctions and not around GABAergic terminals (Cholet *et al.*, 2002). Rose *et al.* (2009) demonstrated that glutamate transporters and Na,K-ATPase pumps are part of the same macromolecular complexes and operate as a functional unit to regulate glutamatergic neurotransmission.

Pharmacological evidence shows that the α2 and α3 isoforms participate in the clearance of K^+ from the extracellular space during intense neuronal activity (Haglund and Schwartzkroin, 1990; Ransom *et al.*, 2000; D'Ambrosio *et al.*, 2002). However, the relative importance of neuronal α3 and glial α2 Na,K-ATPase pumps in K^+ clearance and maintenance of extracellular K^+ concentration within the physiological range during neuronal activity remains unclear.

In cultured astrocytes, the α2 Na,K-ATPase has been found also localized in microdomains that overlay the endoplasmic reticulum, where it is physically (Lencesova *et al.*, 2004) and functionally (Golovina *et al.*, 2003) coupled to the Na^+/Ca^{2+} exchanger, thereby suggesting an additional functional role in the regulation of intracellular Ca^{2+} concentration, particularly in the endoplasmic reticulum. Indeed, elevated levels of cytoplasmic Ca^{2+} ions as well as in the endoplasmic endoplasmic reticulum were measured in cultured astrocytes from *Atp1a2*$^{-/-}$ knock-out (KO) mice (Golovina *et al.*, 2003).

Impaired clearance of neurotransmitters and enhanced neuronal excitation in the amygdala and piriform cortex were shown in *ATP1A2*$^{-/-}$ KO mice at the embryonic stage (Ikeda *et al.*, 2003). These mice die immediately after birth as a result of sever motor deficits that also abolished respiration. Coimmunoprecipitation studies suggest a specific coupling between the α2 Na,K-ATPase and the neuron-specific K^+,Cl^--cotransporter, which excludes Cl^- ions from the cytosol in respiratory center neurons at birth. These data indicate that α2 isoform plays a key role for maintenance of Cl^- homeostasis in neurons and that this role does not seem to be compensated by α1 and α3 isoforms. Therefore, the lack of α2 in *Atp1a2*$^{-/-}$ KO mice causes elevation of intracellular Cl^- concentration that would switch the GABA response from hyperpolarization to depolarization (Ikeda *et al.*, 2004), leading to the functional impairment of the brainstem respiratory neurons and to the lack of spontaneous respiratory activity.

1.2.2. Functional consequences of FHM mutations

Two different FHM1 mouse models were generated by introducing the human FHM1 R192Q or S218L mutations into the orthologous genes (van den Maagdenberg *et al.*, 2004, 2010) and both KI mice show facilitation of CSD threshold and velocity (Eikermann-Haerter *et al.*, 2009, 2011; van den Maagdenberg *et al.*, 2010).

Analysis of the single channel properties of mutant recombinant human P/Q-type Ca^{2+} channels and of the P/Q-type Ca^{2+} current in different neurons of FHM1 R192Q and S218L KI mice revealed that the mutations produce gain-of-function of P/Q-type Ca^{2+} channels, as a consequence of an increased channel open probability. The enhanced Ca^{2+} influx in a wide range of depolarizations is mainly caused by a shift to lower voltages of the channel activation curve which elicits a Ca^{2+} influx through the mutant channels in response to small depolarizations insufficient to open wild type (WT) channels (van den Maagdenberg *et al.*, 2004; Tottene *et al.*, 2002; Pietrobon and Moskowitz, 2013).

The analysis of cortical synaptic transmission in FHM1 KI mice revealed a very interesting differential effect of FHM1 mutations at excitatory and inhibitory synapses. Indeed, Tottene *et al.* (2009) showed that in the FHM1 R192Q KI mice cerebral cortex the gain-of-function of P/Q-type Ca^{2+} channel enhances excitatory synaptic transmission, as a consequence of increased action potential-evoked glutamate release at pyramidal cell synapses; congruently, short-term synaptic depression during trains of action potentials is enhanced. In striking contrast, inhibitory neurotransmission at FS interneuron synapses was unaltered, despite being initiated by P/Q-type Ca^{2+} channels. In agreement with this, analysis of inhibitory neurotransmission in microcultures of cortical neurons from FHM1 R192Q and S218L KI mice, showed that FHM1 mutation does not affect inhibitory transmission at autapses of cortical mutipolar interneurons (Vecchia *et al.*, 2014, 2015).

The increase in glutamate release may explain the facilitation of experimental CSD in FHM1 KI mice. In fact, induction and propagation of CSD in FHM1 R192Q KI mice can be rescued to WT values when glutamate release at pyramidal cell synapses is brought back to WT values by applying sub-saturating concentration of ω-agatoxin IVA (Tottene *et al.*, 2009), a specific blocker of P/Q-type Ca^{2+} channels, indicating a causative link between enhanced glutamate release and CSD facilitation.

These findings demonstrate that FHM1 mutations may differently affect synaptic transmission and short-term plasticity at different cortical synapses, and, as a consequence, very likely alter the neuronal circuits that coordinate and dynamically adjust the balance between excitation and inhibition during cortical activity (Tottene *et al.*, 2009). Functional alterations in these circuits are expected to lead to abnormal processing of sensory information suggesting that these alterations may render the migraineurs cortex vulnerable to CSD ignition in response to migraine triggers such as intense and repetitive sensory stimulation.

FHM2 mutations cause complete or partial loss-of-function of recombinant Na^+/K^+-ATPases due to loss or reduction of catalytic activity and/or more subtle functional impairments or impairment of plasma membrane delivery (Vecchia and Pietrobon, 2012, and references therein). Recently the KI mouse carrying the W887R ATP1A2 mutation, causing FHM2, was generated (Leo *et al.*, 2011). The homozygous mutants die just after birth because of lack of spontaneous respiratory activity due to

functional impairment of the brainstem respiratory neurons (as shown before for the KO mice in paragraph 1.2.1), while the heterozygous mice are viable, fertile and show no apparent clinical phenotype. The mutant α2 Na,K-ATPase protein was barely detectable in the brain of homozygous mutants and reduced to half in the brain of heterozygous mutants, likely as a consequence of endoplasmic reticulum retention and subsequent proteasomal degradation (Leo *et al.*, 2011). *In vivo* analysis of CSD, induced by focal electrical stimulation of the cortex, revealed a decreased induction threshold and an increased velocity of propagation in the heterozygous FHM2 KI mice.

Conflicting findings were obtained from the analysis of mutant recombinant human $Na_V1.1$ channels expressed in non-neuronal cells, pointing to either gain- or loss-of-function effects of FHM3 mutations (Vecchia and Pietrobon, 2012; Cestéle *et al.*, 2013). Although FHM3 mouse models are not available, it was reported that FHM3 in two unrelated families cosegregates with a new eye phenotype of elicited repetitive daily blindness. This new eye phenotype has clinical features similar to those of experimental CSD in the retina (Vahedi *et al.*, 2009), suggesting that also FHM3 mutations may facilitate CSD, by occasionally alteration of neuronal brain excitability.

1.3. Cortex and its organization

The cerebral cortex, the gray matter overlying each brain hemisphere, constitutes nearly 80% of the human brain and is characterized by a double organization defined by layer and columns. The most typical form of neocortex contains six layers, numbered from the outer surface (*pia mater*) of the cortex to the inner white matter (Kandel, 2000; Markram *et al.*, 2004); this laminar organization can be different at functionally different cortices.

Layer 1 (L1, molecular layer) is the most superficial layer, located right beneath the pia mater. It is characterized by relatives few cell bodies and is mainly occupied by the dendrites of the cells located deeper in the cortex and of the axons that travel through or form connections in this layer.

Layer 2 (L2, external granule cells layer) is characterized mainly by small spherical cells called granule cells and in mouse cortex is fused with the layer 3 (L3, external pyramidal layer) which contains a variety of cell types, many of which are pyramidally shaped; the neurons located deeper in layer 3 are typically larger than those located more superficially.

Layer 4 (L4, internal granule cell layer), like layer 2, is populated primarily by granule cells (also named spiny stellate cells as they are star-shaped and with spiny dendrites), which are the principal recipient layer for thalamocortical inputs. The thalamocortical inputs are in turn transmitted from granule cells to layers 2, 3, 5 and 6 (de Kock *et al.*, 2007).

Layer 5 (L5, internal pyramidal layer) contains mainly pyramidally shaped cells typically larger than those in layer 3; layer 5 has been subdivided into a cell-sparse

layer 5A, containing mostly medium-sized pyramidal cells, and a cell-dense layer 5B containing pyramidal neurons of variable size. Layer 5 pyramidal neurons project their axons to subcortical regions and constitute the principal cortical output to excite other cortical areas. Recent evidences indicate that, besides L4, also L5/6 neurons receive thalamocortical inputs (Constantinople and Bruno, 2013).
Layer 6 (L6, polymorphic or multiform layer) is a fairly heterogeneous layer of neurons. It blends into the white matter that forms the deep limit of the cortex and carries axons to and from the cortex. Together with the layer 5, they project back to the thalamus regulating thalamocortical interactions (de Kock *et al.*, 2007).

Neurons in the neocortex are also distributed in functional, vertically oriented columns that traverse the layers. A cortical column is a recurring module of signal processing that would fit within a cylinder of 0.3 - 0.5 mm in diameter. Neurons within a particular column tend to have very similar response properties, presumably because they form a local processing network. The modular concept presumes that the neuronal network in a cortical column performs basic signal transformations, which are then integrated with the activity in other networks and more extended brain areas (Lübke and Feldmeyer, 2007). In particular, in the rodent somatosensory cortex, which processes the information from mouse vibrissae, each functional columns is defined by discrete and well-defined structure in layer 4 known as 'barrel'. These layer 4 barrels are somatotopically arranged in an almost identical fashion to the layout of the whiskers in the snout (Petersen, 2007), and the barrels can be easily visualized in both living and stained brain slices (Petersen and Sakmann, 2000).

The thickness of the cortex does not vary substantially in different species; it is always around 2 to 4 mm thick. The surface area, however, is dramatically larger in higher primates, particularly in the human brain. Thus, the number of neurons, and therefore the number of columns, in the cerebral cortex is one of the crucial determinants of the cortex capacity for information processing (Amaral, 2000).

1.3.1. Cellular populations in the cortex

The neocortical tissue is composed of neuronal and glial cells. Neurons in the cortex can be divided in two principal groups: projection neurons and local interneurons.

Projection neurons have pyramidally shaped cell bodies and constitute the biggest population within the cortex; they are located mainly in layers 3, 5 and 6 and use the excitatory amino acid glutamate as their primary neurotransmitter.

Interneurons, which represent 20-25% of the neurons in the neocortex, use the inhibitory neurotransmitter γ-amino-butyric acid (GABA) (Beaulieu 1993; Fishell and Rudy, 2011) and are located in all layers, where they do not generally create long range projections with their axon.

Several types of GABAergic interneurons have been distinguished based on their morphological diversity, in particular their axonal arborization and, as a consequence, their postsynaptic targets. In fact, different types of inhibitory interneurons inhibit distinct compartments of principal neurons (Rudy *et al.*, 2011). The basket cells have axons that terminate on somatic and perisomatic compartment; the 'chandelier' cells selectively inhibit the axon initial segment; Martinotti cells target distal apical dendrites of pyramidal cells.

Interneurons can also be subdivided in three non-overlapping populations based on the expression of the Ca^{2+}-binding protein parvalbumin (PV), the neuropeptide somatostatin (SOM) and the ionotropic serotonin receptor 5HT3a (5HT3aR) (Isaacson and Scanziani, 2011; Fishell and Rudy, 2011; Rudy *et al.*, 2011). Each population is heterogeneous in terms of morphology and firing properties of the interneurons composing it and likely have different functions in the cortical circuit (Rudy *et al.*, 2011). The PV-expressing group constitutes the largest population of interneurons in the neocortex and includes basket cells and chandelier cells; the large majority of PV interneurons shows FS non-adapting firing. The SOM-expressing group includes the Martinotti cells and a set of neurons that specifically target layer IV. The 5HT3aR-expressing group is heterogeneous and remains to be fully characterized; it includes all of the neurons that express the neuropeptide VIP as well as an equally numerous subgroup of neurons that do not express VIP, and includes neurogliaform cells. (Rudy *et al.*, 2011). A large fraction of Martinotti cells and a fraction of 5HT3aR-expressing interneurons show various types of regular or irregular adapting firing.

The neocortex also has a population of excitatory interneurons, located primarily in L4. These cells have a stellate plexus of dendrites, use the amino acid glutamate as a transmitter and form synapses with neurons near the cell body. These excitatory interneurons are the primary recipients of sensory information received in the neocortex from the thalamus (Amaral, 2000).

Strikingly, in contrast to the large amount of information that exists on the cellular properties of the various types of cortical inhibitory neurons, knowledge of the specific role that each of them plays in orchestrating cortical activity is limited (Isaacson and Scanziani, 2011).

Astrocytes belong to the glia cell class that represents the most abundant cells in the brain. Astrocytes are in strict contact with a high number of neurons, blood vessels and other astrocytes. Astrocytes are also coupled by gap-junctions and form the so-called 'astrocytic syncytium' (Giaume and McCarthy, 1996). A single astrocyte can contact tens of thousands of synapses (Halassa *et al.*, 2007); each astrocyte covers a specific territory with minimal overlapping with the processes of neighboring astrocytes (Halassa *et al.* 2007). Fraction of this territory can be controlled by specialized astrocytes microdomains that include lamellipodia and filopodia that allow highly dynamic interactions with the surrounding synapses and the end-feet of the

glial-vascular interface, from which signals can propagate to the next end-feet without diffusing to the rest of the cell (Perea *et al.*, 2014).

Astrocytes are known to play important roles in the homeostasis of the extracellular environment, regulating the local concentrations of ions and neurotransmitters (K^+ and glutamate clearance; see below) and thus providing the adequate conditions for the appropriate function of neurons and synapses.

Studies of mice that express enhanced green fluorescent protein (EGFP) under the control of the glial fibrillary acid protein (GFAP) promoter have confirmed that the astrocytic cell population is heterogeneous. Expression of GFAP is a prototypical marker for immunohistochemical identification of astrocytes. About half the cells are rich in GFAP and show the typical properties of protoplasmic astrocytes: an irregular cell body with branched processes, low input resistance, a very negative membrane potential, voltage- and time-independent K^+ currents, prominent glutamate uptake and extensive dye coupling, which is indicative of gap-junctional coupling. By contrast, there is also a large population of fluorescent cells that is characterized by low GFAP expression, larger input resistance, lower electronegative membrane potential, voltage-dependent K^+ and Na^+ currents, AMPARs and low glutamate uptake; this population is not coupled through gap junctions (Volterra and Meldolesi, 2005).

1.3.2. Astrocyte-neuron communication

Accumulating evidence obtained by many different groups has demonstrated the existence of a dynamic reciprocal communication between astrocytes and neurons. The term 'tripartite synapse' (Araque *et al.*, 1999) is based on the ability of astrocytes to receive signals from neurons and actively respond to neuronal and synaptic activity with cytosolic Ca^{2+} elevations evoked by neurotransmitters. In turn, this Ca^{2+} elevations stimulate the release of different neuroactive substances, called gliotransmitters, such as glutamate, D-serine, ATP, adenosine, GABA, tumor necrosis factor alpha (TNFα), prostaglandins, atrial natriuretic peptide (ANP), brain-derived neurotrophic factor (BDNF), etc., that can modulate neuronal activity and synaptic physiology (Fig. 1.5; Perea *et al.*, 2009, 2014 and references therein). In addition to modulation of synaptic function, gliotransmitters released from astrocytes play important roles in brain microcirculation (Zonta *et al.*, 2003).

The astrocyte Ca^{2+} elevations are mainly the result of the mobilization of Ca^{2+} stored in the endoplasmic reticulum. The synaptic control of the astrocyte Ca^{2+} signal is based on the fact that astrocytes express a wide variety of functional neurotransmitters receptors, many of which are metabotropic receptors. Astrocyte Ca^{2+} elevations can also occur spontaneously as intrinsic oscillations in the absence of neuronal activity.

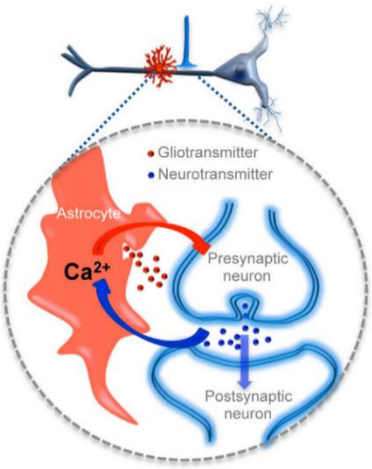

Figure 1.5. Structural and functional relationships of neurons and astrocytes and tripartite synapses (adapted from Navarrete and Araque, 2014).
Scheme of one axon establishing a synapse on an apical dendrite of a prototypical pyramidal neuron and an astrocyte located close to it (in red). The large dashed circle illustrate an enlarged schematic view of the tripartite synapse, where the pre- and postsynaptic neuronal elements (in blue) are surrounded by astrocytic processes (in red). Astrocytes respond with Ca^{2+} elevations to neurotransmitters (blue dots) released during synaptic activity and, in turn, control neuronal excitability and synaptic transmission through the Ca^{2+}-dependent release of gliotransmitters (red dots).

The molecular mechanisms responsible for the release of gliotransmitters are still under debate. Compelling evidence indicate that gliotransmitters release is based on Ca^{2+}- and SNARE protein-dependent mechanisms through vesicle and lysosome exocytosis (Perea and Araque, 2010; Araque *et al.*, 2014). Several Ca^{2+}-independent mechanisms for the release of gliotransmitters have also been proposed, including reversal of glutamate uptake, through connexin hemichannels, pannexin hemichannels, cysteine–glutamate exchanger, pore-forming P2X7 receptors and volume-regulated anion channels (Perea and Araque, 2010). It is noteworthy that all these mechanisms are not mutually exclusive and they might coexist.

1.3.2.1. Astrocytic glutamate uptake

Glutamate is the major excitatory neurotransmitter in the mammalian CNS. However, glutamate is also a potent neurotoxin and glutamate excitotoxicity has been implicated in the pathogenesis of stroke, amyotrophic lateral sclerosis, epilepsy and other neurological diseases. Thus, rapid removal of glutamate from the extracellular space is required for the survival and normal function of neurons.

Glutamate transporters are expressed by many cell types in the CNS, including astrocytes, neurons, oligodendrocytes, microglia and endothelia. Of these, uptake by astrocytes is quantitatively the most important for maintaining normal extracellular glutamate concentrations (Anderson and Swanson, 2000; Tzingounis and Wadiche, 2007). Moreover, by reducing glutamate spillover, glial glutamate uptake may help to isolate synapses, preserving the signal specificity thought to be required for efficient information processing (Danbolt, 2001; Tzingounis and Wadiche, 2007).
Glutamate uptake by astrocytes is mediated by Na^+-independent and Na^+-dependent systems. The Na^+-independent glutamate uptake systems are typically mediated by chloride-dependent glutamate/cystine antiporters, classified as X_c^--type transporters, and represents only a small proportion of total astrocyte glutamate uptake under

normal conditions. The predominant astrocytic glutamate uptake mechanism in the central nervous system is represented by Na^+-dependent systems, through glutamate transporters, that have high affinity for glutamate (Anderson and Swanson, 2000).
Astrocytic glutamate transporters surround the synaptic cleft achieving glutamate uptake against its concentration gradient using electrochemical gradient of Na^+, by coupling transport of three Na^+ and one K^+ down their respective concentration gradients, with inward movement of glutamate and likely one H^+ (Fig. 1.6; Anderson and Swanson, 2000). Because of this coupling, glutamate uptake results in a significant increase in the Na^+ concentration within the fine astrocytic processes.

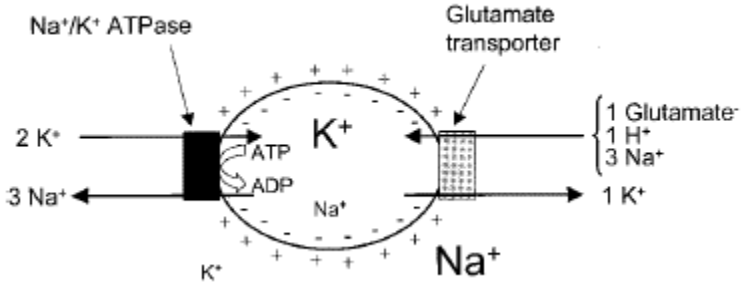

Figure 1.6. Schematic representation of glutamate uptake (Anderson and Swanson, 2000).
The cell membrane potential contributes to the uptake driving force because there is a net inward movement of positive charge with each glutamate transported.

Among the five subtypes that have been identified so far, both glutamate-aspartate transporter (GLAST or EAAT1) and glutamate transporter 1 (GLT1 or EAAT2) are expressed by glial cells (Tzingounis and Wadiche, 2007). Conversely, EAAT3, EAAT4 and EAAT5 are primarily located in neurons.

It is reported that glial transporter expression and glutamate uptake capacity changes during development. In hippocampal astrocytes, the glutamate clearance is slower in juvenile than in adult rats (Diamond, 2005) and it is even slower in neonatal hippocampus (Bergles and Jahr, 1997). Biochemical studies indicate that the transporters expression increases during development (Furuta *et al.*, 1997; Thomas *et al.*, 2011), hence speeding the clearance of synaptically released glutamate and likely restricting the spatial extent of postsynaptic receptor activation. The concentration profile of synaptically released glutamate is also influenced by the geometry of the neuropil (Syková and Nicholson, 2008); narrow, tortuous extracellular spaces prevent transmitter diffusion and slow dilution, thus enhancing postsynaptic receptor activation within and around the synaptic cleft. Ultrastructural and diffusion studies indicate that the extracellular volume fraction decreases by more than one-half between the first postnatal week and adulthood (Sykova and Nicholson, 2008), likely slowing dilution of synaptically released glutamate. Thus, clearance of glutamate released from hippocampus neonatal synapses is mediated primarily by diffusion, whereas clearance in the juvenile depends more on glial uptake. The relative activation of synaptic and extrasynaptic NMDA receptors remains stable over this period,

suggesting that developmental increases in transporter expression compensate for structural changes that slow transmitter dilution (Thomas *et al.*, 2011).

GLT1 and GLAST are heterogeneously expresses during development and in different brain areas. Several line of evidence indicate that in the cortex and hyppocampus, GLT-1 dominates functional uptake in the mature astrocytes while GLAST plays a more prominent role in immature astrocytes (Furuta *et al.*, 1997; Armbruster *et al.*, 2014; Danbolt, 2001). By quantitative immunoblotting it was shown that the number of GLT1 is about four times that of GLAST in the stratum radiatum of mature rat hippocampus (Lehre and Danbolt, 1998). GLAST is the primary glutamate transporter in the Bergmann glial cells of the mature cerebellum and fibrous astrocytes of the ventral white matter tracts of the spinal cord (Furuta *et al.*, 1997).

The glutamate transporters are differentially distributed also at the cellular level; immunoreactivity studies in mice hippocampus indicated that GLT-1 did not entirely cover astrocyte somata and exhibited clusters at processes and at end-feet on blood vessels (Benediktsson *et al.*, 2012; Schreiner *et al.*, 2014); conversely, GLAST immunoreactivity indicated no preferential localization to a specific cellular compartment (Schreiner *et al.*, 2014).

It also reported that the rate of glutamate transport is highly temperature dependent (Q_{10} ~ 3) (Wadiche and Kavanaugh, 1998). Indeed, at physiological temperatures, hippocampal glial transporters are capable of clearing glutamate released evoked by high frequency extracellular stimulation very efficiently; on the contrary, at room temperature, transporters appear overwhelmed during long high frequency stimulation (Diamond and Jahr, 2000). Therefore, temperature effects on glutamate transport may influence the extent to which glutamate can diffuse to neighbouring synapses.

1.3.2.2. Astrocytic potassium uptake

As a consequence of the low baseline concentration of extracellular K^+ and to the limited volume of extracellular space, even modest efflux of K^+ from neurons can elicit considerable changes in the extracellular concentration. These changes can influence a wide variety of neuronal processes, including the maintenance of the resting membrane potential, activation and inactivation of voltage-gated ion channels, the efficacy of synaptic transmission and electrogenic transport of neurotransmitters. One of the most important functions of astrocytes is the clearance of K^+ from the extracellular space, using two systems: net K^+ uptake and a spatial buffer mechanism (Kofuji and Newman, 2004).

Net K^+ uptake can occur by an active process, by the action of Na^+, K^+-ATPase or Na^+-K^+-Cl^- cotransporters. The Na^+ pump plays a principal role in K^+ regulation. The Na^+-K^+-Cl^- transporters are integral membrane proteins that transport Na^+, K^+ and Cl^- ions into cells, often with a stoichiometry of $1Na^+$:$1K^+$:$2Cl^-$.

According to the spatial buffer mechanism, K^+ ions are passively redistributed along the glial syncytium by transferring K^+ from sites of elevated concentration to those with lower concentration. This mechanism depends critically on a high K^+ permeability of the astrocyte cell membrane as well as on the presence of gap junctions between astrocytes: the glial cells express inwardly rectifying K^+ (Kir) channels, with high open probability at the normal resting membrane potential, and form a syncytium in which K^+ currents can traverse relatively long distances. Given this high resting conductance for potassium ions (K^+), the astroglial membrane potential is close to the Nernst equilibrium for K^+ ions and are highly sensitive to changes in the extracellular K^+ levels associated with neuronal activity.

An important biophysical property of Kir channels is that their slope conductance increases with elevations in extracellular K^+ concentration by a square root relation. This unique property of Kir channels allows K^+ conductance increases in glial cells, and therefore, enhanced K^+ clearance rates, when extracellular K^+ concentration is raised. The Kir channels have been recently cloned and over 20 genes are currently known to encode various Kir channel subunits. Kir channels consist of two transmembrane domains bridged by a re-entry loop (P-loop), with intracellular amino and carboxyl termini. The Kir-channel subunits are usually categorized into seven major subfamilies (Kir1 to Kir7) that are diversely regulated by intracellular and extracellular factors. Within the seven described Kir family, the Kir4.1 subtype is almost exclusively expressed by glia in the central nervous system and it is regulated by intracellular ATP (Kofuji and Newman, 2004). Although glia may express additional types of K^+ channels, such as Ca^{2+}- and voltage-dependent K^+ channels, these other channel types are largely inactive at the hyperpolarized glial resting membrane potential. Astrocytes may also express two-pore domain K^+ channels (TASK and TREK), whose contribution to extracellular K^+ concentration regulation remains to be determined (Kofuji and Newman, 2004).

1.3.2.3. Synaptically-activated transporter-mediated current and K^+ current evoked in astrocytes by extracellular stimulation

The extracellular stimulation evokes in astrocytes in acute slices a current characterized by different components (Bergles and Jahr, 1997).

The first short-lived inward current, which is inhibited by application of specific glutamate transporter inhibitor, is the synaptically-activated transporter-mediated current, STC, reflecting glutamate transporter activity. Indeed, glutamate uptake by high affinity transporters is electrogenic, a consequence of the translocation of net positive charge during each transport cycle (see paragraph 1.3.2.1). The STC time course appears to be shaped by the dynamics of glutamate clearance: the STC is slowed by transporter antagonists, which slow glutamate clearance by decreasing uptake capacity (Bergles and Jahr, 1997; Diamond and Jahr, 2000). The STC decay time

course provides a relative measure of the glutamate clearance, whereas the amplitude of the STC reflects the amount of glutamate released at the synapses by extracellular stimulation (Diamond and Jahr, 2000; Diamond, 2005). Indeed, changing stimulus strength causes proportional changes in STC amplitude, with no effects on the STC time course (Diamond and Jahr, 2000).

This transient initial current is followed by a sustained inward current described in the literature as being an inward Ba^+-sensitive K^+ current mainly through Kir channels (Bergles and Jahr, 1997), that decays much more slowly than the STC current (Meeks and Mennerick, 2007; Bernardinelli and Chatton, 2008). This synaptically-activated Ba^+-sensitive K^+ current is a measure of the synaptically-induced increase in extracellular K^+ concentration produced by neuronal K^+ efflux, mostly through voltage gated K^+ channels during the action potential and through the NMDA receptor (Dallérac at al., 2013; Poolos *et al.*, 1987; Shih *et al.*, 2013), and of the accompanying change in driving force on Kir channels of astrocytes, that behave as K^+ electrodes.

A recent study in hippocampus identified, in the astrocytic response evoked by the stimulation, a current partially mediated by GABA transporters (GAT) and Kir4.1-independent K^+ channels (Sibille *et al.*, 2014). Long-lasting GAT currents evoked synaptically have been identified in astrocytes from other brain regions such as the neocortex (Kinney and Spain, 2002), and display slow rise and decay kinetics, in contrast to glutamate transporter-mediate currents.

The different kinetics of fast glutamate transporter-mediated current and slow K^+ and GAT-mediated currents in astrocytes probably reflect differences in extracellular concentrations of glutamate, K^+ and GABA over time, due to distinct release and clearance properties. Indeed, glutamate is mostly released by presynaptic elements at confined synaptic active zones and the close vicinity of glutamate release sites and clustered astroglial glutamate transporters (Melone *et al.* 2009) probably enables efficient fast glutamate clearance. In contrast, the distal location of astroglial GATs to GABAergic synapses (Minelli *et al.* 1996) may underlie the slow kinetics of the synaptically evoked GAT currents. Finally, despite abundant expression of Kir4.1 channels preferentially located on astrocytic processes enwrapping synapses (Higashi *et al.* 2001), the slow astroglial K^+ clearance may originate from uniform extracellular K^+ bulk rises, due to pre- and postsynaptic release of K^+ (Poolos *et al.* 1987; Shih *et al.*, 2013) over large zones, which may be slowly redistributed though gap junction-mediated networks (Pannasch *et al.* 2011).

1.3.3. Excitation/inhibition balance in the cortex

Synaptic excitation and inhibition are inseparable events in the cortex (Isaacson and Scanziani, 2011). The interactions between GABAergic interneurons and glutamatergic principal cells are reciprocal: interneurons inhibit principal cells and are excited by them. In fact, the connectivity between these two neuronal classes is quite

high: individual interneurons can inhibit more than 50% of principal cells located within about 100 μm and receive excitatory input from a large fraction of them (Kapfer *et al.*, 2007; Fino *et al.*, 2013). Thus, not only GABAergic interneurons are excited in proportion to the level of local network activity, but also they directly influence it through their inhibitory feedback. This simple connectivity pattern is ubiquitous in cortex and forms the basis for so-called feedback or recurrent inhibition.

Of course, not all cortical excitation received by inhibitory interneurons is locally generated. Cortical cells receive excitatory inputs via long-range axons originating from subcortical nuclei, as well as from other cortical regions and different cortical layers. These excitatory afferent inputs diverge onto both principal cells and interneurons, generating feedforward inhibitory circuits. Interestingly, the same afferent fibers make stronger excitatory connections onto interneurons than they do on principal cells, thereby ensuring that even minimal levels of afferent input generate inhibition in cortical circuits (Gabernet *et al.*, 2005).

In addition to principal cells, GABAergic interneurons also make inhibitory contacts onto each other and the connectivity between interneurons is highly reciprocal. This mutual connectivity between interneurons is also able to shape spatial and temporal features of cortical inhibition (Isaacson and Scanziani, 2011).

Because of this massive interconnection, excitation and inhibition increase and decrease together during physiological cortical activity and alterations of this relationship shift cortical activity to hyperexcitable (epileptiform) or silent (comatose) state. Thus, excitation-inhibition balance each other and this balance is important for proper cortical functions. However, despite the overall proportionality of excitation and inhibition, their exact ratio is not constant. For example, stimulus intensity or shape can affect the excitation-inhibition balance and excitation-inhibition balance can change over a short timescale as a result of adaptation, depending on stimulation history and rate (Isaacson and Scanziani 2011).

How excitation-inhibition balance is established during development is largely unknown. Consistent with the central importance of excitation-inhibition balance, a variety of neurological and psychiatric disorders are currently viewed as pathologies of brain excitability and are thought to involve or even be caused by disruption of this delicate equilibrium. Among these pathologies are migraine, mental retardation, Rett syndrome, fragile X syndrome, autism spectrum disorders and epilepsy. A growing number of mutations in genes coding for proteins involved in neurotransmission (such as Ca^{2+} channels, proton pumps, synaptic vesicle components, pre- and post-synaptic constituents) have been found in familiar cases of these pathologies (Poduri and Lowenstein, 2011; Rajakulendran *et al.*, 2010; Vecchia and Pietrobon, 2012).

1.4. Cortical network electrical activity

Cortical neurons receive the great majority of their synaptic inputs from neurons within the local network (more or less 1 mm distant) (Binzegger *et al.*, 2004). As a consequence of this dense and local connectivity, the cerebral cortex exhibits spontaneous, persistent high synchronous activity in the absence of any external stimulation, such as during natural sleep or anesthesia (Steriade *et al.*, 2001; Petersen *et al.*, 2003; Buzsaki, 2010; Poulet and Petersen, 2008). This ongoing activity is revealed by the rhythmic and synchronous oscillation of the membrane potential of populations of neurons and can be measured by electroencephalography (EEG) or extracellular (or intracellular) recordings *in vivo*.

The spatial and temporal patterns of spontaneous activity in the cortex differ markedly across the various physiological conditions; EEG records, as time dependent signals, are decomposed into five main frequency bands, ranging from low frequency delta (< 4 Hz) and theta (4-8 Hz) waves, commonly found during slow-wave sleep, through alpha (8-12 Hz) and beta (13-30 Hz) waves, associated with an awake and alert brain, to gamma waves (30-100 Hz), associated with intense multimodal information processing.

1.4.1. Slow oscillations and their neuronal counterparts, up- and down-states

In the cortex, the most well studied pattern of recurrent network activity is that of the 'slow' (<1 Hz) oscillation, characterized by slow large amplitude membrane potential fluctuations that occur synchronously in nearby neurons (Steriade *et al.*, 2001; Petersen *et al.*, 2003; Poulet and Petersen, 2008). This fluctuations consist in rhythmic cycles of sustained depolarization (of 15-25 mV), called up-states, that can be subthreshold or can generate action potentials, followed by the cessation of firing and the rescue of the membrane resting potential, called down-states (Steriade *et al.*, 1993; Haider *et al.*, 2006; Petersen *et al.*, 2003; Sanchez-Vives and McCormick, 2000).

Several lines of evidence confirm that both excitatory and inhibitory neurons fire during up-states. Indeed, the up-states are generated by large synchronous bursts of spontaneous excitatory and inhibitory postsynaptic currents, which arise from correlated activity of a large population of presynaptic connected neurons generated through recurrent synaptic network activity within cortical circuitry (Petersen *et al.*, 2003; Shu *et al.*, 2003; Sanchez-Vives and McCormick, 2000; Haider *et al.*, 2006; Wilson, 2008; Okun and Lampl, 2008). This reflects the architecture of local cortical circuits, in which pyramidal cells are connected to other pyramidal cells and to inhibitory interneurons, in such a way that maintain a dynamic balance between excitation and inhibition during up-states (see paragraph 1.3.3). Long-range

connections play a key role in the communication, propagation and synchronization of this locally generated activity (Haider and McCormick, 2009 and references therein). While the recurrent excitation of cortical pyramidal cells during the up-states appears to originate from other pyramidal neurons, the source of the robust inhibitory potentials is less known. Fast-spiking GABAergic interneurons are one likely input, since these are highly active (Steriade *et al.*, 2001; Haider *et al.*, 2006; Fanselow and Connors, 2010; Tahvildari *et al.*, 2012). The importance of fast GABAergic inhibition in controlling persistent activity is supported by the fact that blocking $GABA_A$ receptors transforms up-states into epileptiform bursts (Sanchez-Vives and McCormick, 2000; Shu *et al.*, 2003).

The slow oscillations are thought to be essential for memory formation and consolidation (Chauvette *et al.*, 2012). Growing evidence supports the view that the transition of memories from a labile, hippocampal-dependent state to a stable or consolidated, hippocampal-independent state depends on activity-driven plasticity processes that take place during sleep (Hoffman *et al.*, 2007; Mölle and Born, 2011).

1.4.2. Initiation, propagation and termination of up-states

Spontaneous slow oscillations are disrupted by disconnection of intracortical pathway while survive thalamic lesions and transection of the corpus callosum (Steriade *et al.*, 1993). Moreover, spontaneous up-states similar, although at a lower frequency, to the ones observed *in vivo*, have also been reported *in vitro* in brain slices of many cortical regions (Sanchez Vives and McCormick, 2000), maintained in a solution with divalent ions concentrations similar to those found in natural cerebrospinal fluid (Cossart *et al.*, 2003; Sanchez-Vives and McCormick, 2000; Shu *et al.*, 2003). These findings indicate that the up-state activity originates intrinsically within the cortex (Steriade *et al.*, 1993; Sanchez-Vives and McCormick 2000), via recurrent excitatory and inhibitory intracortical interactions, and then transmitted to other brain areas.

Recent evidences suggests that the full expression of the slow oscillation requires the balanced interaction of both neocortex and thalamus (Crunelli and Hughes, 2010; Crunelli *et al.*, 2015; David *et al.*, 2013; Lemieux *et al.*, 2014). Nevertheless, the extent of the thalamic contribution to network activity is still a matter of discussion. As neocortical neurons, almost all thalamic neurons exhibit the slow oscillation with their up- and down- states occurring quasi-synchronously, both locally and with cortical neurons. In thalamocortical slices from adult mice, the cutting of the connections between thalamus and cortex reduced the frequency of up-states (Rigas and Castro-Alamancos, 2007). Similarly, recordings from anesthetized and behaving cats indicate that full or partial cortical deafferentation that removes thalamic inputs to the neocortex dramatically reduced the expression of slow oscillations in affected cortical areas (Lemieux *et al.*, 2014).

The mechanisms underlying generation and maintenance of spontaneous up-states activity within the cortex are still under debate: three hypotheses on the origin of the up-states in local networks have been proposed (Chauvette *et al.*, 2010; Timofeev and Chauvette, 2011 and references therein).

The first one is the 'spontaneous release hypothesis'; according to this hypothesis, spontaneous transmitters release in large neuronal populations, occurring during a down state, occasionally depolarizes some cells to the firing threshold, thus initiating an active state in the network (Timofeev *et al.*, 2000; Bazhenov *et al.*, 2002). Therefore, activity may start in any neuron, although cells receiving largest excitatory convergence will have higher probability of being activated before the others in the network.

According to the second proposed mechanism, the transition from silence to activity is mediated by intrinsic firing of layer 5 pyramidal neurons, which are depolarized and generate some spikes between the active states, when other cortical neurons are silent (Sanchez-Vives and McCormick, 2000). This so called 'layer 5 neuron hypothesis' predicts that activity always originates in these neurons and then it propagates to other cortical layers.

The third hypothesis attributes transitions from silent to active states to the selective synchronization of spatially structured neuronal ensembles involving a small number of cells (Cossart *et al.*, 2003). The 'selective synchronization' hypothesis predicts that even during the silent states, some neurons of the network still generate irregular spontaneous firing.

Recent findings suggest that spontaneous recurrent cortical activity depends also on the coordination between the activity of electrically excitable cells and the neuromodulation by inexcitable glial cells (Poskanzer and Yuste, 2011; Fellin *et al.*, 2009). Indeed, the stimulation of a single astrocyte *in vitro* can activate the astrocytic network and double the number of up-states, whereas inhibition of astrocytic activity, with a Ca^{2+} chelator, blocks half of the up-states (Poskanzer and Yuste, 2011). Moreover, *in vivo* recordings in combination with astrocyte-specific molecular genetics showed that the inhibition of gliotransmission affects cortical slow oscillations, reducing up-states duration (Fellin *et al.*, 2009).

Recent studies provide insights on the contribution of specific cortical layers to the initiation and propagation of spontaneous recurrent cortical activity.

Extracellular multiple-unit recordings in ferret cortical slices revealed that the slow oscillation seems to be initiated in layer 5, as an excitatory interaction between pyramidal neurons, and propagates through the neocortex (Sanchez-Vives and McCormick, 2000).

More recently, multisite field potential recordings, extracellular multiunit and intracellular recordings from closely located neurons *in vivo* in the cat neocortex revealed that the active states could start at any depth, but activation of large pyramidal cells from deep layers was more likely to occur first (Chauvette *et al.*, 2010). This is

probably due to the large excitatory convergence on the layer 5 cells; indeed, given their broad projection, there might be a higher probability for spontaneous synaptic inputs summation in these cells than in neurons in other layers, leading to firing and activation of the network.

Using a combination of intracellular recordings and of fast optical imaging with voltage-sensitive dyes in thalamocortical-connected slices of rat barrel cortex, it was shown that a single thalamic input typically triggers an up-state that initiates within a column following a preferential L4 → L2/3 → L5 sequence, and then propagates via layer 2/3 and layer 5 to neighboring columns. However, layer 5, but not layer 2/3, is crucial for the spread of excitation both within a column and across columns. Indeed, layer 5 can sustain and propagate activity to neighboring columns in the absence of layer 2/3. Conversely, layer 2/3 cannot sustain activity in the absence of the underlying layer 5, and often fails to propagate activity to neighboring columns. Thus, layer 5 amplifies activity in local layer 2/3 networks and distributes it over many columns within the primary sensory cortex (Wester and Contreras, 2012).

A further confirmation of the specific role of layer 5 neurons in sustaining and propagating up-states comes from a recent *in vivo* study using optogenetic activation of infragranular or supragranular neurons. Optogenetic activation of a subset of pyramidal neurons located in layer 5 generated network activity that resembled spontaneous up-states, whereas photoinhibition of these same neurons substantially attenuated ongoing up-states. In contrast, light activation and inhibition of layer 2/3 cells modestly affects spontaneous slow activity (Beltramo *et al.*, 2013). The differential role of layer 5 and layer 2/3 neurons in slow oscillation may be linked to the better ability of layer 5 excitatory neurons to propagate depolarization within and across cortical layers.

The mechanisms underlying the termination of up-states are also unclear. Phase transitions from up-state to down-state can be triggered by the build-up of activity-dependent K^+ conductances (Sanchez-Vives and McCormick, 2000; Shu *et al.*, 2003; Sanchez-Vives *et al.*, 2010). Other activity-dependent mechanisms such as synaptic depression may also participate in the termination of the up-states (Mann *et al.*, 2009; Parga and Abbott, 2007). $GABA_B$ receptors appear to selectively contribute to the termination of up-states in layer 2/3 pyramidal neurons in rat entorhinal cortex slices, because $GABA_B$ antagonists drastically prolong the up-state duration and impair the ability of layer 1 stimulation to terminate up-states (Mann *et al.*, 2009).

2. AIM OF WORK (I)

Missense mutations in the gene encoding the pore forming subunit of P/Q-type Ca^{2+} channel are associated with familial hemiplegic migraine type 1 (FHM1), a rare form of autosomal dominant subtype of migraine with aura (Pietrobon and Moskowitz, 2013). KI mice carrying the R192Q mutation show gain of function of P/Q-type Ca^{2+} channels that determines an increased influx of Ca^{2+} in neurons, including pyramidal cells, and an increased probability of glutamate release (Pietrobon, 2010; Tottene *et al.*, 2009). It was recently found in our laboratory that the frequency of the up-state activity recorded in acute cortical slices, resembling spontaneous slow oscillations *in vivo*, is increased in FHM1 KI mice (Fabbro, Sessolo, Vecchia, Conti and Pietrobon, manuscript in preparation).

To further investigate the role of P/Q-type Ca^{2+} channels in the spontaneous recurrent cortical activity underlying the up-states, I studied the effect of blocking the P/Q-type Ca^{2+} channels on up-state activity recorded in acute slices of mouse somatosensory cortex.

Given that at many cortical synapses P/Q- and N-type Ca^{2+} channels cooperate in controlling synaptic transmission, I also investigated the effect of blocking N-type Ca^{2+} channels on up-state activity.

3. RESULTS (I)

In this study, spontaneous recurrent cortical activity was studied using patch clamp techniques in somatosensory cortex brain slices of WT mice from postnatal day 16 to 19 (P16-19), at room temperature. To increase membrane excitability and facilitate the occurrence of spontaneous activity, I routinely recorded from slices maintained in an extracellular solution (see details in Materials and Methods, paragraph 8.4.4.1), with higher K^+ concentration and lower Ca^{2+} and Mg^{2+} concentrations. The spontaneous recurrent activity in current clamp mode was recorded in layer 2/3 pyramidal neurons at the resting potential without injecting current. The spontaneous activity is characterized by rhythmic cycles of depolarization, called up-states, on which action potentials (APs) can be generated, and repolarisation at the resting potential, called down-states, in which there is the cessation of firing, as shown form the representative trace recorded from a layer 2/3 pyramidal cell in current clamp (Fig. 3.1).

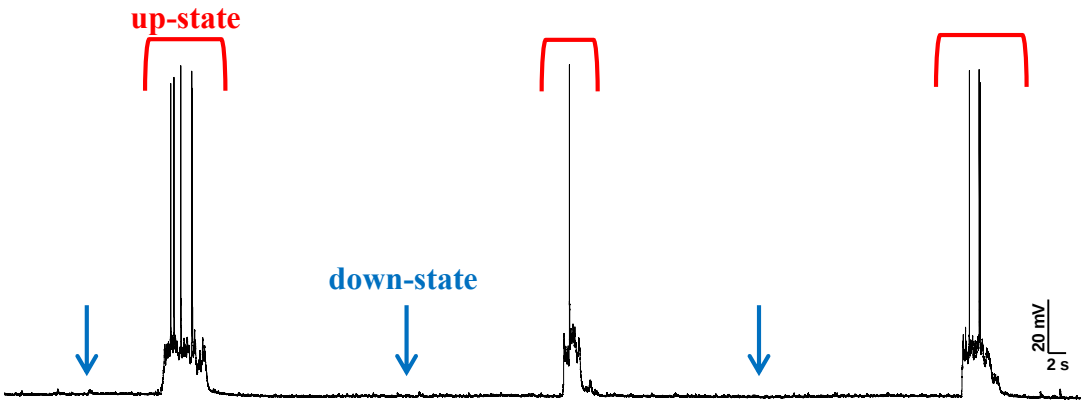

Figure 3.1 Representative current clamp trace from a layer 2-3 pyramidal cell showing up- and down-states spontaneous activity.
The AP firing is only localized during the depolarization of the membrane potential. In the recording trace, blue arrows point examples of down-states while up-states are indicated in red.

The up-states can be characterized in terms of duration, amplitude and frequency of occurrence. The up-states duration was measured from their onset to their returning to the resting potential; the amplitude was estimated as the difference between the potential preceding the event and the mean value of the depolarization; the frequency was expressed as the number of up-states occurring per minute.
The mean frequency of the up-states in my experimental conditions was 1.6 ± 0.1 up-states/minute (n=24 slices). Given the low frequency of neuronal spontaneous oscillations, to obtain an accurate evaluation of this activity, it was necessary to monitor the activity for long periods of time (twenty to thirty minutes). From the same

set of experiments, I derived also the mean duration, that was 5.3 ± 0.3 seconds (n=24 slices), and the mean amplitude, 16.7 ± 0.7 mV (n=24 slices).

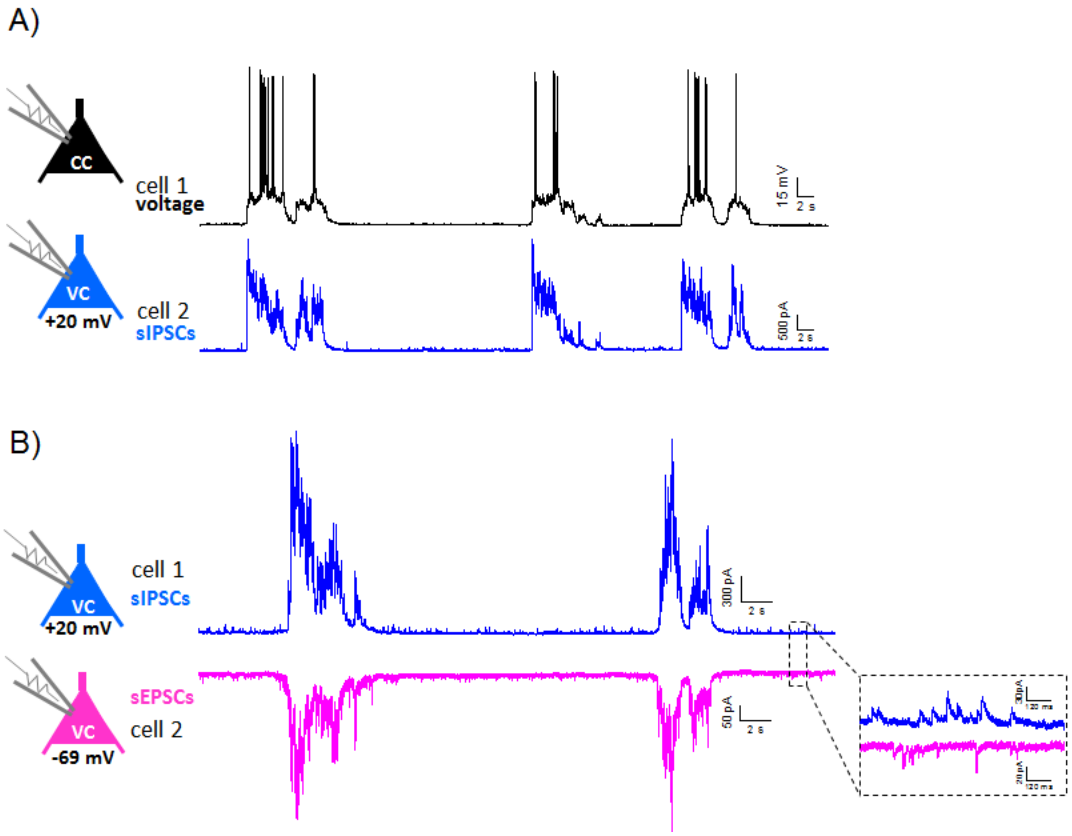

Figure 3.2. Synchronous barrages of sEPSCs and sIPSCs drive the up-states.
A) Double patch-clamp recording, from layer 2/3 of somatosensory cortex in acute slice, in current clamp in one cell and in voltage clamp at the reversal potential for EPSCs (+20 mV) to record sIPSCs in the other.
B) Double voltage clamp recording, from layer 2/3 of somatosensory cortex in acute slice, of sIPSCs (at the reversal potential of the EPSCs, +20 mV) in one cell and of sEPSCs (at the reversal potential of the IPSCs, -69 mV) in the other. In the inset, representative expanded traces of uncorrelated activity composed by low amplitude random inputs.
CC: current clamp recording of spontaneous recurrent cortical activity. VC: voltage clamp recording of sPSCs.

As shown in Fig. 3.2 by the dual patch clamp recordings from two nearby layer 2/3 pyramidal neurons, the up-states are generated by large synchronous barrages of excitatory and inhibitory postsynaptic currents (sEPSCs and sIPSCs), which arise from correlated activity of a large population of presynaptic connected neurons due to spontaneous recurrent network activity (Petersen *et al.*, 2003; Okun and Lampl, 2008). The sEPSCs reflect all the excitatory synaptic inputs from excitatory neurons that make synapses onto the recorded pyramidal cells and are active during spontaneous cortical activity. On the other hand, the sIPSCs are due to the activity of the interneurons synaptically connected to the recorded pyramidal cells. To isolate the

excitatory and inhibitory inputs onto the recorded pyramidal cells, I recorded the sEPSCs at the reversal potential for the inhibitory inputs (-69 mV) and the sIPSCs at the reversal potential of the excitatory inputs (+20 mV), with a cesium containing intracellular solution. The large bursts of sIPSCs, in blue, occur synchronously with large bursts of sEPCSs, in magenta. Besides being synchronous, the large bursts of sEPSCs and sIPSCs have amplitudes that are linearly correlated indicating that the larger the excitatory drive in the local circuit the larger the inhibitory one.

As shown in Fig. 3.3, up-state activity was rapidly and completely abolished by application of saturating concentration of D-AP5 (50 μM), an NMDA glutamate receptor antagonist (n=9 slices). Similarly, the up-state activity disappeared after the application of NBQX (50 μM), an AMPA glutamate receptor inhibitor (n=5 slices, data not shown).

The spontaneous recurrent cortical activity was also completely abolished by application of cadmium (Cd^{2+}, 200 μM), that blocks all the voltage-gated Ca^{2+} channels and hence synaptic transmission (n=4; Fig. 3.4).

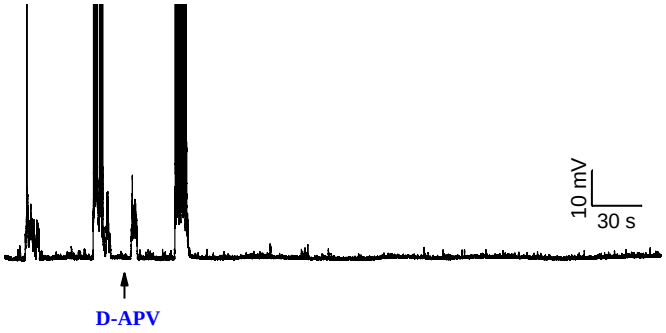

Figure 3.3. Effect of NMDA receptors inhibition on spontaneous recurrent cortical activity.
Current clamp recording of up-state activity from a layer 2/3 pyramidal cell in somatosensory cortex slice, before and after application of D-AP5 (50 μM), a NMDA receptors inhibitor. The arrow indicates the beginning of the inhibitor application during the recording.

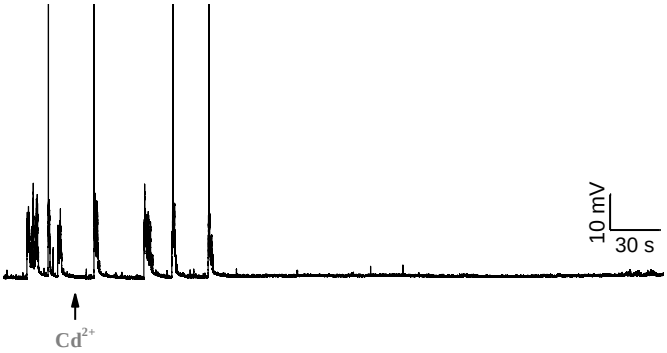

Figure 3.4. Effect of Cd^{2+} application on spontaneous recurrent cortical activity.
Current clamp recording of spontaneous recurrent cortical activity from a layer 2/3 pyramidal cell in somatosensory cortex brain slice, before and after application of Cd^{2+} (200 μM). The arrow indicates the beginning of inhibitor application.

These results show that spontaneous cortical up-states depend on synaptic transmission and in particular on the excitation provided by both, NMDA and AMPA

receptors, without which they do not occur (in agreement with previous data; McCormick *et al.*, 2003; Seamans *et al.*, 2003; Favero and Castro-Alamancos, 2013).

FHM1 KI mice, carrying the R192Q mutation, show a gain-of-function of the channels that determines an increased influx of Ca^{2+} in neurons, including pyramidal cells, and an increased probability of glutamate release at cortical pyramidal cells synapses. Recent findings in our laboratory (Fabbro, Sessolo, Vecchia and Pietrobon, manuscript in preparation) show that the up-states frequency is larger in KI than WT mice, as shown in the Fig. 3.5, suggesting that the gain-of-function of P/Q-type Ca^{2+} channels facilitates the mechanisms of up-states generation and/or decreases the refractory period after an up-state. To further investigate the role of P/Q-type Ca^{2+} channels in the generation of up-states (and in general in the recurrent network activity underlying the up-states), I studied the effect of inhibition of P/Q-type Ca^{2+} channels on the up-state activity in WT mice.

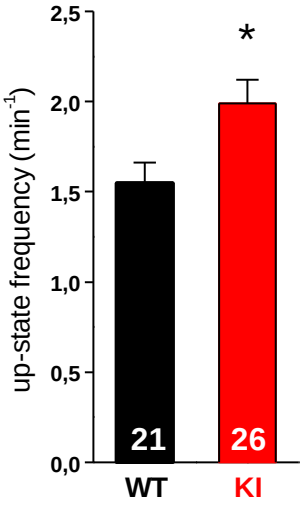

Figure 3.5. Histograms of up-states frequency in WT and KI mice.
Up-states frequency was measured from current clamp recordings in somatosensory brain slice obtained from P16-18 old WT (in black) and age-matched R192Q KI mice (in red). The frequency is expressed as number of events per minute of recording. * = $p < 0.05$.

I performed patch clamp recordings to compare in the same experiment the up-states activity in control condition and after application of saturating concentrations of a specific P/Q-type Ca^{2+} channels blocker, ω-agatoxin IVA (400 nM, ω-AgaIVA).
Given the increased frequency of up-states in FHM1 KI mice, with a gain-of-function mutation in P/Q type Ca^{2+} channels, one would expect that the block of these channels would result in a reduced frequency of the up-states in WT mice. Surprisingly, instead, the block of P/Q-type Ca^{2+} channels transformed the up-states into events resembling interictal epileptiform discharges (Fig. 3.6A). These events have the same frequency of the up-states but are characterized by a larger depolarization amplitude (57 ± 1 mV versus 19 ± 2 mV, n=6 slices) and shorter duration (0.36 ± 0.03 seconds versus 5.4 ± 0.2 seconds, n=6 slices) than the up-states (Fig. 3.6B).

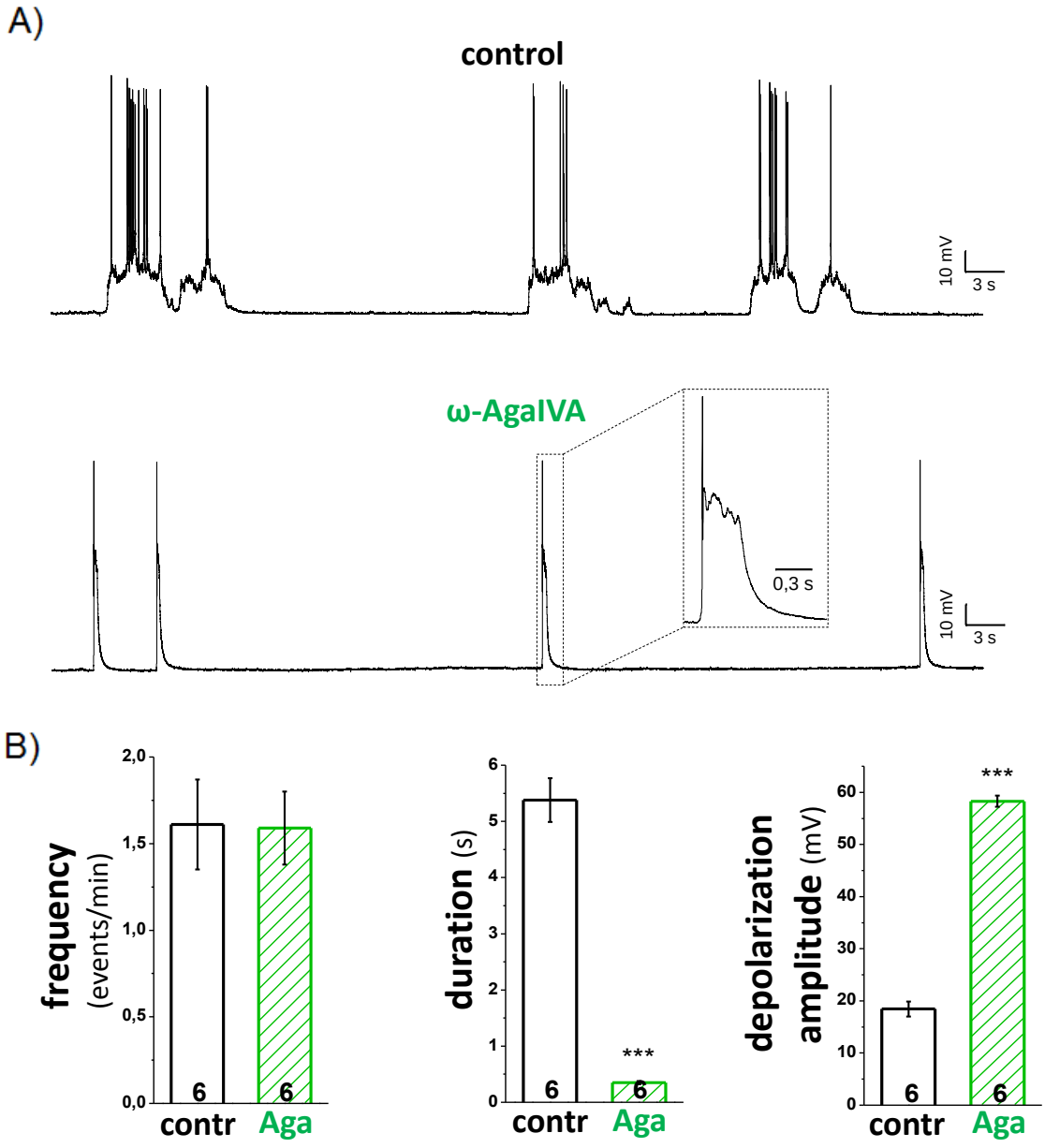

Figure 3.6. The spontaneous recurrent cortical activity is transformed in simil-interictal epileptiform activity by the block of P/Q type Ca^{2+} channels.

A) Current clamp recording of spontaneous cortical activity from a layer 2/3 pyramidal cell of somatosensory cortex in acute slice obtained from P16 old WT mice, in control condition (upper trace) and after 10 minutes of ω-AgaIVA (400 nM) application (bottom trace).

Inset: magnification of a representative simil-interictal epileptiform event.

B) The histograms report the mean value for frequency, duration and depolarization amplitude of the up-states in control condition (contr) and of the simil-interictal epileptiform events after 10 minutes of ω-AgaIVA (Aga, 400 nM) application, measured in current clamp recordings of spontaneous recurrent cortical activity from layer 2/3 pyramidal cells of somatosensory cortex in acute slice obtained from P16-19 old WT mice (n=6 slices). *** = $p < 0.001$.

The mean frequency measured in a larger sample, including also voltage clamp recordings, provides a similar results: 1.4 ± 0.1 min^{-1} in control versus 1.3 ± 0.2, min^{-1} in ω-AgaIVA, n=23 slices.

To explain the transformation of up-states into simil-interictal epileptiform events by ω-AgaIVA, I hypothesized that the block of P/Q-type Ca^{2+} channels produces a stronger reduction of the inhibitory compared to excitatory synaptic transmission during the network activity underlying the up-states, resulting in a shift of the excitation-inhibition balance during the spontaneous activity towards excitation. To test this hypothesis, the total sEPSCS and sIPSCs were measured in voltage clamp in layer 2/3 pyramidal cells during the spontaneous network activity before and after the application of ω-AgaIVA (Fig. 3.7).

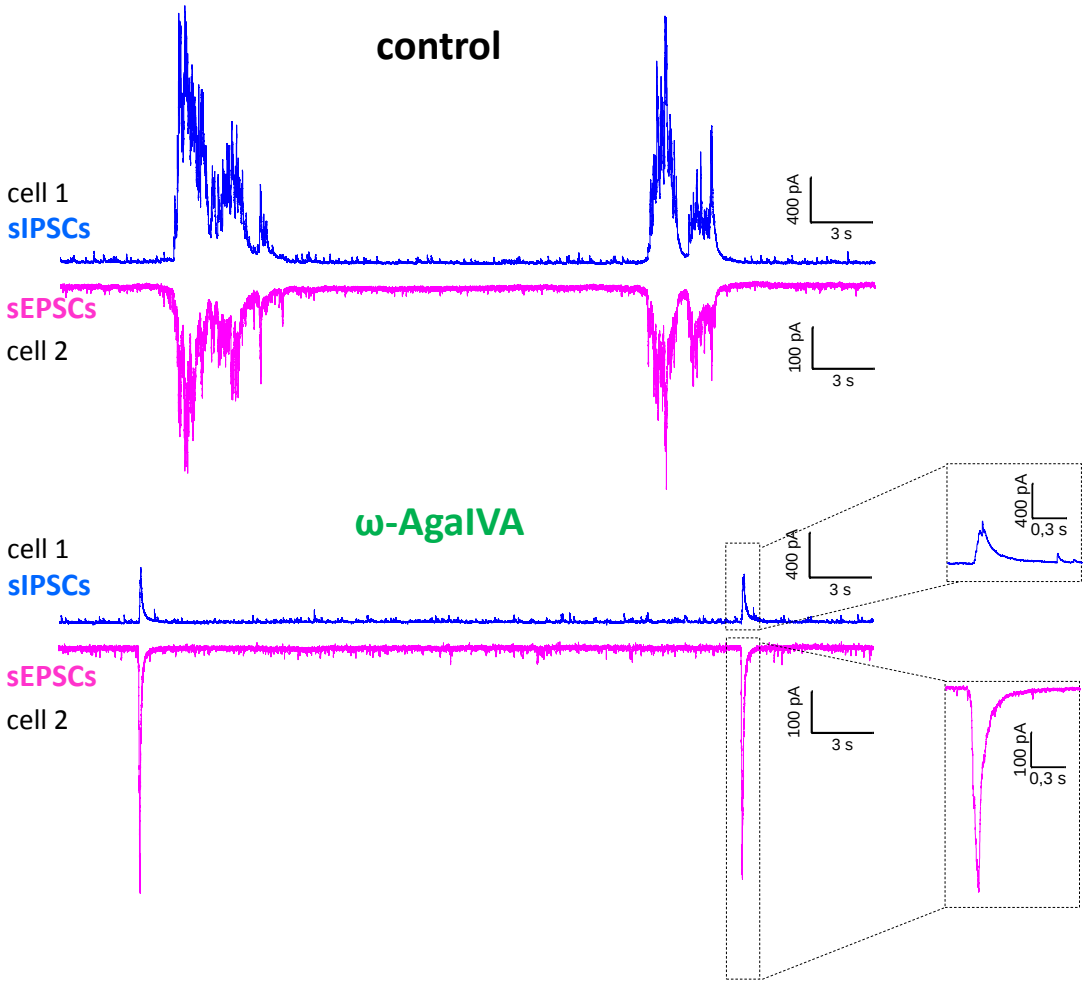

Figure 3.7. Representative recordings in voltage clamp of sEPSCs and sIPSCs from layer 2/3 pyramidal cells of WT mice in control condition and after the block of P/Q-type Ca^{2+} channels. Double voltage clamp recordings of sIPSCs in cell 1 (at the reversal potential of EPSCs, +20 mV) and sEPSCs in cell 2 (recorded at the reversal potential of IPSCs, -69 mV) in control condition (upper traces) and after 10 minutes of ω-AgaIVA (400 nM) application (botton traces).

To quantify the effect of the P/Q-type Ca^{2+} channels block, I measured the mean excitatory and inhibitory synaptic conductance (G_e and G_i) of the sEPSCs and sIPSCs bursts that generate the up-states in control and the simil-interictal epileptiform events in the presence of ω-AgaIVA, in pyramidal cells. To derive mean G_e and G_i, I obtained

the mean excitatory and inhibitory currents by integrating the sEPSCs and sIPSCs bursts to measure the synaptic charge of each burst, which was then divided by the burst duration; the mean synaptic currents were then divided by the driving force (assuming a linear relationship between current and voltage).
The block of P/Q-type Ca^{2+} channels reduced both G_e and G_i, but the reduction of G_i (71 ± 3%) was much larger than that of G_e (13 ± 8%). As a direct consequence, the G_e/G_i ratio increased from 0.2 ± 0.0 in the control condition to 0.6 ± 0.1 in ω-AgaIVA, becoming in ω-AgaIVA 3.3 ± 0.3 times larger than in control (Fig. 3.8).
This results confirm the initial hypothesis that the simil-intericat epileptiform activity produced by the block of P/Q type Ca^{2+} channels is generated through an imbalance of the excitation-inhibition equilibrium towards excitation, due to a bigger reduction of inhibitory than of excitatory synaptic transmission.

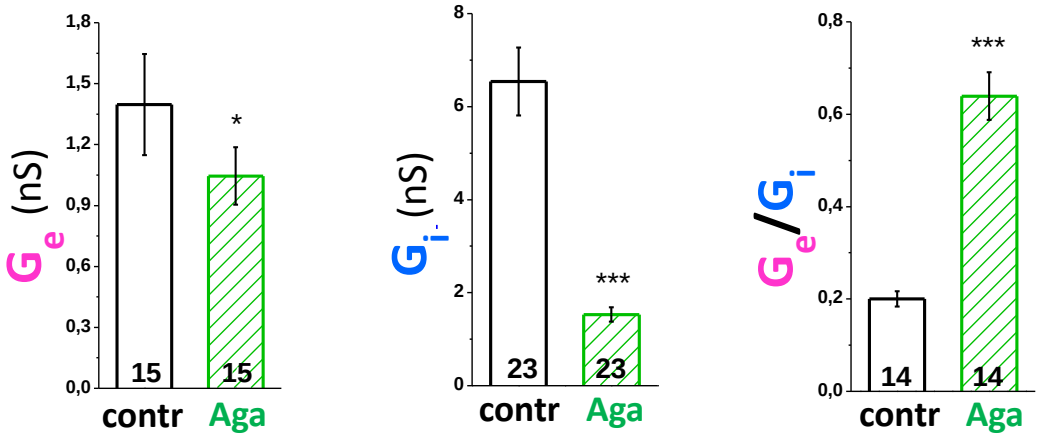

Figure 3.8. The block of P/Q-type Ca^{2+} channels shifts the excitation-inhibition balance in favor of excitation.
The histograms report the mean excitatory and inhibitory synaptic conductances (G_e and G_i) and their ratio before (contr) and after (Aga) the block of P/Q-type Ca^{2+} channels by ω-AgaIVA (400 nM) application. The mean G_e and G_i in individual pyramidal cells were derived, as described in the text, from the mean synaptic currents obtained by integrating the sEPSCs and sIPSCs bursts recorded at different voltages. * = $p < 0.05$; *** = $p < 0.001$.

The relative small reduction of G_e after the block of P/Q-type Ca^{2+} channels was surprising, given that cortical excitatory synaptic transmission at many pyramidal cells synapses depends predominantly on P/Q-type Ca^{2+} channels (Rozov *et al.*, 2001; Ali and Nelson, 2006; Tottene *et al.*, 2009; Sessolo *et al.*, unpublished data).
To better understand this result, I measured G_e and G_i in the initial period of application of the drug, i.e. the period in which the drug has not yet blocked all the channels.
As shown from both, the time course of G_e and the traces in Fig. 3.9, partial block of P/Q-type Ca^{2+} channels strongly reduced G_e of individual sEPSCs bursts. After being reduced to a minimal value, G_e started to increase to reach a value that is only slightly lower than the control. The increase in G_e coincided with the transition from sEPSCs

bursts resembling those underlying the up-states to a different type of network activity, that eventually leads to that underlying the simil-interictal epileptiform events.

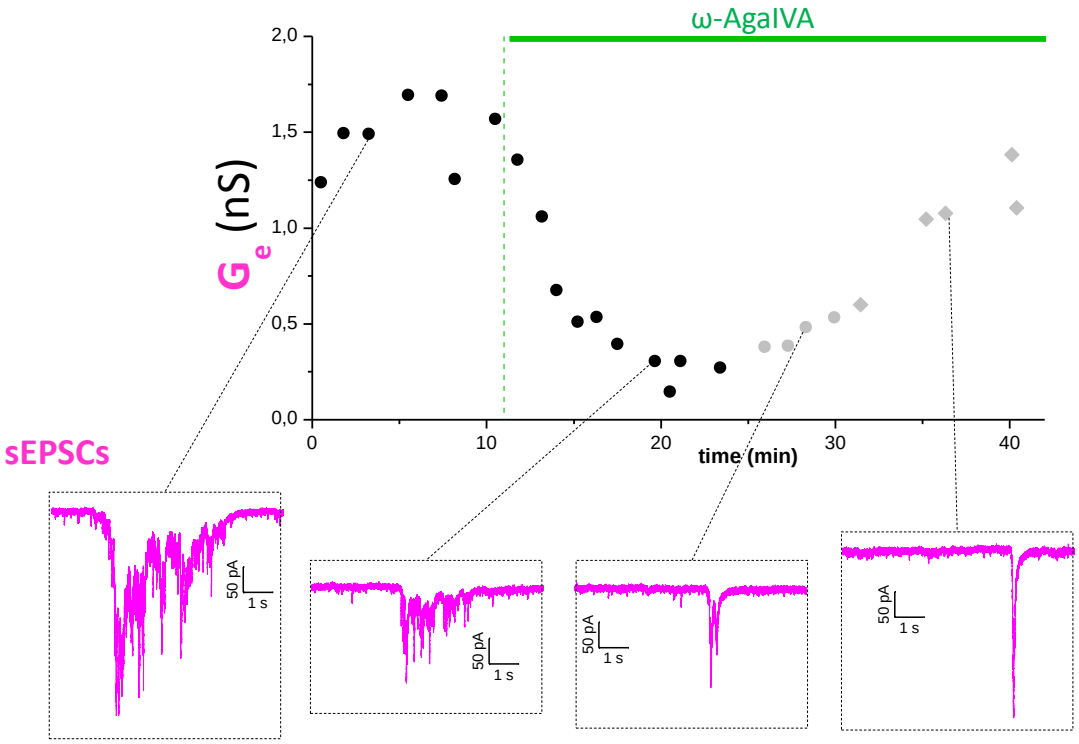

Figure 3.9. Immediately after addition of ω-AgaIVA, G_e of individual sEPSCs bursts was inhibited.

The upper graph shows the time course of changes in G_e of individual sEPSCs bursts after addition of ω-AgaIVA (400 nM), in a representative voltage clamp recording from a layer 2/3 pyramidal cell at -69 mV: the black points represent up-state-generating events; the gray points represent events that eventually result in simil-interictal epileptiform discharges. The bottom traces are representative sEPSCs bursts.

Double voltage-clamp recordings, to record simultaneously the sEPSCs and sIPSCs bursts in two cells, show that the transition from sPSCs bursts to a different type of network activity occurs when G_e/G_i increases above a critical value (Fig. 3.10). During this transition, ω-AgaIVA strongly reduced both G_e and G_i (Fig. 3.10A); after a brief period in which G_e and G_i decreased in parallel and the excitation-inhibition balance remained unaltered, G_i was reduced relatively more than G_e and, as a consequence, the G_e/G_i ratio progressively increases. When this ratio reached a critical value, 2.2 ± 0.1 times larger than the control (n=7 slices), the network activity changed and G_e started to increase reaching a value similar to that in control. At this time, G_e was reduced by 53 ± 6% while G_i was reduced by 74 ± 4% (Fig. 3.10B).

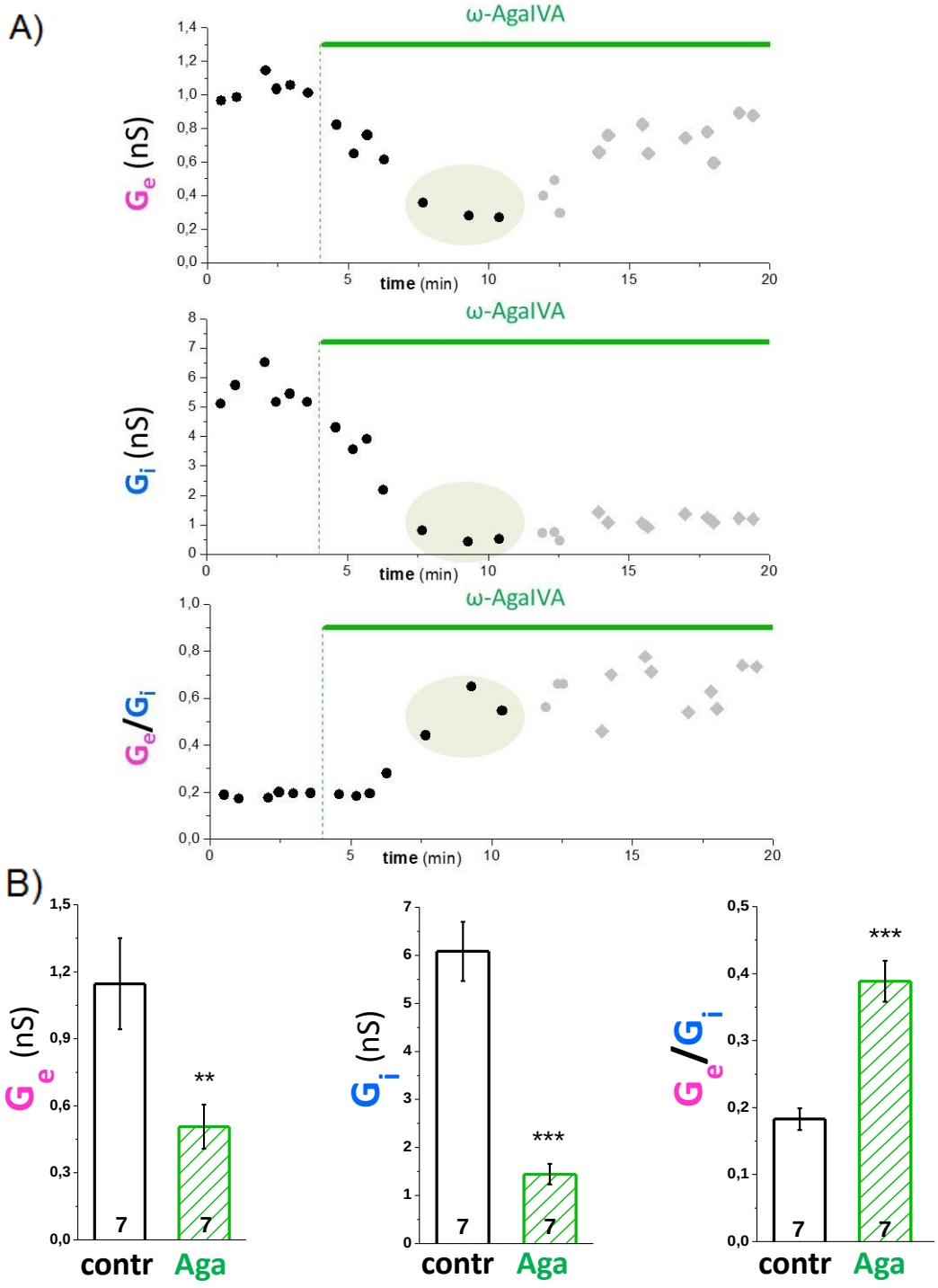

Figure 3.10. After addition of ω-AgaIVA, both G_e and G_i of individual sEPSCs and sIPSCs bursts were inhibited.

A) Time course of G_e, G_i and G_e/G_i obtained in a double voltage clamp recording, measuring the sEPSCs bursts in one cell and the sIPSCs in the other. In black are reported up-state-generating events; the grey points represent events that eventually results in simil-interictal epileptiform discharges.

B) The bar plots report the mean G_e and G_i and their ratio in control (contr) and after application of ω-AgaIVA (Aga, 400 nM) calculated at the time indicated with the green circle in panel A, where inhibition of G_e and G_i is maximal. At this time point, also G_e/G_i was calculated. ** = $p < 0.01$; *** = $p < 0.001$.

A possible interpretation of the fact that, after reaching the maximal inhibition, G_e starts to increase is that as a consequence of the shift of excitation-inhibition balance towards excitation (G_e/G_i 2.2 ± 0.1 times larger than the control), the pyramidal cells increase their firing frequency leading to an increased number of active excitatory synapses during the network activity that compensates for the reduced glutamate release at each synapse. In agreement with this interpretation, preliminary double patch clamp recordings in voltage clamp in one cell and in current clamp in the other, show that at the time of maximal inhibition of G_e and G_i (and increase of G_e/G_i above a critical value, Fig. 3.10), there was an increase in the firing frequency of pyramidal cell during the up-state (and a decrease in the duration of the up-states, preliminary data not shown) (Fig. 3.11).

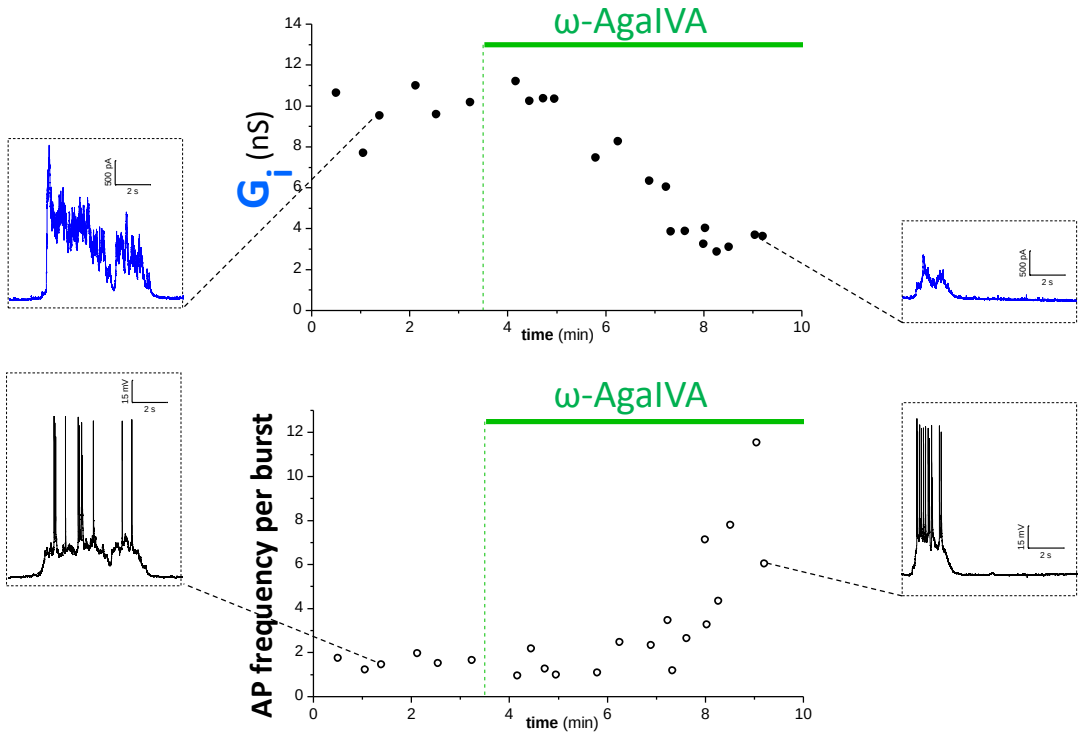

Figure 3.11. The inhibition of G_i leads to increased firing rate of pyramidal cells.
Representative double patch clamp recording, measuring the sIPSCs bursts in voltage clamp in one pyramidal cell and the up-states in current clamp in the other.
On the top: time course of G_i. On the bottom: time course of the AP frequency per burst recorded in current clamp. The AP frequency was measured as the ratio between the number of AP fired during an up-state and the duration of the up-state (Hz).
In both the panels, the insets show representative events.

These data indicate that P/Q-type Ca^{2+} channels have a dominant role in controlling both excitatory and inhibitory synaptic transmission onto pyramidal cells during the spontaneous recurrent network activity that underlies the up-states. However, the block of P/Q-type Ca^{2+} channels reduces recurrent inhibition more than recurrent excitation and shifts the cortical excitation-inhibition balance towards excitation. This

suggests that, in the cerebral cortex, P/Q-type Ca^{2+} channels play a more prominent role in controlling inhibitory compared to excitatory synaptic transmission.

Given that at many cortical synapses, P/Q- and N-type Ca^{2+} channels cooperate in controlling synaptic transmission, I also investigated the role of the N-type Ca^{2+} channels in the spontaneous recurrent network activity.

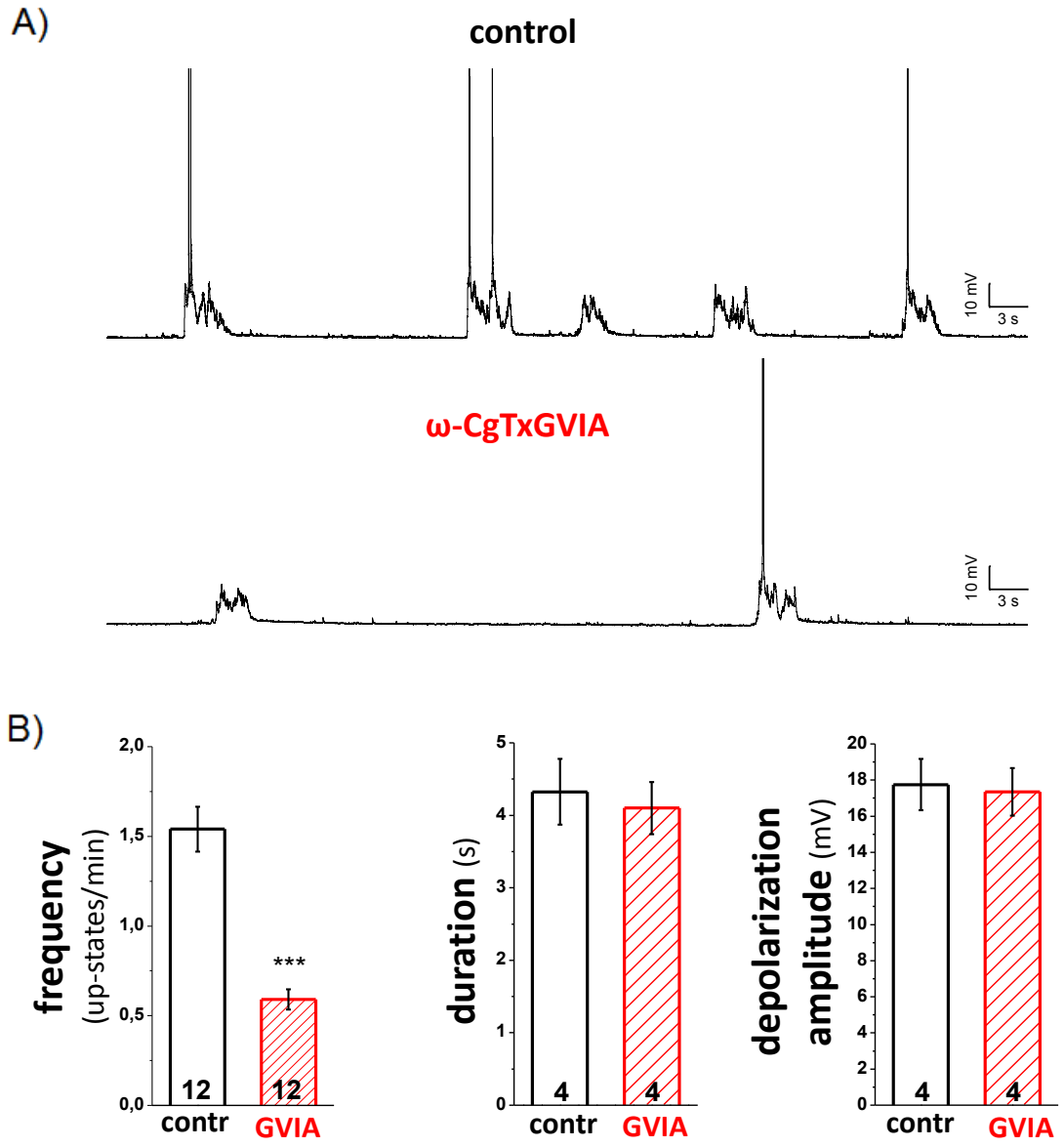

Figure 3.12. Effect of blocking the N-type Ca^{2+} channels on spontaneous recurrent cortical activity.

A) Current clamp recording of spontaneous recurrent cortical activity from a layer 2/3 pyramidal cell of somatosensory cortex in acute slice of WT P18 old mice, in control condition and after 10 minutes of application of ω-CgTxGVIA (1 µM), a specific blocker of N-type Ca^{2+} channels.

B) The histograms report the mean value for frequency, duration and depolarization amplitude of the up-states in control condition and after 10 minutes of ω-CgTxGVIA (1 µM) application, in patch-clamp recordings of spontaneous recurrent cortical activity from layer 2/3 pyramidal cells of somatosensory cortex in acute slice obtained from P16-19 old WT mice. The mean frequency was measured in current clamp and voltage clamp recordings (n=12 slices), while the up-states duration and depolarization amplitude were derived from current clamp recordings (n=4 slices). *** = $p < 0.001$.

I first performed current clamp recordings before and after application of ω-conotoxin GVIA (1 µM, ω-CgTxGVIA), a highly specific blocker of N-type Ca^{2+} channel, in order to evaluate the effect of the block of this channel on spontaneous up-states. In contrast with the block of P/Q-type Ca^{2+} channels**,** blocking N-type Ca^{2+} channels significatively reduced the frequency of the up-states by 61 ± 3%, without modifying the duration and the depolarization amplitude (Fig. 3.12): indeed, the duration and amplitude of up-states after ω-CgTxGVIA application were not significantly different from those observed in control conditions. These results suggest that N-type Ca^{2+} channels play a critical role in the control of the frequency of the up-states.

I analyzed the effect of the block of N-type Ca^{2+} channels on the barrages of sEPSCs and sIPSCs, by performing double voltage clamp recordings. The block of N-type Ca^{2+} channels had a relatively small effect on the mean G_e and G_i of the sEPSCs and sIPSCs bursts underlying the up-states. G_i was reduced relatively more than G_e and, as a consequence, G_e/G_i increased by 54 ± 11% (Fig. 3.13), but this increase was not sufficient to transform up-states in simil-interictal eplipetiform events, as happened after the block of P/Q-type Ca^{2+} channels.

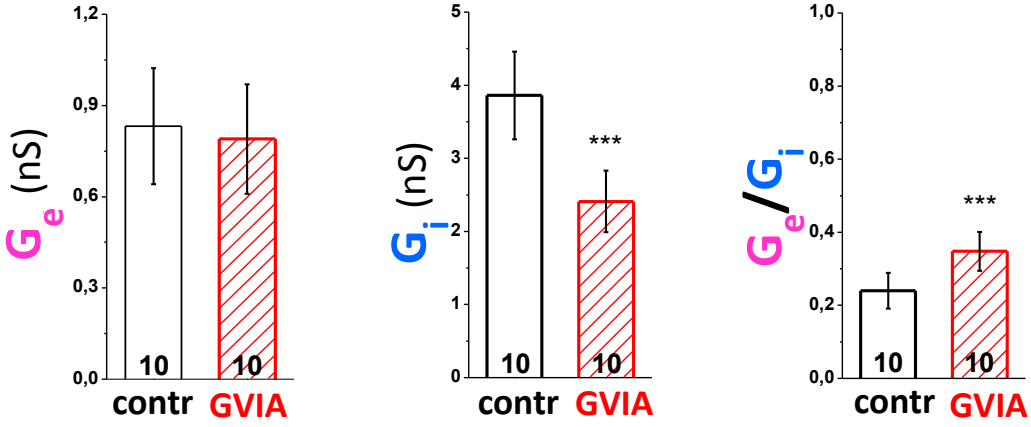

Figure 3.13. After addition of ω-CgTxGVIA, G_i of individual sIPSCs bursts, but not G_e of individual sEPSCs bursts, is inhibited.

The bar plots report the mean G_e and G_i and their ratio before and after 10 minutes of ω-CgTxGVIA (1 µM) application. In ω-CgTxGVIA, G_e is not inhibited while there is a 34 ± 6% inhibition of G_i and G_e/G_i is 1.5 ± 0.1 times larger than in control. *** = $p < 0.001$.

6. Discussion (I)

I investigated the effect of blocking P/Q- and N-type Ca^{2+} channels on the spontaneous up-states, recorded from layer 2/3 pyramidal neurons in acute cortical slices, that resemble slow oscillation *in vivo* (Steriade *et al.*, 1993). To facilitate the occurrence of spontaneous up-states, the slices were maintained in an extracellular solution with ionic composition mimicking that of the brain cerebrospinal fluid, with relatively high K^+ and low Ca^{2+} and Mg^{2+} concentrations (see details in Materials and Methods, paragraph 8.4.4.1; Sanchez-Vives and McCormick, 2000; Rigas and Castros-Alamancos, 2007), and a high perfusion flux was used to maximize slice oxygenation (Hájos *et al.*, 2009). Under these conditions, I was able to record spontaneous up-states occurring at 1.6 ± 0.1 min^{-1}, with a duration of 5.3 ± 0.3 seconds and a depolarization amplitude of 16.7 ± 0.7 mV. The mean frequency of up-states occurrence is lower and the mean duration of the up-states is larger in my recordings than those reported *in vivo* (Steriade *et al.*, 1993; Sanchez-Vives and McCormick, 2000; Fellin *et al.*, 2009). Given the evidence that the thalamus actively contributes to the generation of the slow oscillation (Crunelli and Hughes, 2010; Crunelli *et al.*, 2015; David *et al.*, 2013; Lemieux *et al.*, 2014), the fact that the thalamocortical connections are cut in coronal slices likely contributes to the lower frequency of up-states. In addition, the differences in frequency and duration of the up-states probably in part reflect the fact that my recordings were performed at room temperature, unlike physiological temperature in the studies *in vivo* (Steriade *et al.*, 1993; Sanchez-Vives and McCormick, 2000; Haider *et al.*, 2006; Fellin *et al.*, 2009) and the higher temperature used in some studies *in vitro* (33-36°C; Sanchez-Vives and McCormick, 2000; Shu *et al.*, 2003; Rigas and Castros-Alamancos, 2007; Wester and Contreras, 2012). Indeed, in a recent study on ferret cortical slices, the up-states frequency decreased while the up-states duration increased when the temperature was lowered from a physiological temperature of 36°C to 32°C (Reig *et al.*, 2010).

In agreement with previous studies, I showed that the block of NMDA and AMPA receptors suppresses spontaneous cortical up-states (McCormick *et al.*, 2003; Seamans *et al.*, 2003; Favero and Castro-Alamancos, 2013), indicating that the up-states depend critically on the excitation provided by both NMDA and AMPA receptors. I also showed that Cd^{2+} application, which blocks all the voltage-gated Ca^{2+} channels and hence the synaptic transmission, completely abolishes the up-states. These results are consistent with the evidence that the up-states are driven by large synchronous barrages of sEPSCs and sIPSCs, arising from correlated activity of a large population of presynaptic connected neurons generated through recurrent synaptic network activity within cortical circuitry (Petersen *et al.*, 2003; Shu *et al.*, 2003; Sanchez-Vives and McCormick, 2000; Haider *et al.*, 2006; Wilson, 2008; Okun and Lampl, 2008).

Given that at many cortical synapses neurotransmitter release and synaptic transmission are predominantly mediated by P/Q- and N- type Ca^{2+} channels, the network silencing by Cd^{2+} application points toward a critical role of these two voltage-gated Ca^{2+} channels in the generation and/or expression of spontaneous up-states in slices. Uncovering the role of P/Q-type Ca^{2+} channels is particularly interesting since gain-of-function mutations in the gene encoding the pore forming subunit of P/Q-type Ca^{2+} channel are associated with FHM1, a rare form of autosomal dominant subtype of migraine with aura (Pietrobon and Moskowitz, 2013). KI mice carrying the R192Q mutation show an increased Ca^{2+} influx through P/Q-type Ca^{2+} channels in neurons, including cortical pyramidal cells, and an increased probability of glutamate release at cortical pyramidal cells synapses (Pietrobon, 2010; Tottene e al., 2009). It was recently found in our laboratory that the frequency of the up-states, recorded in acute cortical slices, is increased in FHM1 KI mice (Fabbro, Sessolo, Vecchia and Pietrobon, manuscript in preparation). As up-states are synaptically generated, the increased frequency in FHM1 KI mice is consistent with the hypothesis that the enhanced glutamate release may lead to an increased probability of sEPSCs summation, due to an increase in the frequency of sEPSCs.

By comparing the activity before and after application of ω-agatoxin IVA (a specific pharmacological blockers of P/Q-type Ca^{2+} channel; ω-AgaIVA), I showed that the block of P/Q-type Ca^{2+} channels transforms the up-states into events resembling interictal epileptiform discharges. The evaluation of the mean excitatory and inhibitory synaptic conductances (G_e and G_i) during the control up-states and the simil-interictal epileptiform events in ω-agaIVA, demonstrated that this change in the network activity occurs when G_e/G_i increases above a critical value (3.3 ± 0.3 times larger than in control), as a consequence of a larger reduction of recurrent inhibition than of recurrent excitation, by P/Q-type Ca^{2+} channels blocker (13 ± 8% inhibition of G_e and 71 ± 3% of G_i). Given that cortical excitatory synaptic transmission at many pyramidal cells synapses depends predominantly on P/Q-type Ca^{2+} channels (Pietrobon, 2010; Ali and Nelson, 2006; Tottene *et al.*, 2009; Zaitsev *et al.*, 2007; Rozov *et al.*, 2001), the small reduction of G_e was surprising. However, by evaluating the fraction of inhibition of G_e and G_i in the initial period of application of the blocker, I showed that 1) both G_e and G_i are strongly reduced when only a fraction of P/Q-type Ca^{2+} channels are blocked, but G_i is reduced relatively more than G_e (53 ± 6% and 74 ± 4% maximal inhibition of G_e and G_i respectively); 2) after reaching the maximal inhibition, G_e starts to increase toward a value similar to that in control condition. A possible explanation for this observation comes from preliminary findings of an increased firing rate of pyramidal cells at the time of maximal inhibition of G_e. The increase in pyramidal cell firing frequency might lead to an increased number of active excitatory synapses during the network activity that compensates for the reduced glutamate release at each synapse.

These results indicate that P/Q-type Ca^{2+} channels have a dominant role in controlling both excitatory and inhibitory synaptic transmission onto pyramidal cells during the spontaneous recurrent network activity that underlies the up-states. However, the block of P/Q-type Ca^{2+} channels reduces recurrent inhibition more than recurrent excitation and shifts the cortical excitation-inhibition balance towards excitation. This suggests that, in the cerebral cortex, P/Q-type Ca^{2+} channels play a more prominent role in controlling inhibitory compared to excitatory synaptic transmission. When, as a consequence of the block of P/Q-type Ca^{2+} channels, G_e/G_i increases above a critical value, the spontaneous network activity changes and the up-states are transformed into events resembling simil-interictal epileptiform discharges.

The data are consistent with the hypothesis that impairment of cortical inhibitory synaptic transmission may contribute to the generation of the epileptic phenotype in spontaneous mouse mutants and humans with loss-of-function mutations in P/Q-type Ca^{2+} channel (Pietrobon, 2007, 2010 and references therein). Actually, this is supported by a recent study demonstrating that conditional ablation of P/Q-type Ca^{2+} channels in cortical interneurons results in severe generalized epilepsy, due to impairment of GABA release from fast-spiking interneurons (Rossignol *et al.*, 2013).

Interestingly, blocking N-type Ca^{2+} channels with ω-conotoxin GVIA (ω-CgTxGVIA) has a completely different effect on spontaneous cortical activity. The block of this channel, reduces the frequency of the up-states without changing up-states duration and depolarization amplitude, indicating that N-type Ca^{2+} channels play a critical role in controlling up-states frequency. By measuring G_e and G_i, I found that the excitation-inhibition balance is less affected by block of N-type Ca^{2+} channels than by block of P/Q-type Ca^{2+} channels: after the block of N-type Ca^{2+} channels, G_e/G_i increases (1.5 ± 0.1 times larger in ω-CgTxGVIA than in control) but not sufficiently to transform up-states in simil-interictal eplipetiform events.

These results suggest that the frequency of the up-states seems not to be correlated to the G_e/G_i ratio measured in layer 2/3 pyramidal neurons during the up-states. Indeed, in ω-AgaIVA there is not a change in the frequency of the events, even if the G_e/G_i triplicates, conversely, in ω-CgTxGVIA, the small increase of the ratio is accompanied to a large reduction of the up-states frequency. The data might suggest a different role of N-type Ca^{2+} channels in cortical physiology in layer 2/3 and in the layer where relevant cells for up-states generation are.

5. AIM OF WORK (II)

Familial hemiplegic migraine type 2 (FHM2) is caused by mutations in *ATP1A2*, the gene encoding the α2 subunit of the Na,K-ATPase (De Fusco *et al.*, 2003). In the brain, α2 subunit is expressed primarily in neurons during embryonic development but almost exclusively in astrocytes in the adult (Moseley *et al.*, 2003). The FHM2 mutations cause loss-of-function of recombinant α2 Na,K-ATPase (Bottger *et al.*, 2012). In the brain of heterozygous FHM2 W887R KI mice, the α2 Na,K-ATPase protein is reduced to half while there is almost no expression in the brain of embryonic homozygous FHM2 W887R KI mice. *In vivo* experiments in heterozygous FHM2 KI mice, carrying the human mutation W887R, showed a facilitation of experimental CSD (Leo *et al.*, 2011).

The mechanisms underlying facilitation of experimental CSD in FHM2 KI mice remain unknown. The aim of the project is to investigate these mechanisms in acute brain slices of mouse somatosensory cortex. I first tested whether in an *in vitro* model it was possible to observe the facilitation of experimental CSD observed for heterozygous FHM2 KI mice *in vivo*; to study experimental CSD, I induced CSD by applying pulses of high KCl onto the slices surface (Tottene *et al.*, 2009). After setting the conditions in which facilitation of CSD was observed *in vitro*, I investigated three possible mechanisms that may underlie the facilitation of CSD in FHM2 KI mice:

The specific localization and functional coupling of the α2 Na,K-ATPase to glutamate transporters in astrocyte processes, surrounding cortical glutamatergic synapses (Cholet *et al.*, 2002), suggests that glutamate uptake into astrocytes during cortical activity could be impaired as a consequence of the loss-of-function of α2 Na,K-ATPase. Given that activation of NMDA receptors plays a key role in the positive feedback cycle that ignites CSD (Tottene *et al.*, 2011; Pietrobon and Moskowitz, 2014), an inefficient clearance of glutamate in FHM2 KI mice could be a mechanism underlying CSD facilitation.

To test whether the rate of glutamate clearance by astrocytes is reduced in heterozygous FHM2 KI mice, I measured the synaptically-activated glutamate transporter-mediated current (STC), evoked in cortical astrocytes of layer 1 by extracellular electrical stimulation in the same layer, in acute cortical slices. Either single pulse stimulation or trains of stimuli at high frequencies (50 and 100 Hz) were delivered. I isolated the STC pharmacologically by applying TFB-TBOA, a glutamate transporter antagonist, in order to measure the STC decay time course that provides a relative measure of the rate of glutamate clearance.

Pharmacological evidences indicate that α2 and/or α3 Na,K-ATPase participate in the clearance of K^+ from the extracellular space during intense neuronal activity (D'Ambrosio *et al.*, 2002; Kofuji and Newman, 2004); however, the relative importance of these two pumps remains unclear. If α2 Na,K-ATPase is important in

this clearance, then its loss of function may results into an increase of extracellular K^+ concentration during neuronal activity. Given that most models of CSD include local increase of extracellular K^+ concentration above a critical value as a key event for the initiation of CSD (Pietrobon and Moskowitz, 2014), an inefficient clearance of K^+ might lead to a facilitation of CSD.

In order to investigate if K^+ clearance is reduced, I measured the decay time course of the synaptically-activated K^+ current, through Kir channels, evoked in cortical astrocytes of layer 1 by electrical stimulation.

The tight coupling of α2 Na,K-ATPase with the Na^+/Ca^{2+} exchanger at plasma membrane microdomains that overlie the endoplasmic reticulum, suggests that Ca^{2+} homeostasis could be impaired as a consequence of the loss-of-function of α2 Na,K-ATPase. Indeed, elevated levels of Ca^{2+} ions in the cytoplasm and in the endoplasmic reticulum were measured in cultured astrocytes from *ATP1A2*$^{-/-}$ KO mice (Golovina *et al.*, 2003). An increased release of gliotransmitters, including glutamate, consequent to increased release of Ca^{2+} from intracellular stores in response to synaptic activity could be implicated in CSD facilitation.

I first investigated whether the Ca^{2+} content was increased in the Ca^{2+} stores. I obtained an indirect measure of the amount of Ca^{2+} in the stores, by measuring in cultured cortical astrocytes the Ca^{2+} transients induced by ionomycin in Ca^{2+}-free medium.

I then performed measurements of the threshold for CSD induction and the velocity of CSD propagation in acute cortical slices of FHM2 KI mice, before and after application of cyclopiazonic acid (CPA), a SERCA inhibitor, which depletes the intracellular Ca^{2+} stores preventing most of the release of gliotransmitters.

6. RESULTS (II)

6.1. Does W887R FHM2 mutation facilitate the induction and the propagation of experimental cortical spreading depression (CSD) induced in cortical slices by high KCl pulses?

In an *in vivo* study on heterozygous FHM2 KI mice, it was found that FHM2 W887R mutation facilitates the induction and the propagation of CSD induced by focal electrical stimulation of the cortex (Leo *et al.*, 2011). The authors observed a more than 30% decreased threshold for CSD induction and a nearly 40% increased velocity of CSD propagation (Leo *et al.*, 2011).

I tested whether I could confirm CSD facilitation by the W887R FHM2 mutation in our *in vitro* model of experimental CSD. In this *in vitro* model, brief pulses of high KCl of increasing duration were applied onto layer 2/3 surface of acute brain slices of mouse somatosensory cortex, until a CSD was observed as inferred by the spreading of changes in intrinsic optic signal (IOS) and by the typical depolarization recorded from a pyramidal cell located usually 600 μm apart from the KCl pipette. The duration of the first pulse eliciting a CSD was taken as CSD threshold and the rate of horizontal spread of the change in IOS as CSD velocity (see details in Materials and Methods paragraph 8.5; Tottene *et al.*, 2009).

I first studied experimental CSD in somatosensory cortex slices obtained from young mice, at the age of postnatal days (P) 16-18, at room temperature, i.e. the same experimental conditions that were previously used in our laboratory for the study of CSD in a mouse model of FHM1 (Tottene *et al.*, 2009). Under these conditions, in contrast with what was obtained in FHM1 KI mice and what was seen in the *in vivo* study in FHM2 KI mice, I found that CSD threshold and velocity are similar in WT and FHM2 KI mice (Fig. 6.1).

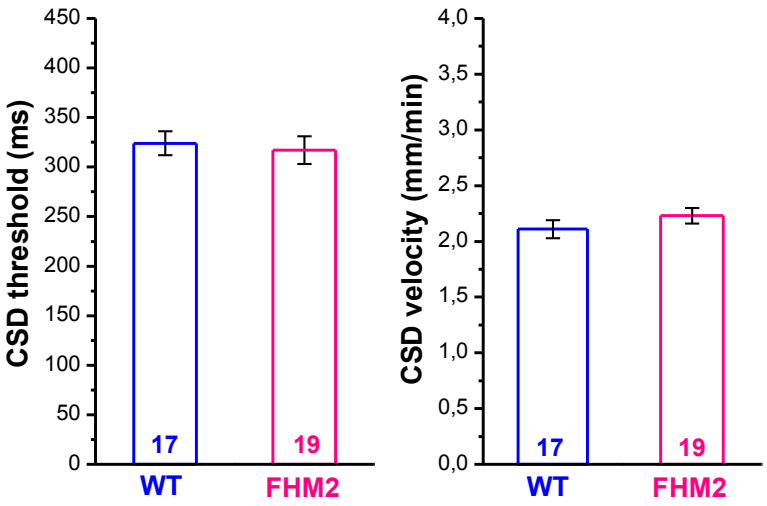

Figure 6.1. CSD threshold and velocity were similar in WT and FHM2 KI P16-18 old mice at room temperature.
The bar plots show the mean values of threshold for CSD induction (on the left) and of velocity of CSD propagation in WT (in blue) and FHM2 KI mice (in magenta). CSD was induced in layer 2/3 of somatosensory cortex slices from P16-18 old mice at room temperature.

In order to verify the hypothesis that the different findings *in vitro* and *in vivo* were due to the different age of the animals (P16-18 versus adult) and/or to the different temperature (room temperature versus physiological temperature), I repeated the experiments first using mice of older age and then increasing the temperature.
In somatosensory cortex slices from one month old mice (P28-29), I observed a significantly 13% lower threshold for CSD induction and also a 8% higher velocity of CSD propagation in FHM2 KI mice than in WT mice (Fig. 6.2).

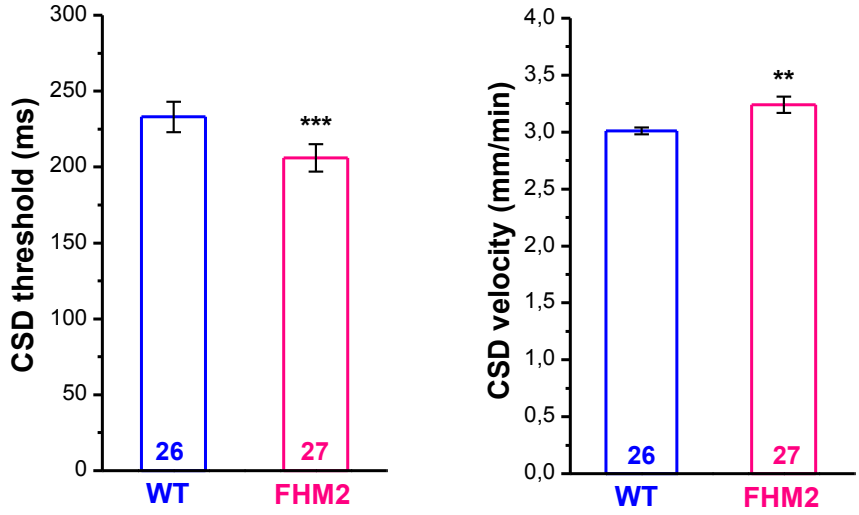

Figure 6.2. The threshold for CSD induction was lower and the velocity of CSD propagation was higher in FHM2 KI mice compared to WT mice, in P28-29 old mice at room temperature.
The bar plots show the mean values of threshold for CSD induction (on the left) and of velocity of CSD propagation in WT (in blue) and FHM2 KI mice (in magenta). CSD was induced in layer 2/3 of somatosensory cortex slices, obtained from P28-29 old mice, at room temperature.
** = $p < 0.01$; *** = $p < 0.001$.

I tried older than one month old mice and I observed a small increase in the gain of function effect of the mutation. Indeed, using P34-35 old mice, I observed a significantly 20% lower threshold for CSD induction and a 20% higher velocity of CSD propagation in FHM2 KI mice than in WT mice (Fig. 6.3).
These data are in agreement with the *in vivo* results, even though the difference between WT and FHM2 KI mice were still smaller than those reported in the *in vivo* study (Leo *et al.*, 2011).
I then assessed the temperature effect carrying out the experiments at higher temperature (30°C). Using P34-35 old mice and increasing the temperature, I found a remarkable large increase of the gain of function effect of the mutation, with values actually similar to the ones found in the *in vivo* study (Leo *et al.*, 2011): I observed a significantly 38% lower threshold for CSD induction and a 26% higher velocity of CSD propagation in the FHM2 KI mice than in WT mice (Fig. 6.4).

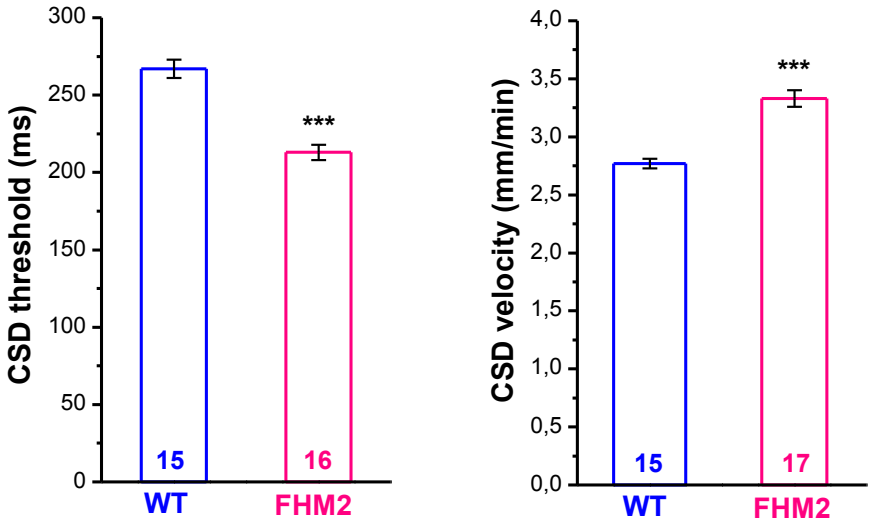

Figure 6.3. The threshold for CSD induction was lower and the velocity of CSD propagation was higher in FHM2 KI mice compared to WT mice, in P34-35 old mice at room temperature.
The bar plots show the mean values of threshold for CSD induction (on the left) and of velocity of CSD propagation in WT (in blue) and FHM2 KI mice (in magenta). CSD was induced in layer 2/3 of somatosensory cortex slices, obtained from P34-35 old mice, at room temperature. *** = $p < 0.001$.

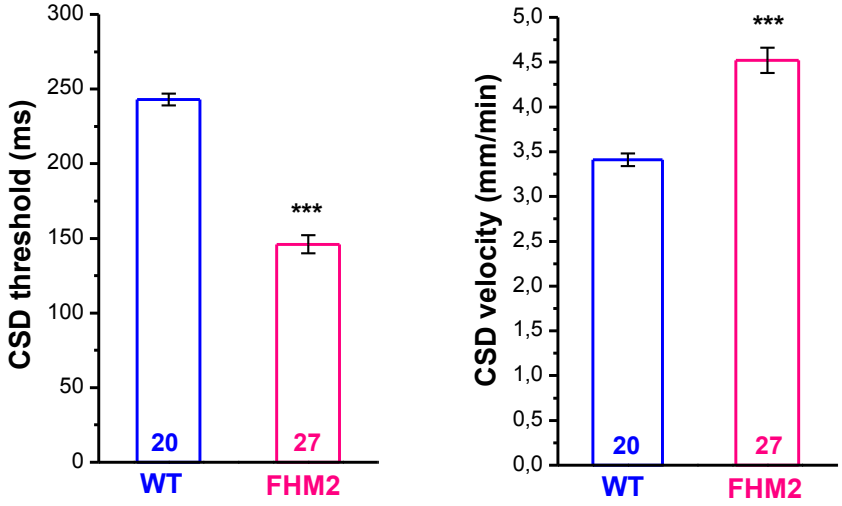

Figure 6.4. At 30°C, the gain of function effect of the mutation was increased in FHM2 KI P34-35 old mice.
The bar plots show the mean values of threshold for CSD induction (on the left) and of velocity of CSD propagation in WT (in blue) and FHM2 KI mice (in magenta). CSD was induced in layer 2/3 of somatosensory cortex slices, obtained from P34-35 old mice, at 30°C. *** = $p < 0.001$.

Although slightly smaller than that of old mice, a large facilitation of experimental CSD was also observed at 30°C with P22-23 old mice: I observed a significantly 25% lower threshold for CSD induction and a 21% higher velocity of CSD propagation in the FHM2 KI mice than in WT mice (Fig. 6.5).

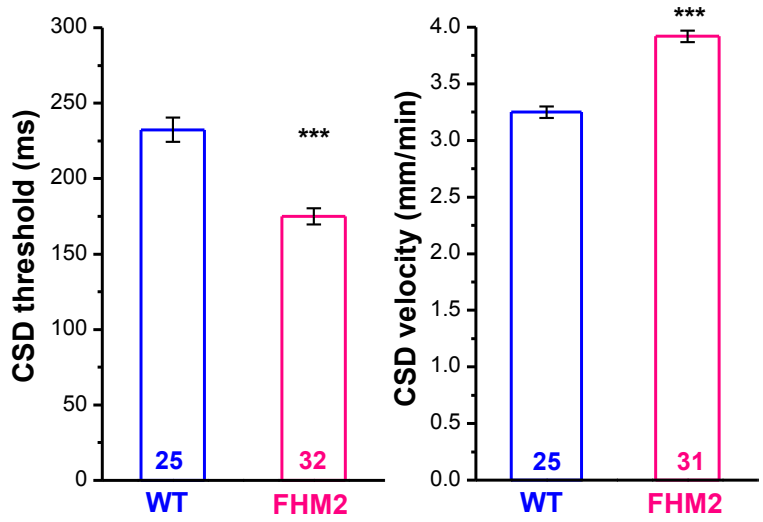

Figure 6.5. Facilitation of experimental CSD in acute cortical slices of P22-23 old FHM2 KI mice at 30°C.
The bar plots show the mean values of threshold for CSD induction (on the left) and of velocity of CSD propagation in WT (in blue) and FHM2 KI mice (in magenta). CSD was induced in layer 2/3 of somatosensory cortex slices, obtained from P22-23 old mice, at 30°C. *** = $p < 0.001$.

Taken together these data confirm that the FHM2 mutation facilitates threshold of CSD induction and velocity of CSD propagation in our *in vitro* model of experimental CSD. More important, I set the experimental condition to study the mechanisms of increased CSD susceptibility in FHM2 KI mice.
Considering the technical difficulties of working with slices of old mice (e.g. slice healthy and cells survival), I decided to perform all further experiments at 30° C using brain slices from P22-23 old mice.

6.2. Does the loss-of-function of α2 Na,K-ATPase result in an impaired astrocyte-mediated clearance of glutamate from the synaptic cleft during cortical neuronal activity?

To answer this question, I took advantage of the fact that the transport of one glutamate molecule is coupled to the cotransport of three Na^+ and one H^+ in exchange for one K^+. Therefore, the glutamate transporters are electrogenic and more important, the glutamate released during synaptic activity induces measurable current in astrocytes.
I placed a stimulating electrode in layer one (layer 1) in brain slices of somatosensory cortex obtained from WT and FHM2 KI mice. I recorded in voltage clamp mode from astrocytes, held at -80 mV, located in the same layer 200 µm apart from the electrode. The astrocytes inward current evoked by electrical stimulation of layer 1 neuronal afferents was measured in the presence of a cocktail of antagonists of AMPA (10 µM NBQX), NMDA (50 µM D-AP5 and 20 µM MK-801) and $GABA_A$ (20 µM

bicuculline) receptors (Bergles and Jahr, 1997; Bernardinelli and Chatton, 2008), to block postsynaptic current flow (see below).

As shown in Fig. 6.6, the astrocytic inward current elicited by a single pulse stimulation consists of two components. The fast transient component of this current is blocked by application of 15 µM TFB-TBOA (TBOA), a glutamate transporter antagonist, and it represents the so-called astrocytic synaptically-activated glutamate transporter-mediated current (STC), generated by the uptake of the glutamate, through the astrocytic glutamate transporters, released by the stimulation. Beside the STC, there is a sustained TBOA-insensitive current that mainly represents a K^+ current mediated by Kir channels (Fig. 6.6, green trace; see below and see details in Introduction, paragraph 1.3.2.3).

The STC was isolated pharmacologically by subtracting the response to a single pulse stimulation recorded in the presence of TBOA from that recorded in control condition (Fig. 6.6, blue trace) (Diamond, 2005).

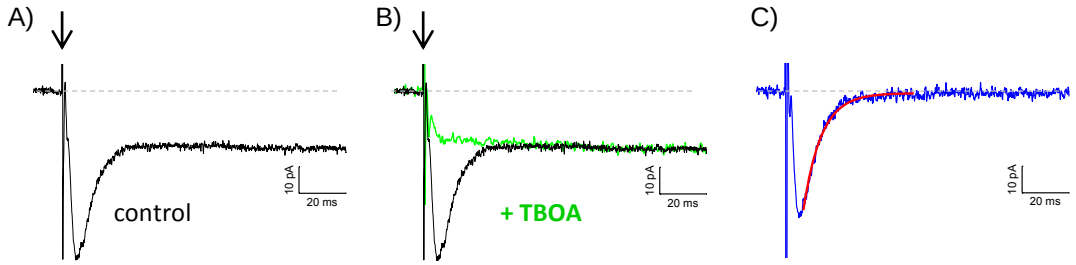

Figure 6.6. Synaptically-activated inward currents evoked in a layer 1 cortical astrocyte by extracellular stimulation.

A) Representative whole-cell current trace, recorded at 30°C from a layer 1 astrocyte (V = -80 mV) in an acute coronal slice of barrel cortex from a P22 WT mouse, in response to a single pulse stimulation of 100 µA in amplitude and 100 µs in duration (stimulation frequency of 0.05 Hz) in control condition in the presence of AMPA, NMDA and $GABA_A$ receptors blockers (in black; as described in the text).

B) Besides the inward current recorded in control condition (in black), the response to single pulse stimulation recorded in the presence of TBOA (15 µM) is reported in green. The transient current is the STC while the sustained current is the TBOA-insensitive current, mainly mediated by Kir channels.

C) Synaptically-activated glutamate transporter-mediated current (STC; in blue) isolated by subtracting the response to a single pulse in the presence of TBOA from that recorded in control condition. The STC decay was fitted with a single exponential function (in red) to measure the time constant (τ).

In the three panels, the dashed grey line indicates the baseline and the arrow points the stimulus.

The STC decay time course provides a relative measure of the rate of glutamate clearance (i.e. how rapidly synaptically released glutamate is taken up from the extracellular space) and it is independent of the intensity of extracellular stimulation (Bergles and Jahr, 1997; Diamond and Jahr, 2000; Diamond, 2005): the STC is slowed by transporter antagonists, which slow glutamate clearance by decreasing uptake capacity (Bergles and Jahr, 1997; Diamond and Jahr, 2000). If the rate of glutamate

clearance by astrocytes in FHM2 KI mice is decreased, I expect a slower time course of the STC.

I derived a measure of the rate of glutamate clearance by fitting the STC decay with a single exponential function and measuring the decay time constant (τ; see details in Materials and Methods, paragraph 8.4.6.2): the larger the value of τ of STC decay, the slower is the rate of glutamate clearance.

I measured the τ of STC decay in WT and FHM2 KI mice and I observed that the τ of STC decay is 16% higher in FHM2 KI (8.16 ± 0.24 ms, n=10 slices) compared to WT mice (7.03 ± 0.20 ms, n=14 slices) (Fig. 6.7, on the left).

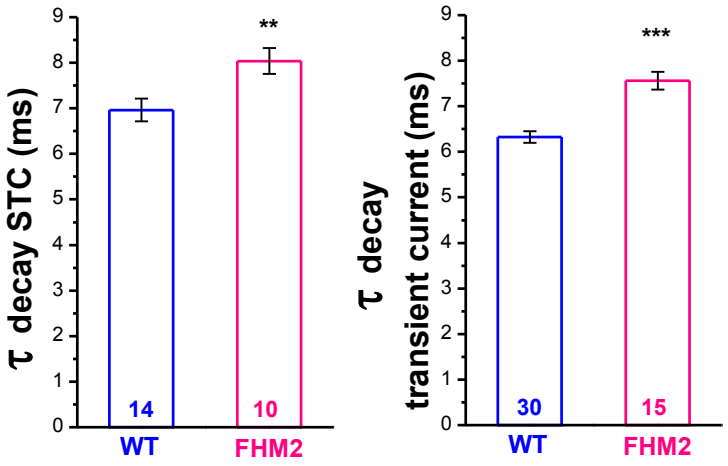

Figure 6.7. The rate of the clearance of glutamate released by a single pulse stimulation was reduced in FHM2 KI mice.
The bar plots report the mean value of the τ of the decay measured for STC (pharmacologically isolated; on the left) and for the transient current (without pharmacological isolation; on the right) evoked by single pulse stimulation in WT (in blue) and FHM2 KI mice (in magenta). ** = $p < 0.01$; *** = $p < 0.001$.

To test whether it was possible to verify the impairment of the glutamate clearance without pharmacological isolation of the STC current from the transient current elicited by single pulse stimulation, I measured the τ of the decay of the transient current. The τ decay of the STC, pharmacologically isolated, was slower than the τ of the decay of the transient current, without pharmacological isolation, due to the sustained TBOA-insensitive component. Nevertheless, comparing the τ of the decay of the transient current in WT and FHM2 KI mice, I obtained a result similar to that observed for the STC (pharmacologically isolated): the τ of the decay of the transient current evoked by a single pulse stimulation was 20% slower in FHM2 KI than in WT mice (Fig. 6.7, on the right).

These results indicate that in FHM2 KI mice, the rate of glutamate clearance evoked by a single pulse stimulation is significantly reduced.

In another set of experiments, I measured the STC evoked by a train of 10 pulses at high frequency (50 and 100 Hz). The idea behind is that a train of stimuli might better mimic the trigger of CSD rather than a single pulse; additionally, a train

of stimuli will lead to a larger amount of glutamate released and, therefore, one may expect a bigger impairment in the glutamate clearance by astrocytes in FHM2 KI compared to WT mice.

In this case, I measured the τ of the decay of the STC evoked by the last pulse of the train. As for the single stimulus, I first tried to isolate the STC by applying TBOA and subtracting the trace in the presence of TBOA from that in control condition. After TBOA application, the short-lived current elicited by each pulse was inhibited but the sustained TBOA-insensitive current increased with time, making the subtraction impossible (Fig. 6.8).

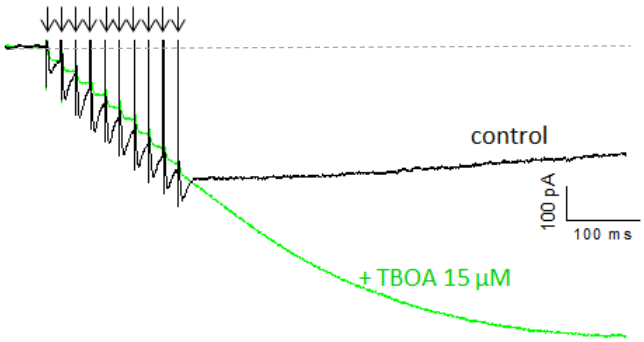

Figure 6.8. Synaptically-activated inward currents evoked in a layer 1 cortical astrocyte by a train stimulation.
Representative whole-cell current traces, recorded at 30°C from a layer 1 astrocyte (V = -80 mV) in an acute coronal slice of barrel cortex from a P22 WT mouse, in response to a train stimulation of ten pulses of 100 µA in amplitude and 100 µs in duration at 50 Hz, in control condition (in black) and after application of TBOA (15 µM; in green). In TBOA, the STC was inhibited while the TBOA-insensitive current increased with time. The dashed grey line indicates the baseline and the arrows point the stimuli.

I worked out another way to isolate the STC of the tenth pulse in the train, based on the finding that the sustained TBOA-insensitive current increased in a linear fashion along the train (Fig. 6.9).

In experiments in which single pulse and double pulse stimulation were alternated, I isolated the response to the second pulse by subtracting the current evoked by the first pulse to the current evoked by the paired pulses. The measure of the TBOA-insensitive current amplitude revealed that the TBOA-insensitive current amplitude of the isolated response to the second pulse was similar to that of the first pulse (Fig. 6.9).

Similarly, in experiments in which trains of 9 pulses and trains of 10 pulses were alternated, the response to the tenth pulse was isolated by subtracting the response to 9 pulses form that to 10 pulses: the amplitude of the sustained TBOA-insensitive current of the isolated response to the tenth pulse was similar to that of the first pulse (Fig. 6.9).

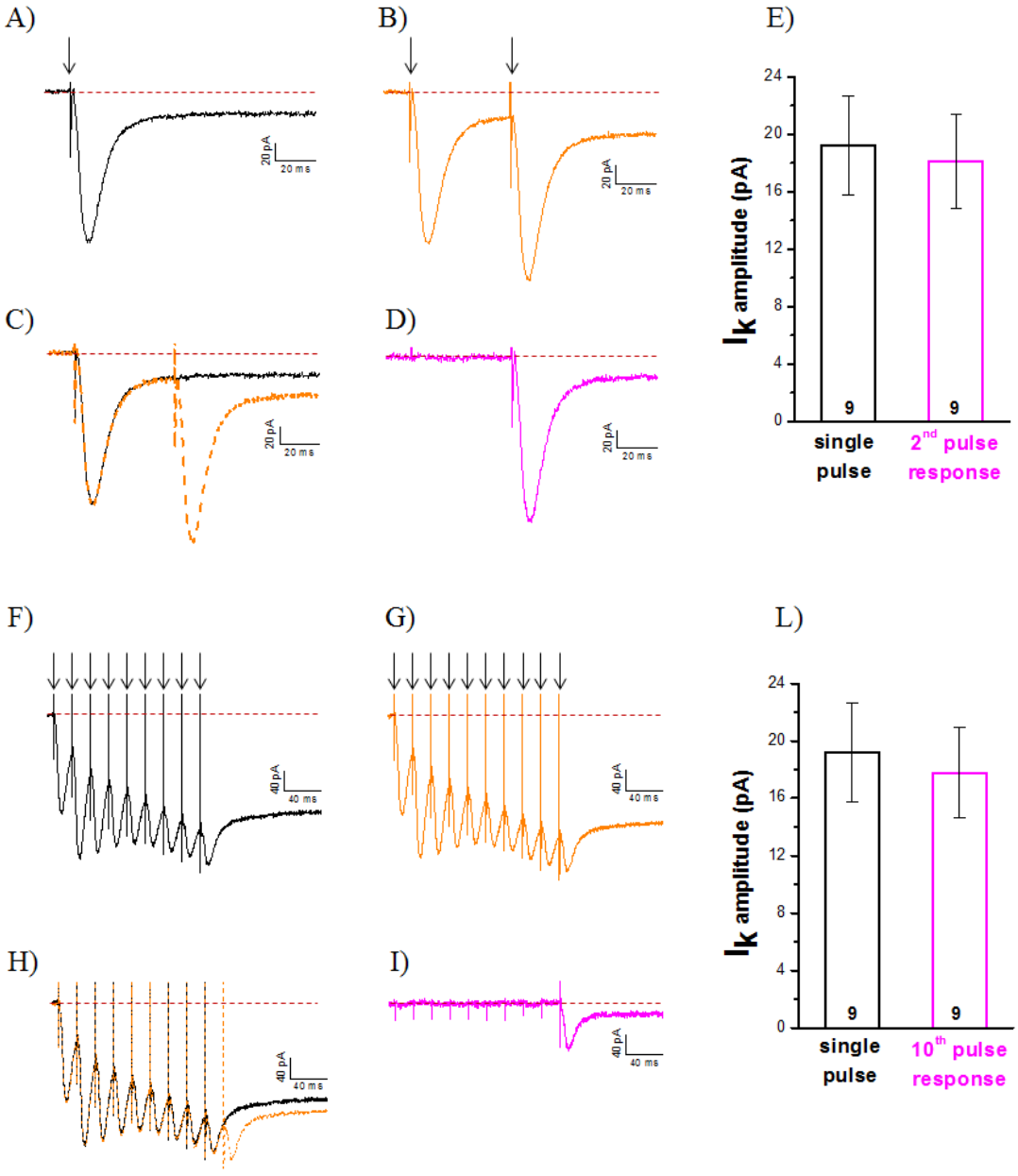

Figure 6.9. The TBOA-insensitive current amplitude increased in a linear fashion.

A-D) Representative whole-cell current traces recorded at 30°C from a layer 1 astrocyte (V = -80 mV) in an acute coronal slice of barrel cortex from a P23 WT mouse: a single pulse stimulation (A, in black) was alternated to a paired pulse stimulation (B, in orange). By subtracting the two traces (C, single pulse in black and paired pulses in dashed orange are superimposed), the response to the second pulse was isolated (D, in magenta).

F-I) 9 pulses (F, in black) and 10 pulses (G, in orange) at 50 Hz were subtracted (H, 9 pulses in black and 10 pulses in dashed orange are superimposed) to obtain the response to the tenth pulse (I, in magenta).

The red dashed line in A-I panels indicates the baseline and the arrows point the stimuli.

E, L) The bar plots report the mean values of the TBOA-insensitive current amplitude for the single pulse and the isolated response to the second pulse or to the tenth pulse.

To isolate the STC of the tenth pulse of the train, I recorded in the same experiment the response to 9 and 10 pulses in control condition and that to single pulse in the presence of TBOA. I derived the response to the tenth pulse, as shown just before, by subtracting the response to 9 pulses form that to 10 pulses. The TBOA-insensitive current evoked by the single pulse recorded in the presence of TOBA was then subtracted from the isolated response to the tenth pulse, to obtain the STC of the tenth pulse of the train (Fig. 6.10).

Thus, I could compare WT and FHM2 KI mice glutamate clearance during the train: I found that the τ of the decay of the STC of the last pulse in the train was largely increased in FHM2 KI. In particular, using a 50 Hz train, the glutamate uptake is 28% slower in FHM2 KI than in WT mice (Fig. 6.11). I went even at higher frequency stimulation, at 100 Hz: in this case, the glutamate uptake was 43% slower in FHM2 KI than in WT mice (Fig. 6.11).

This suggests that the slowdown of the glutamate clearance by astrocytes is higher in FHM2 KI mice after a train of action potential compared to the one observed following one pulse stimulation.

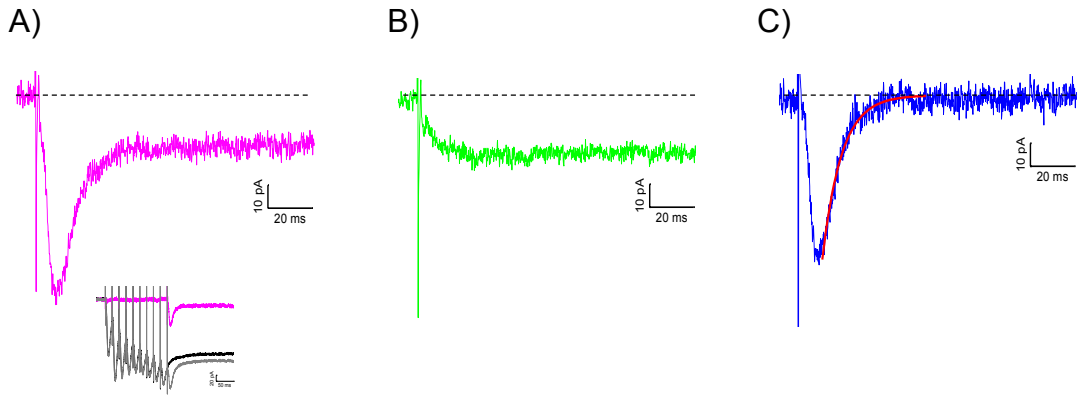

Figure 6.10. STC of the tenth pulse of a train stimulation.

A) Representative response to the tenth pulse (in magenta) of a train stimulation (at 50 Hz), isolated by subtracting the current elicited by a 9 pulses stimulation from that by a 10 pulses one. In the inset, the currents evoked by 9 (in black) and 10 (in grey) pulses and the isolated response to the tenth pulse (in magenta) are shown superimposed to remember how I isolated the response to the tenth pulse.

B) Representative TBOA-insensitive current elicited by a single pulse stimulation in the presence of TBOA (15 μM; in green).

C) STC of the tenth pulse obtained by subtracting the TBOA-insensitive current elicited by the single pulse in the presence of TBOA (shown in green in panel B) from the isolated tenth pulse (shown in magenta in panel A). The decay fitting, from which τ was measured, is reported in red.

The black dashed line, in the three panels, signs the baseline.

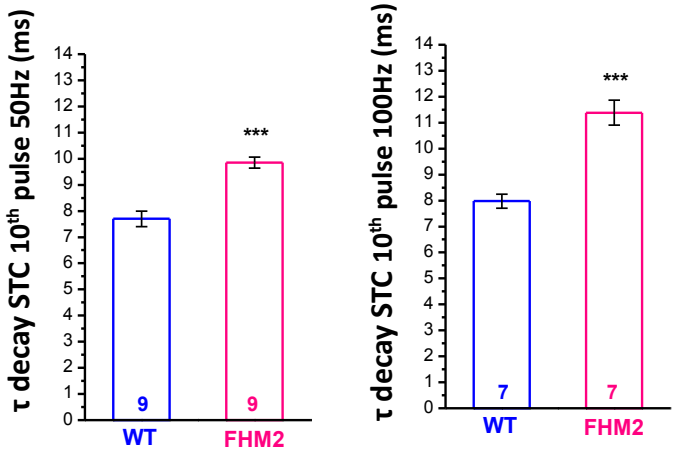

Figure 6.11. The τ of the decay of the STC evoked by a train stimulation was largely increased in FHM2 KI.
Bar plot of the mean value of τ of the decay measure for STC evoked by a train stimulation at 50 Hz (on the right) and at 100 Hz (on the left), in WT (in blue) and FHM2 KI (in magenta) mice. *** = $p < 0.001$.

It has been shown that the STC amplitude is proportional to the glutamate release evoked at the synapses by the extracellular stimulation; in fact, the amplitude of the STC varies proportionally with stimulus strength (Bergles and Jahr, 1997; Diamond and Jahr, 2000). Therefore, I was surprised to find that the STC amplitude after a single pulse stimulation was higher in FHM2 KI than in WT mice (Fig. 6.12). If the amplitude of the STC current is proportional to the glutamate released at the synapses by extracellular stimulation, the finding in Fig. 6.12 suggests that in FHM2 KI mice the extracellular stimulation elicits a larger glutamate release than in WT mice.

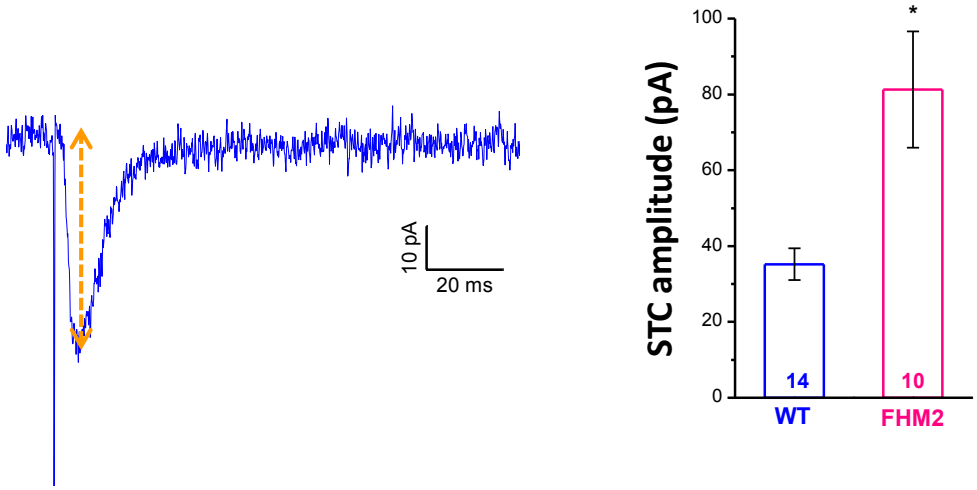

Figure 6.12. The STC amplitude, elicited by single pulse stimulation, was larger in FHM2 KI than in WT mice.
A) Representative STC evoked by single pulse stimulation; the amplitude of the response is indicate by orange arrow. B) The bar plot reports the mean values of amplitude of STC evoked by a single stimulation measured in WT and FHM2 KI mice. * = $p < 0.05$

If the glutamate release was actually increased in FHM2 KI mice, I would expect changes in the short-term plasticity and in particular an increase in the short-term

depression of the glutamate release (Tottene *et al.*, 2009). Comparing the amplitude of the glutamate current of the first pulse and of the tenth pulse in FHM2 KI and WT mice, I found that in WT mice there was no change while in FHM2 KI mice the STC amplitude evoked by the tenth pulse in the train was 54% lower compared to that evoked by the first pulse (Fig. 6.13).
This is consistent with a larger short-term depression of glutamate release in FHM2 KI compared to WT mice and is consistent with the conclusion that, indeed, in FHM2 KI mice the evoked glutamate release is higher than in WT mice.

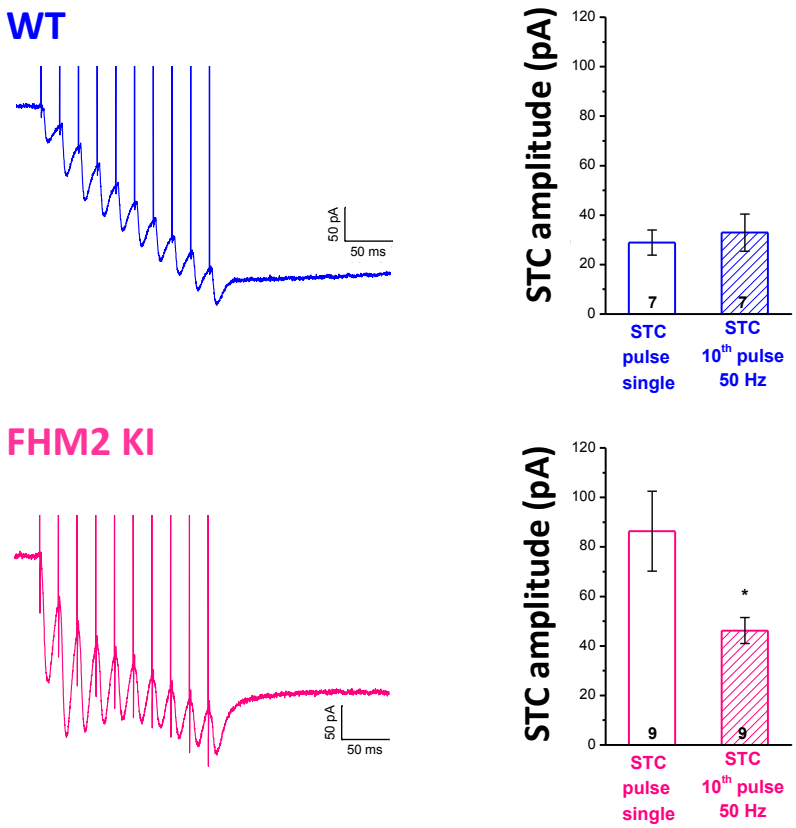

Figure 6.13. The short-term depression of glutamate release was larger in FHM2 KI compared to WT mice.
On the left: representative responses to 10 pulses stimulation at 50 Hz, in WT mice (on the top, in blue) and in FHM2 KI mice (on the bottom, in magenta). On the right: Bar plots report the mean values of amplitude of STC evoked by a single pulse stimulation and by a train stimulation at 50 Hz, in WT mice (on the top, in blue) and in FHM2 KI mice (on the bottom, in magenta). * = $p < 0.05$.

All together, these data indicate that the τ decay of the STC is larger in FHM2 KI compared to WT mice and that the difference is greater after a train of pulses with increasing frequency of the stimulation than after a single pulse. This supports my working hypothesis that the loss-of-function of the pump results in an impairment of glutamate clearance and suggests that the impairment increases with increases frequency of cortical activity. Surprisingly, also evoked glutamate release appears

increased in FHM2 KI mice as previously shown in FHM1 KI mice (Tottene *et al.*, 2009). Therefore, both the reduced clearance of glutamate and the increased evoked glutamate are expected to lead to CSD facilitation in FHM2 KI mice.

6.3. Is the clearance of K^+ by astrocytes during cortical neuronal activity impaired as a consequence of the loss-of-function of α2 Na,K-ATPase?

To answer this question, I measured the sustained TBOA-insensitive current elicited by extracellular stimulation (for simplicity, I refer to it as K^+ current from now on; Fig. 6.14). This sustained slowly decaying current is a measure of the synaptically-induced increase in extracellular K^+ concentration produced by neuronal K^+ efflux and of the accompanying change in driving force on Kir channels of astrocytes (Meeks and Mennerick, 2007; Bernardinelli and Chatton, 2008). Indeed, from literature, it is known that the amplitude of this K^+ current depends on the extracellular K^+ concentration elevation induced by electrical stimulation; thus, the larger the K^+ elevation induced by extracellular stimulation, the larger is the K^+ current recorded from astrocytes. The decay kinetics of this current provides an indirect measure of the rate of K^+ clearance from the interstitial space by astrocytes during neuronal activity.

To investigate whether K^+ clearance is impaired in FHM2 KI mice, I recorded the current evoked in astrocytes by extracellular stimulation in the absence of receptor blockers and I measured the τ of the decay of the sustained K^+ current in WT and FHM2 KI mice.

As shown in Fig. 6.14-6.15, in the absence of synaptic receptors blockers, the K^+ current was about three times larger than after the blockers application (10 µM NBQX, 50 µM D-AP5, 20 µM MK-801 and 20 µM bicuculline). Indeed, in the absence of receptors blockers (i.e. physiological conditions), the most of the K^+ efflux that causes extracellular K^+ concentration elevation is through the NMDA receptors (Poolos *et al.*, 1987; Shih *et al.*, 2013; see details in Introduction, paragraph 1.3.2.3).

In a still limited number of experiments, I found that the τ of the decay of the K^+ current evoked by 50 and 100 Hz train stimulation was similar in WT (2.4 ± 0.2 ms, n=7 slices at 50Hz; 2.5 ± 0.1 ms, n=6 slices at 100Hz) and FHM2 KI (2.8 ± 0.3 ms, n=9 slices at 50Hz; 2.6 ± 0.2 ms, n=7 slices at 100Hz) mice.

These results suggest that there are no changes in the rate of K^+ clearance in FHM2 KI mice that can lead to CSD facilitation.

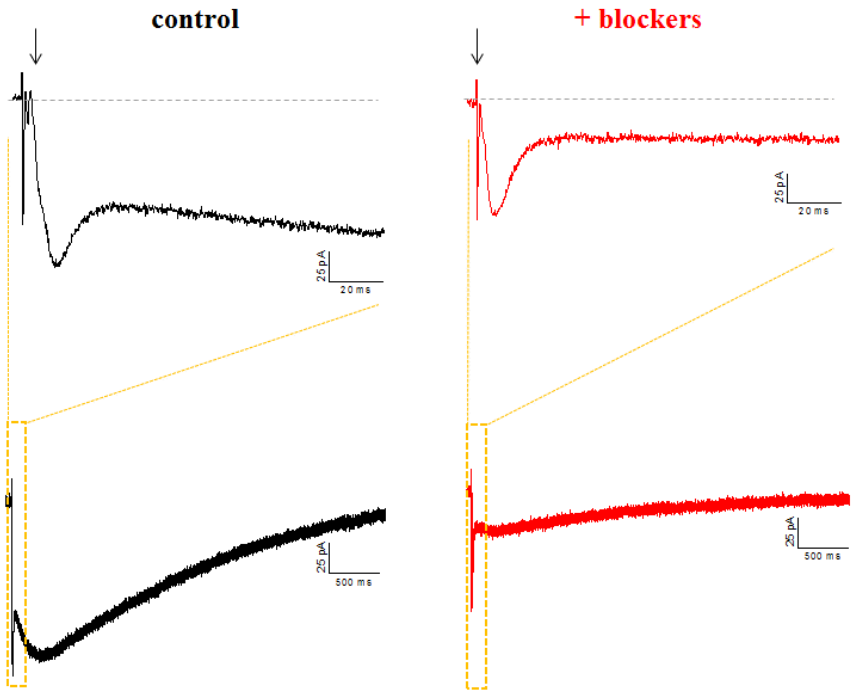

Figure 6.14. The K^+ currents evoked in a layer 1 cortical astrocyte by extracellular stimulation is a slowly decaying current.
On the top, representative response to a single pulse stimulation, before (control, on the left, in black) and after (+blockers, on the right, in red) synaptic transmission blockers application (10 µM NBQX, 50 µM D-AP5, 20 µM MK-801 and 20 µM bicuculline). The fast transient current is the STC while the slowly decaying current is the TBOA-insensitive current, mainly mediated by Kir channels.
On the bottom, the same recordings are shown on a compress scale in order to better visualize the slow decay kinetic of the K^+ current.

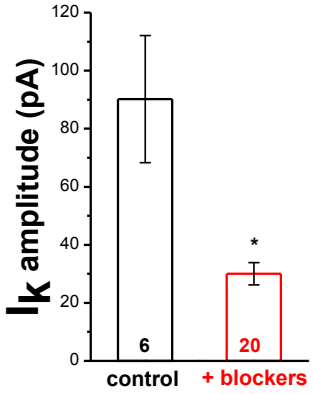

Figure 6.15. The K^+ current amplitude was larger in the absence than in the presence of receptors blockers.
The bar plot reports the mean values of the K^+ currents amplitude before (control, in black) and after synaptic receptors blockers application (+blockers, in red). * = $p < 0.05$.

6.4. Is Ca^{2+} content in the intracellular Ca^{2+} stores of astrocytes in FHM2 KI mice increased and does Ca^{2+} release from stores contribute to the facilitation of experimental CSD in FHM2 KI mice?

In astrocytic primary culture at 7-10 days *in vitro* (DIV), we measured the Ca^{2+} transient using astrocytes loaded with Fura-2 in response to the addition of ionomycin

in a Ca^{2+} free (EGTA-containing) medium (Fig. 6.16; in collaboration with Prof. Paola Pizzo). It is possible to obtain an indirect measure of the amount of Ca^{2+} in the stores by measuring the area under the curve. In FHM2 KI mice the amount of Ca^{2+} released from the intracellular Ca^{2+} stores by ionomycin was nearly 60% higher compared to the WT mice. This finding indicates that Ca^{2+} content is increased in the intracellular Ca^{2+} stores of astrocytes in FHM2 KI mice.

Given this result, I tested whether the increased Ca^{2+} concentration into the astrocytes contributed to facilitation of experimental CSD in FHM2 KI mice. I therefore investigated whether depleting the intracellular Ca^{2+} stores with cyclopiazonic acid (CPA), a SERCA inhibitor, and hence inhibiting gliotransmitters release affected CSD.

I measured threshold and velocity of K^+-induced CSD in acute cortical slices of FHM2 KI and WT mice in the absence and in the presence of CPA (50 µM). I used CPA concentration that completely inhibits the Ca^{2+} responses elicited in astrocytes by KCl pulses (both subthreshold and threshold for CSD induction), without significantly affecting the Ca^{2+} responses in neurons (Andrea Urbani, PhD thesis).

In FHM2 KI mice, depletion of the astrocytes intracellular Ca^{2+} stores with CPA increased CSD threshold and decreased CSD velocity towards WT values. Although both threshold and velocity remained different from those of the WT (Fig. 6.17).

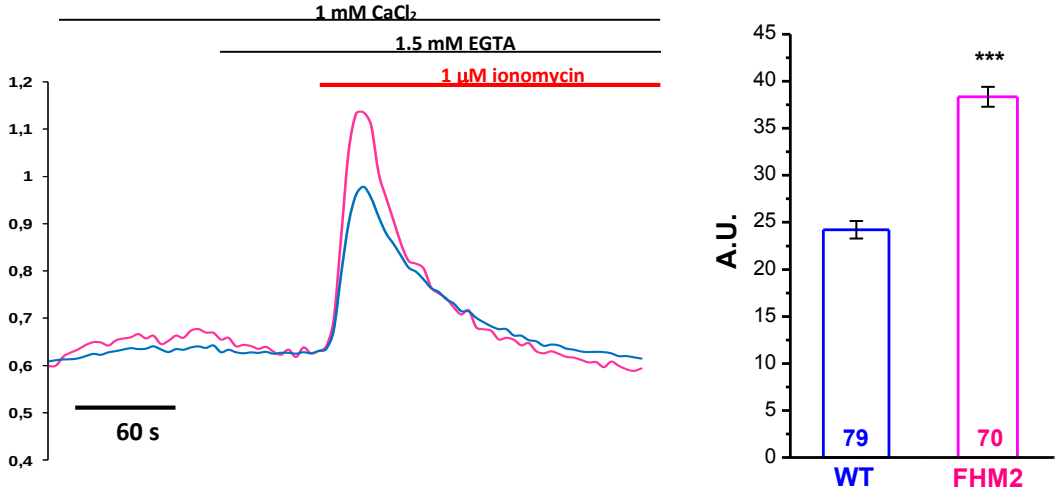

Figure 6.16. Increased $Ca2^+$ content in the intracellular stores of cortical astrocytes in culture from FHM2 KI mice.

The Ca^{2+} transients were measured in astrocytes primary cultures (DIV 7-10), obtained from P7-8 old WT and FHM2 KI mice. On the left, representative traces of Ca^{2+} concentrations, expressed as the ratio F340/F380, obtained from single WT (in blue) and FHM2 KI (in magenta) astrocytes loaded with Fura-2, in an experiment in which EGTA (1.5 mM) and ionomycin (1 µM) were added, as indicated. The area under the Ca^{2+} transient curve of individual astrocytes was calculated to obtain an indirect measure of the Ca^{2+} content in the stores. The average values in WT and FHM2 KI are shown on the right (mean area: 24.2 ± 0.9 A.U. n=79 WT versus 38.3 ± 1.1 A.U. n=70 KI). *** = $p < 0.001$.

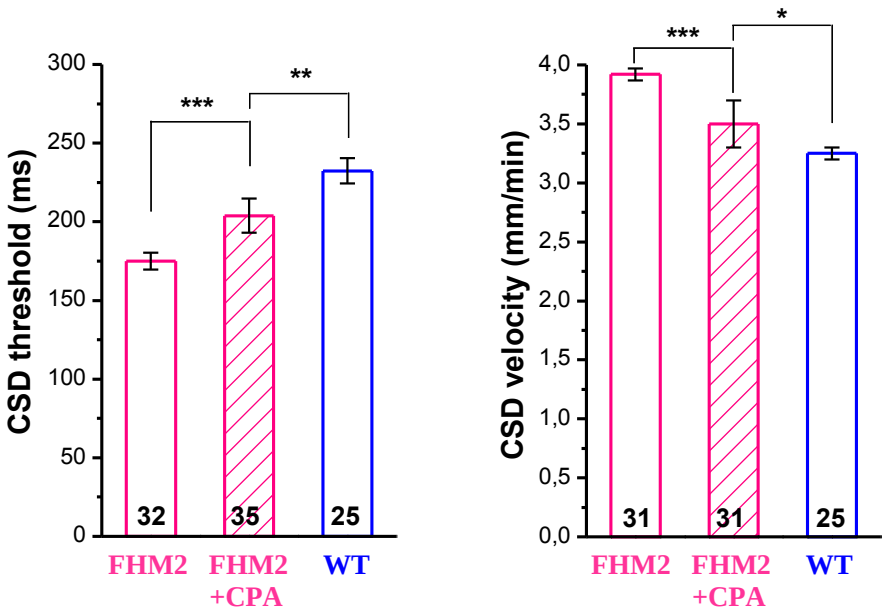

Figure 6.17. In FHM2 KI mice, depletion of the astrocytes intracellular Ca^{2+} stores increased threshold for CSD induction and decreased velocity of CSD propagation.
Threshold for CSD induction (on the left) and velocity of CSD propagation (on the right) were measured in somatosensory cortex slice from P22-23 old FHM2 KI old mice at 30°C in the absence (in magenta) and in the presence of CPA (50 µM) (in striped magenta). The correspondent values for WT mice are reported in blue. * = $p < 0.05$; ** = $p < 0.01$; *** = $p < 0.001$.

In contrast, in WT mice, depletion of astrocytes intracellular Ca^{2+} stores with CPA did not affect CSD threshold and velocity (Fig. 6.18).

These results indicate that depletion of Ca^{2+} stores reduces the facilitation of CSD in FHM2 KI mice, without affecting threshold for CSD induction and velocity of CSD propagation in WT mice. All together these data suggest a role of increased Ca^{2+} concentration inside the intracellular stores in astrocytes of FHM2 KI mice in the facilitation of experimental CSD in FHM2 KI mice, probably as a consequence of a larger release of gliotransmitters.

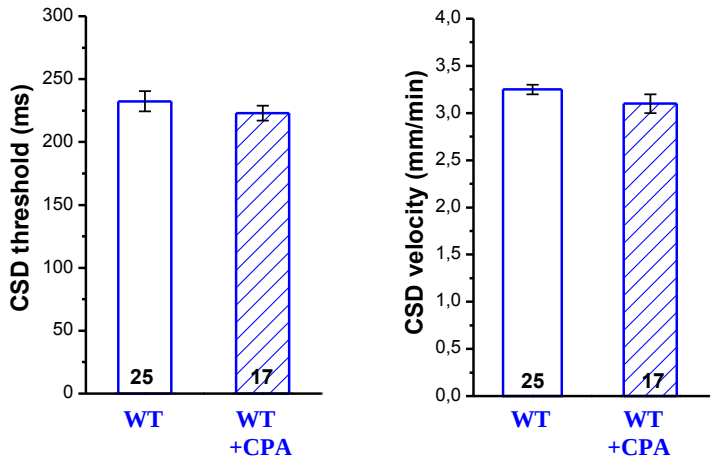

Figure 6.18. In WT mice, the threshold for CSD induction and velocity of CSD propagation were not affected by depletion of the astrocytes intracellular Ca^{2+} stores.
Threshold for CSD induction (on the left) and velocity of CSD propagation (on the right) were measured in somatosensory cortex slice from P22-23 old WT old mice at 30°C before (in blue) and after application of CPA (50 µM) (in striped blue).

7. DISCUSSION (II)

Recent *in vivo* experiments in heterozygous FHM2 W887R KI mice showed that the loss-of-function of α2 Na,K-ATPase leads to an increased threshold for CSD induction and a decreased velocity of CSD propagation (Leo *et al.*, 2011). I found that experimental CSD, induced in brain slices by high KCl pulses, is facilitated in P22-23 old mice, at 30°C: under these conditions, CSD has significantly 25% lower threshold of induction and 21% higher velocity of propagation in FHM2 KI compared to WT mice, with values similar to those observed in the *in vivo* study (Leo *et al.*, 2011). I investigated three possible mechanisms that underlie the facilitation of CSD in FHM2 KI mice, in acute brain slices of mouse somatosensory cortex.

I first studied whether the loss-of-function of α2 Na,K-ATPase results in an impaired astrocytes-mediated clearance of glutamate from the synaptic cleft during cortical neuronal activity. Given that glutamate uptake through astrocytes glutamate transporters is electrogenic, as the transport of one glutamate molecule is coupled to the cotransport of three Na^+ ions and one H^+ ion in exchange for one K^+ ion, I studied the rate of glutamate clearance by astrocytes electrophysiologically. I measured the inward current evoked in astrocytes of layer 1 by extracellular electrical stimulation of the same layer, in acute cortical slices of P22-23 old mice at 30°C (i.e. the same conditions in which I observed CSD facilitation in FHM2 KI mice), in the presence of synaptic receptors blockers (Bergles and Jahr, 1997; Bernardinelli and Chatton, 2008). The astrocytes inward current elicited in slices by a single pulse stimulation consists of two components. The fast transient current, blocked by application of TBOA (a glutamate transporter antagonist), is the STC generated by the uptake of glutamate, mediated by the astrocytic glutamate transporters. Beside the STC, there is a sustained TBOA-insensitive current that mainly represents a K^+ current mediated by Kir4.1 channels, due to the synaptically-induced increase in extracellular K^+ concentration. Given that, in physiological condition, most of the K^+ efflux that causes extracellular K^+ concentration elevation is through the NMDA receptors (Poolos *et al.*, 1987; Shih *et al.*, 2013; see details in Introduction, paragraph 1.3.2.3), I recorded the STC in the presence of synaptic receptors blockers, to reduce the entity of this slowly decaying K^+ current and facilitate the isolation of the STC component.

The time constant (τ) of STC decay provides a relative measure of how rapidly synaptically released glutamate is taken up from the extracellular space (Bergles and Jahr, 1997; Diamond and Jahr, 2000; Diamond, 2005), i.e. a slowed τ of STC decay reflects a slowed rate of glutamate clearance. I isolated the STC pharmacologically (Diamond, 2005) and I measured the τ of STC decay by fitting the STC decay with a single exponential function (see details in Materials and Methods, paragraph 8.4.6.2). The value of the τ of STC decay I measured in layer 1 cortical astrocytes from WT P22-23 old mice at 30°C (6.96 ± 0.25 ms, n=14) is similar to that previously reported

in adult (> P60 old) rat hippocampal astrocytes (6.17 ± 0.95 ms, n=5; Diamond *et al.*, 2005). Measurements of the τ of STC decay in FHM2 KI mice revealed that the clearance of glutamate released by single pulse stimulation is 20% slower in FHM2 KI than WT mice.

I measured also the τ of STC decay evoked by the last pulse of a train stimulation at 50-100 Hz, in FHM2 KI and WT mice. The idea behind is that a train of stimuli might better mimic the trigger of CSD rather than a single pulse. Additionally, as a train of stimuli will lead to a larger amount of glutamate released, one may expect a bigger impairment in the glutamate clearance by astrocytes in the FHM2 KI compared to WT mice. I found that the slowing of glutamate clearance in FHM2 KI mice was more pronounced after a train stimulation than a single pulse and increased with increasing frequency of the train stimulation: the glutamate clearance was 28% slower at 50 Hz and 43% slower at 100 Hz in FHM2 KI than WT mice.

My data show that the loss-of-function of the α2 Na,K-ATPase in FHM2 KI mice causes an impairment of the glutamate clearance. This is likely linked to the specific localization and functional coupling between α2 Na,K-ATPase and the glutamate transporters in astrocyte processes surrounding cortical glutamatergic synapses (Cholet *et al.*, 2002; Rose *et al.*, 2009). The loss-of-function of the pump might lead to a decreased density of glutamate transporters on the astrocytes plasma membrane or to a slowing of the glutamate transporter activity due to an increase in the Na^+ intracellular local concentration.

Glial cells express two types of glutamate transporters, GLAST and GLT1 (Tzingounis and Wadiche, 2007), whose expression is different during development and among brain areas.

The exact type of glutamate transporter involved in the glutamate uptake by layer 1 astrocytes in P22-23 old mice is unknown. However, several lines of evidence indicate that in the cortex and hippocampus, GLT-1 dominates functional uptake in the mature astrocytes while GLAST plays a more prominent role in immature astrocytes (Furuta *et al.*, 1997; Armbruster *et al.*, 2014; Danbolt, 2001). According to this, a recent study in mouse cortical brain slices, showed a large inhibition by DHK (a specific inhibitor of GLT1) of the STC elicited in P26-34 astrocytes of the deep cortical layers by photolysis of caged glutamate. This indicates that in astrocytes, only slightly older than those I used, GLT1 plays a major role in the glutamate clearance in the cortex.

Interestingly, unpublished findings (in collaboration with Prof. Fiorenzo Conti) show that in layer 2/3 perisynaptic astrocytic processes of FHM2 KI mice both total and membrane densities of GLT1 are significantly reduced compared to WT. This reduction of GLT1 is consistent with my result of an impaired clearance of glutamate by FHM2 KI astrocytes and suggests that a decreased density of GLT1 contributes to it.

I surprisingly found that the STC amplitude after a single pulse stimulation was higher in FHM2 KI than in WT mice. Given that the STC amplitude is proportional to

the glutamate release evoked at the synapses by the extracellular stimulation (Bergles and Jahr, 1997; Diamond and Jahr, 2000), my result suggests that extracellular stimulation elicits a larger glutamate release in FHM2 KI than in WT mice. Comparing the amplitude of the glutamate current of the first pulse and of the tenth pulse of a train stimulation in FHM2 KI and WT mice, I found that in WT mice there was no change while in FHM2 KI mice the STC amplitude evoked by the tenth pulse was 54% lower compared to that evoked by the first pulse. This finding is consistent with a larger short-term depression of glutamate release in FHM2 KI compared to WT mice and supports the conclusion that in FHM2 KI mice the evoked glutamate release is higher than in WT mice. The mechanisms underlying this surprising finding remain unknown. Both the reduced clearance of glutamate and the increased evoked glutamate release may be implicated in the facilitation of CSD in FHM2 KI mice, as these mechanisms are expected to lead to an enhanced activation of NMDA receptors. Activation of NMDA receptors by glutamate released from recurrent cortical pyramidal cell synapses plays a key role in the positive feedback cycle that provokes CSD (Pietrobon and Moskowitz, 2014). In FHM1 KI mice, the causal link between increased glutamate release and facilitation of experimental CSD has been demonstrated (Tottene *et al.*, 2009). Indeed, in FHM1 KI mice, CSD threshold is restored to the WT value by restoring evoked glutamate release to the WT value through partial inhibition of P/Q-type Ca^{2+} channels (Tottene *et al.*, 2009).

The observation that age of the animals and recording temperature are two critical experimental conditions to observe CSD facilitation, in brain slices of FHM2 KI mice, is consistent with a critical role of impaired glutamate clearance in CSD facilitation. Indeed, the glutamate uptake capacity changes during development (Bergles and Jahr, 1997; Diamond, 2005; Thomas *et al.*, 2011): in hippocampal astrocytes, the SCT are faster in adult than in juvenile and in juvenile than in neonatal rats (Diamond, 2005; Bergles and Jahr, 1997), in agreement with biochemical studies indicating also that the glutamate transporters protein levels increase during development (Furuta *et al.*, 1997; Thomas *et al.*, 2011). Additionally, it is also reported that the rate of glutamate transport is highly temperature dependent (Wadiche and Kavanaugh, 1998; Diamond and Jahr, 2000). At physiological temperatures, hippocampal glial transporters are capable of clearing glutamate released by high frequency extracellular stimulation very efficiently, whereas, at room temperature, transporters appear overwhelmed during long high frequency stimulation.

The second potential mechanism of CSD facilitation that I studied is the impaired clearance of K^+ by astrocytes during cortical neuronal activity. Given the astrocytes high resting conductance for K^+ ions due to high density of Kir channels, the astrocytes are highly sensitive to changes in the extracellular K^+ levels associated with neuronal activity (Kofuji and Newman, 2004). A measure of the external K^+ increase produced by neuronal stimulation is provided by the TBOA-insensitive slowly decaying current, that is mainly due to K^+ influx through Kir channels and is

proportional to the change in K^+ Nernst potential consequent to neuronal K^+ efflux produced by electrical stimulation (Meeks and Mennerick, 2007; Bernardinelli and Chatton, 2008). The τ of the decay of this K^+ current provides an indirect measure of the rate of K^+ clearance by astrocytes. I measured the τ of the decay of the K^+ current elicited in layer 1 astrocytes by extracellular stimulation of the same layer in the absence of synaptic receptors blockers. Preliminary experiments showed that the τ of the decay of the K^+ current evoked by train stimulation was similar in WT and FHM2 KI mice, likely indicating that there are no changes in the rate of K^+ clearance in FHM2 KI mice compared to WT. Pharmacological evidence indicates that α2 and/or α3 Na,K-ATPase participate in the clearance of K^+ during intense neuronal activity (Haglund and Schwartzkroin, 1990; Ransom *et al.*, 2000; D'Ambrosio *et al.*, 2002), but the relative importance of these two pumps remains unclear. If confirmed after increasing the sample, my data suggest that the α2 Na,K-ATPase plays a minor role in K^+ clearance. The observation of an unaltered CSD duration in the *in vivo* study between FHM2 KI and WT mice (Leo *et al.*, 2011) is consistent with this conclusion, since in hippocampal slices it has been showed that blocking α3 and α2, by local administration of ouabain (a Na,K-ATPase inhibitor), CSD duration increases (Haglund and Schwartzkroin, 1990).

These data suggest that CSD facilitation in FHM2 KI mice is not primarily due to an impaired K^+ clearance by astrocytes, as a consequence of the 50% reduction in the amount of α2 Na,K-ATPase (Leo *et al.*, 2011).

I finally investigated whether the Ca^{2+} content in the intracellular Ca^{2+} stores of astrocytes in FHM2 KI mice is increased. By integrating the Ca^{2+} transient, induced in cultured cortical astrocytes by ionomycin in Ca^{2+}-free medium, I obtained an indirect measure of the Ca^{2+} amount in the stores. I found that in FHM2 KI mice the amount of Ca^{2+} released from the intracellular Ca^{2+} stores by ionomycin was nearly 60% higher compared to WT mice, indicating that the Ca^{2+} content is increased in the intracellular Ca^{2+} stores of astrocytes in FHM2 KI mice. This finding is in agreement with previous measurements of elevated levels of Ca^{2+} ions in the cytoplasm and in the endoplasmic reticulum in cultured astrocytes from in *ATP1A2*$^{-/-}$ KO mice (Golovina *et al.*, 2003).

The increased Ca^{2+} content in the stores is probable a consequence of the tight coupling of the α2 Na,K-ATPase with the Na^+/Ca^{2+} exchanger at plasma membrane microdomains that overlay the endoplasmic reticulum (Lencesova *et al.*, 2004; Golovina *et al.*, 2003). Indeed, the Na^+/Ca^{2+} exchanger activity is regulated by the Na,K-ATPase, via its influence on the Na^+ electrochemical gradient across the plasma membrane. Therefore, the reduction of the Na^+ concentration gradient across the plasma membrane at the level of this microdomains, caused by the loss-of-function of α2 Na,K-ATPase, may result in local accumulation of Ca^{2+} in the space between the plasma membrane microdomain and the adjacent endoplasmic reticulum, which can account for the enhanced Ca^{2+} concentration into the Ca^{2+} stores.

I then investigated whether the increased Ca^{2+} concentration into the astrocytes contributes to facilitation of experimental CSD in FHM2 KI mice. By evaluating CSD threshold and velocity before and after depletion of intracellular Ca^{2+} stores by CPA (a SERCA inhibitor), I observed that depletion of Ca^{2+} stores reduces the facilitation of CSD in FHM2 KI mice, without affecting CSD in WT mice. These data suggest a role of increased Ca^{2+} concentration inside the intracellular stores in astrocytes in the facilitation of experimental CSD in FHM2 KI mice. A possible underlying hypothesis is that the increased Ca^{2+} content may lead to a larger release of gliotransmitters, including glutamate, in response to synaptic activity.

8. MATERIALS AND METHODS

8.1. Animals

The study of spontaneous recurrent cortical activity (described in Results I) was performed using WT C57Bl/6J mice (genetic background: 87.5 %). The study was performed using both male and female mice from postnatal day 16 to 19 (P16-19), and summary data show results from both sexes.

All the experiments to study the mechanisms of susceptibility to CSD in a mouse model of FHM2 (described in Results II) were performed on brain slices from heterozygous KI mice carrying the human W887R mutation in the *ATP1A2* orthologous gene (as described in Leo *et al.*, 2011) and the corresponding WT mice. FHM2 KI mice in the following age range P16-18, P22-23, P28-29 and P34-35, together with age-matched WT mice were used. Experiments from WT and KI mice of similar age were alternated on a daily basis. Both male and female mice were used and summary data show results from both sexes. For confirmatory genotyping of the heterozygous FHM2 KI mice, DNA was extracted from finger, ear clip or tail and analyzed by PCR using the previously described primers (Leo *et al.*, 2011).

Mice were housed under constant temperature (22 ± 1°C), humidity (50%) and acoustic isolation conditions with a 12 hours light/dark cycle, and were provided with food and water *ad libitum*.

All experimental procedures were carried out in accordance with the Italian Animal Welfare Act and approved by the local authority veterinary service.

8.2. Coronal cortical slices preparation

Acute coronal slices of the barrel cortex were prepared for both the projects.

8.2.1. Solutions

standard Artificial Cerebrospinal Fluid (sACSF*)*: NaCl 125 mM, KCl 2.5 mM, $MgCl_2$ 1 mM, $CaCl_2$ 2 mM, $NaHCO_3$ 25 mM, NaH_2PO_4 1.25 mM, glucose 25 mM, minocycline 50 nM, saturated with 95% O_2 and 5% CO_2 (pH 7.4 with NaOH).

Gluconate Cutting Solution (GCS): KGluconate 130 mM, KCl 15 mM, EGTA 0.2 mM, HEPES 20 mM, glucose 25 mM, kynurenic acid 2 mM, minocycline 50 nM saturated with 100% O_2 (pH 7.4).

Mannitol Cutting Solution (MCS): D-mannitol 225 mM, glucose 25 mM, KCl 2.5 mM, NaH_2PO_4 1.25 mM, $NaHCO_3$ 26 mM, $CaCl_2$ 0.8 mM, $MgCl_2$ 8 mM, kynurenic acid 2 mM, minocycline 50 nM, saturated with 95% O_2 and 5% CO_2 (pH 7.4).

GCS, MCS and sACSF contain minocycline (SIGMA), a microglia inhibitor, to prevent immune responses. GCS and MCS contain also kynurenic acid (Abcam Biochemicals), a NMDA receptor blocker, to prevent excitotoxicity during slices cutting.

8.2.2. Slices preparation

Slice cutting protocol adopted in our laboratory has been developed by Dr. Stephane Dieudonné (*École Normale de Paris*) working in Prof Philippe Ascher's group. This protocol (described in Dugué *et al.*, 2005) is characterized by the presence of the GCS, which mimics the intracellular ionic composition to enhance the recovery of neurons after cutting; moreover, the concentration of extracellular Ca^{2+} is set to 0 mM to prevent neuronal activity, thus preventing excitotoxicity.

Mice were anesthetized with isofluorane and decapitated; the whole head was immediately put into ice-cold ACSF, where the scalp was removed and the skull opened. The brain was quickly removed and placed, with its ventral surface up, in fresh an ice-cold ACSF solution. A cut perpendicular to the anteroposterior axis was made to remove the cerebellum and to create a basis surface for fixing the brain to the slicer stage. The tissue was then lightly blotted on filter paper and glued with cyanoacrylate glue onto the stage of a vibratome (Leica VT1000S) with the pial surface toward the blade. The glue was allowed a few seconds to dry and then the tissue was totally immersed in an ice-cold (2-3°C) GCS. A few (depending on brain size) slices were cut and discarded; the remaining tissue was cut into 350 μm thick slices and left and right hemispheres were separated. Slices putatively containing the barrel cortex were transferred at room temperature (RT) for 1 minute in MCS. This solution present an ionic composition intermediate between GCS and sACSF solution and allowed an intermediate recovery passage for slices before being transferred in sACSF solution. Slices were then transferred in sACSF solution at 30°C for 30 minutes and finally at RT for 30 minutes, to allow neurons recovering from the cutting procedure. Each slice was maintained for at least 20 minutes in recording solution before being used for electrophysiological recordings.

All the experiments were performed within 6 hours from the decapitation of the animal.

8.3. Patch clamp technique

The patch clamp technique allows single channel or whole cell currents to be recorded with the advantage of controlling the intracellular medium.

A glass micropipette with an open tip diameter (~1-2 μm) is filled with a suitable solution that usually matches the cytoplasm ionic composition. The pipette contains a silver electrode covered with silver chloride that is connected to a feedback amplifying

system (patch clamp amplifier). To avoid contact of the tip with eventual impurities present in the bath solution, which may hinder the formation of a good seal, a positive pressure is applied inside the pipette. A high resistance seal between the pipette and the cell membrane (in the order of GΩ) is formed by pressing the pipette against the membrane and by applying a light suction through a suction tube connected to the pipette holder. The high resistance of this seal makes it possible to record currents with high resolution and low noise.

Once the giga-ohm seal is established, the positive pressure previously applied to the pipette is released and four different configurations can be obtained (Molleman, 2003):

1) cell-attached: the membrane patch is conserved and not broken. This configuration allows measurements of single channel current (if a channel or more are present in the patch) without altering cytosolic environment. Because the pipette is on the extracellular side of the membrane, it is usually filled with bathing solution.

2) inside-out: it is obtained from cell-attached configuration by withdrawing the pipette from the cell. The result is now a vesicle attached to the pipette tip. The vesicle can be destroyed by exposure to air, i.e. the pipette is briefly lifted above the bath. This leaves a patch with the cytosolic side facing the bath. The intracellular surface of the membrane patch faces the bath solution.

3) outside-out: it is obtained by simply pulling away the patch pipette from a whole-cell configuration. The membrane will eventually break and, owing to the properties of the phospholipids, fold back on itself into a patch covering the pipette. The intracellular surface of the patch faces the solution contained in the pipette.

4) whole-cell: the membrane patch is ruptured by applying further suction and then the pipette solution and the electrode make direct electrical contact with the cytoplasm. As patch pipette tip is sufficiently wide (around 1 μm diameter) to allow washout of the cytoplasm by the pipette filling solution, the composition of the intracellular fluid can be considered equal to that of the pipette filling solution. This configuration allows the measurement of the current flowing through all the channels expressed in the plasma membrane or of the voltage changes of the whole cell. In the whole-cell configuration, the experimenter can manipulate the intracellular composition changing the ionic composition of the intracellular filling solution, but unknown cytosolic factors relevant to the subject of study can be unwittingly washed out. To avoid the latter, perforated patch-clamp was used, where electrical contact with the cytosol is established by adding a membrane-perforating agent to the pipette solution. The agent (nystatin or amphotericin B) perforates the membrane so that only small molecules such as ions can pass through, leaving the cytoplasm's organic composition largely intact.

All the experiments presented in this thesis (Results I and II) were performed by using the patch clamp technique in whole-cell configuration.

8.3.1. Patch clamp mode

The patch clamp technique offers the possibility to perform experiments in two different configurations: the voltage clamp and the current clamp.

The voltage clamp method (or voltage clamp recording mode) allows recording of ionic currents across the cell membrane at potential set by the operator (holding potential); this is achieved by a current-voltage converter that produces a voltage output that is proportional to the current input. In this way, any deviation of the recorded potential from the holding potential is instantly corrected by compensatory current injection; this current is an accurate representation (but opposite in sign) of the ionic current over the membrane under investigation.

The current clamp method (or current clamp recording mode) allows recording of the membrane potential variations after injections into a cell of amounts of current (even null) through the recording electrode.

Unlike the voltage clamp mode, in the current clamp mode the membrane potential is not clamped but can vary freely and the amplifier records spontaneous voltage variations or voltage deflections evoked by stimulations. Similarly to the voltage clamp recording mode, the current flow through the electrode produces a voltage drop across the electrode that depends on the product of the current and of the resistance of the electrode and this voltage drop will add to the recorded potential. In current clamp mode, the bridge balance control is used to balance out this voltage drop so that only the membrane potential is recorded. A differential amplifier is used to subtract a scaled fraction (the scaling factor is the pipette resistance) of the current from the voltage recorded in order to give the true membrane potential. The capacitance of the pipette is also corrected with the pipette capacitance neutralization function.

8.4. Patch clamp setup and recordings

During experiments, brain slices were put in a submerged recording chamber mounted on the stage of an upright microscope (Nikon Instruments, Eclipse E600FN) and held down with a handmade harp. The slice was continuously perfused with fresh extracellular solution saturated with 95% O_2 and 5% CO_2 at 3-6 mL/min using a peristaltic pump (Gilson, Miniplus 3). The extracellular solutions first passed through 5 ml syringes to avoid bubbles reaching the perfusion chamber and to create a break in the solution lines thus preventing these acting as aerials for noise; the solutions reached then the experimental chamber. Drugs were applied through separate perfusion lines. Lines were primed to speed up the application (the time for solution exchange was approximately 2 minutes).

Experiments described in Results (I) were performed at RT using a flow rate of 3 mL/min.

Experiments presented in Results (II) were conducted at RT or at 30°C, as indicated, with in general a flow rate of 3 mL/min. An exception to this are the

experiments to evaluate CSD threshold and velocity at 30°C, in which the flow rate was increased to 6 mL/min, in order to ensure the best oxygenation of the slice, critical for CSD recordings (Takano *et al.*, 2007).

8.4.1. Microscope

Slices observations and recordings were made with an upright microscope (Nikon Instruments, Eclipse E600FN) using infrared differential interference contrast (IR DIC) optics to introduce contrast into nonabsorbent objects. Light is first polarized and then passed through Wollaston prism, which splits light into two quasi-parallel beams. The light then passes through the specimens so that some beams will pass through the object and others to the edge of it. Beams that pass through the object will be slightly refracted with respect to those that do not. Both of the beams then pass through another Wollaston prism, which recombines them. Finally, the light passes through a polarizing filter. Beams that have been refracted by an object will appear a different shade to those that have not, due to constructive or destructive interference on recombination of the beams, giving a perception of contrast.

Slices were first visually inspected with a 10X objective and then with a water immersion objective (60X) for a detailed observation of cells and for the electrophysiological recordings.

Two CCD cameras (Hamamatsu Photonics K.K., Hitachi) were fitted on the microscope and connected to a monitor for a live view acquisition on two different displays.

The microscope and the manipulators were supported by an anti-vibration table (Micro-g, TMC) and surrounded by a homemade Faraday cage.

8.4.2. Electrophysiological setup

For both projects, electrical signals were recorded through a Multiclamp 700B patch-clamp amplifier connected to an analogical to digital converter (Digidata 1550) interface and pClamp software (all from Axon Instruments).

The CV-7B headstage contains a current to voltage (I-V) converter used in voltage clamp mode and a voltage follower used in current clamp mode. A recording electrode filled with the intracellular medium described before is introduced in an appropriate holder containing a silver chloride wire linking the electrode to the headstage. A silver chloride earth electrode links the bath to the headstage. The headstage is connected to a motorized micromanipulator (Luigs & Neumann) allowing precise positioning of the electrode under microscopic control.

All the experiments have been done using whole-cell single or double patch clamp recordings in current clamp or voltage clamp mode. For dual, simultaneous

patch clamp experiments to record the spontaneous recurrent cortical activity (Results I), cells were 100-150 μm apart from each other.

8.4.3. Cell identification

All the experiments were performed on coronal slices of somatosensory cortex (barrel cortex). This cortical area was recognized by the presence of barrel-like typical structures in the layer 4 (Petersen, 2007). In order to standardize the condition of slices healthy, recordings were made only from slices in which the number of death cells at 45 μm depth was not greater than 3 in a 228 X 172 μm field.

8.4.3.1. Pyramidal cells identification

Recordings of the spontaneous recurrent cortical activity (Results I) were performed on layer 2/3 pyramidal cells of barrel cortex. The cells recorded were deeper than 45 μm from the surface with a dendritic arborization almost parallel to the plane of the cut. The pyramidal cells were first visually identified according to their soma shape (triangular soma with two basal dendrites, a main apical dendrite that elongates to the layer 1 and the axon spreading in the deeper layers or other cortical regions) (Fig. 8.1a-b).

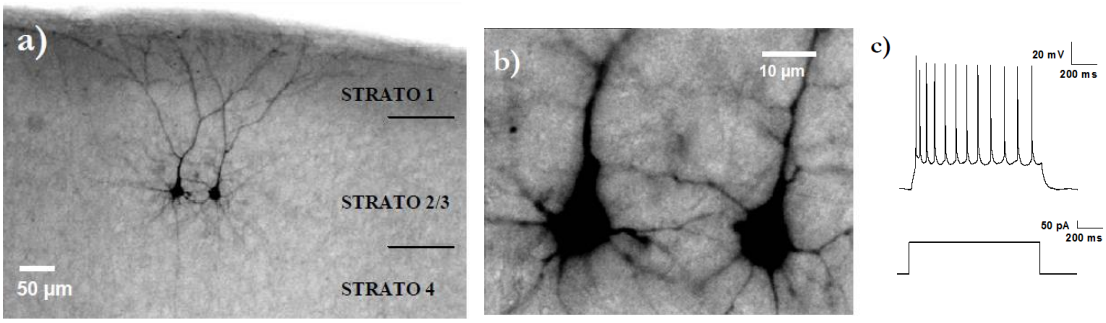

Figure 8.1. Morphological and electrophysiological characterization of pyramidal cells in layer 2/3 of somatosensory cortex in WT mice brain slice.

a, b) A pair of pyramidal cells was recorded simultaneously in layer 2/3 of somatosensory cortex. Both cells were filled with biocytin during whole-cell recording and processed with the Vector ABC method. The pictures were acquired with an upright microscope using a DIC optics. On the left, a 10X magnification; on the right, a 60X magnification.

c) Electrophysiological response of a pyramidal cell to a depolarizing step (200 pA injection). The cell depolarizes from -70 mV and fires action potentials.

Additionally, the characteristic AP-firing induced by supra-threshold current injections of increasing amplitudes up to 400 pA in current-clamp was evaluated (Fig. 8.1c). The firing of pyramidal cells indeed shows a typical spike frequency adaptation

and the maximal frequency of firing is close to 20 Hz; the second AP in a series is wider than the first, and the development of an adaptive hump as the cell is further depolarized is generally observed (Reyes *et al.*, 1998).

8.4.3.2. Astrocytes identification

The recordings presented in Results (II) were made from visually identified astrocytes in layer 1 of barrel cortex, deeper than 45 μm from the surface. The astrocytes were identified according to their typical morphological and electrophysiological properties; these cells were firstly visually identified by their small soma (diameter 5-10 μm), low input resistances (34 ± 4 MΩ, n=31 cells), high resting potentials (79 ± 1 mV, n=31 cells), passive membrane properties and lack of APs (Matthias *et al.* 2003; Mishima and Hirase, 2010).
In particular, the astrocyte was patch clamped and the voltage response to 400 ms current pulses from -50 pA to +250 pA with 50 pA steps (7 steps total) was recorded; all the recorded cells had current-voltage relationships close to linear (Fig. 8.2).

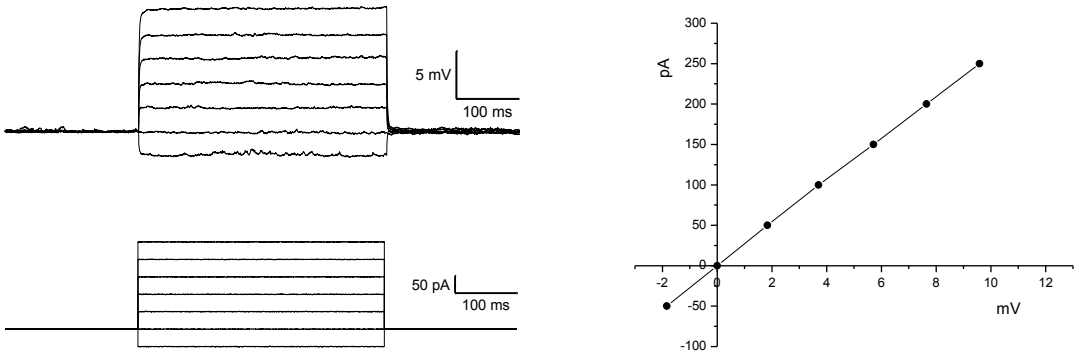

Figure 8.2. Electrophysiological characterization of an astrocyte in layer 1 of somatosensory cortex in acute brain slice.
On the left: representative whole-cell voltage response of an astrocyte to depolarizing steps (from -50 to +250 pA current injection). On the right: representative linear, quasi-ohmic I-V curve, usually recorded in astrocytes.

Only cells exhibiting this passive electrophysiological phenotype were used for further study, as these are the astrocyte subtypes known to take up glutamate (Matthias *et al.* 2003). Occasionally, members of a second class of glial cells were encountered (complex astrocytes, recognized by a less negative potential, a higher membrane resistance and a non-linear I-V curve; Bernardinelli and Chatton, 2008) and were not included in this study.

8.4.4. Solutions

8.4.4.1. Extracellular solutions

The experiments described in Results (I) were performed using a Modified Artificial Cerebrospinal Fluid (mACSF): 125 mM NaCl, 3.5 mM KCl, 1 mM $CaCl_2$, 0.5 mM $MgCl_2$, 25 mM $NaHCO_3$, 1.25 mM NaH_2PO_4, 25 mM Glucose, saturated with 95% O_2 e 5% CO_2 (pH 7.4 with 5% CO_2).

The extracellular solution (mACSF) differs from the sACSF solution because of a concentration of K^+ ions slightly higher and a relatively lower concentration of Ca^{2+} and Mg^{2+} ions, which make mACSF solution more similar to the cerebrospinal fluid than sACSF solution. Under these conditions, the spontaneous activity of cortical circuitry is increased compared to that observed in the presence of standard solution (Sanchez-Vives *et al.*, 2000).

For the experiments presented in Results (II), I used a mACSF solution (with 1 mM Mg^{2+}, more similar to the concentration in the cerebrospinal fluid than 0.5 mM used for up-states recordings) to measure CSD threshold and velocity. The composition of the extracellular solution used for the recordings from astrocytes was: 125 mM NaCl, 2.5 mM KCl, 1 mM $MgCl_2$, 1 mM $CaCl_2$, 25 mM $NaHCO_3$, 1.25 mM NaH_2PO_4, 25 mM glucose, saturated with 95% O_2 and 5% CO_2 (pH 7.4 with NaOH). This extracellular solution is similar to the sACSF solution, except for the reduced Ca^{2+} content to 1 mM (instead of 2 mM) and for the absence of minocycline.

8.4.4.2. Intracellular solutions

The electrodes were filled with different intracellular solutions depending on the recording mode.

For current clamp recordings from neurons, the pipette solutions contained (in mM): 114 K-gluconate, 6 KCl, 4 MgATP, 0.3 NaGTP, 10 Na-Phosphocreatine, 10 HEPES (pH 7.25 with KOH, osmolarity 300 mOsm with sucrose).

The internal solution for voltage clamp recordings from neurons contained (in mM): 114 CsMetansulfonate, 6 KCl, 4 MgATP, 0.3 NaGTP, 10 Na-Phosphocreatine, 5 QX-314, 10 HEPES (pH 7.25 with KOH, osmolarity 300 mOsm with sucrose). The use of cesium instead of potassium allowed reducing the leak currents underlined by potassium fluxes. QX-314 was used to block Na^+ channels and prevent unwanted unclamped APs.

The internal solution for voltage clamp recordings from astrocytes contained (in mM): 115 K-gluconate, 6 KCl, 4 MgATP, 0.3 NaGTP, 10 Na-Phosphocreatine, 10 HEPES, 5 glucose (pH 7.25 with KOH, osmolarity 295 mOsm with sucrose).
The intracellular medium was filtered using a 0.2 μm filter (Sartorius).

8.4.4.3. Drugs and toxins

Concentrations used for the experiments in Results (I): D-AP5 50 µM (Abcam Biochemicals), NBQX 10 µM (Abcam Biochemicals), ω-AgaIVA 400 nM (Peptide Institute Inc.), ω-CgTxGVIA 1 µM (Bachem), QX-314 5 mM (Abcam Biochemicals).

Concentrations used for the experiments in Results (II): CPA 50 µM (Abcam Biochemicals), TFB-TBOA 15 µM (Tocris), D-AP5 50 µM (Abcam Biochemicals), NBQX 10 µM (Abcam Biochemicals), bicuculline 20 µM (Abcam Biochemicals), MK-801 20 µM (Abcam Biochemicals).

Cytochrome C (0.1 mg/ml, Sigma-Aldrich) was added to the solutions with peptide toxins.

8.4.5. Electrodes

8.4.5.1. Recording electrode

Patch-clamp pipettes were obtained from borosilicate capillaries (Wiretrol II 5-000-2050), previously polished by fire and alcohol, using the puller P-95 (Sutter Instruments). The resistance of pipettes in the bath used for recordings from neurons ranged between 3 and 5 MΩ, while to record astrocytes the resistance was 5-7 MΩ.

8.4.5.2. Stimulating electrode

The layer 1 neuronal fibers (Results II) were stimulated using a concentric bipolar electrode (WPI TM33CCINS Tungsten 3" 76 Imp 10-15K Probe outer diameter 0.016 insulated 400 microm, core diameter 003" 76 microm y 0.4mm, X dim w/polyimide .005" 127 microm). The stimulating electrode was lowered into the bath and advanced towards the zone to be stimulated using a micromanipulator (Luigs & Neumann). The stimulating electrode was positioned at least 200 µm apart from the patch pipette in layer 1. The stimulating electrode was connected to a constant voltage isolated stimulator (Digitimer LTD) and neuronal afferent fibers were stimulated by applying a single pulse stimulus of 100 µsec of 100 µA, a double pulses at 20 Hz frequency and 10-9 pulses stimulation at 50 Hz and 100 Hz frequencies.

8.4.6. Data acquisition and analysis

Current and voltage clamp recordings from neurons (Results I) were acquired using Clampex 10.4 at a sampling rate of 10 kHz and filtered at 1-4 kHz using a 8-pole Bessel filter built within the software and analyzed using Clampfit 10.4 of the pClamp suite (PClamp 10.4, Axon, Molecular Devices).

Signals in voltage clamp from astrocytes (Results II) were low-pass filtered at 2 kHz and sampled at 10 kHz.

Data were corrected offline for the calculated liquid junction potential (LJP) of each solution: LJP measured at the pipette tip was -10 mV for the intracellular solution used in voltage clamp recordings from neurons and astrocytes, -12 mV for the intracellular solution used in current clamp recordings from neurons and -12 mV for intracellular solution used for recordings from astrocytes. LJP should be added to all voltages to obtain the correct values of membrane potential in whole-cell recordings (Neher, 1992).

8.4.6.1. Recordings and analysis of spontaneous recurrent cortical activity

Only pyramidal cells with a resting potential between -70 mV and -80 mV and an access resistance below 30 MΩ (with less than 25% variation) were included in the analysis.

The spontaneous recurrent activity in current clamp mode was recorded at the resting potential without injecting current. The up-states duration was measured from their onset to their retuning to the resting potential (or, if a double exponential decay was present, to the end of the first phase of the exponential decay). In the analysis of the effect of P/Q-type Ca^{2+} channels block, the duration of both up-states and simil-interictal epileptiform events was measured at half amplitude. The amplitude was estimated as the difference between the potential preceding the events and the mean value of the depolarization. The frequency was expressed as the number of up-states per minute.

Pyramidal neurons were voltage-clamped at the Cl^- reversal potential (-69 mV) for spontaneous excitatory postsynaptic currents (sEPSCs) recordings and at the reversal potential for excitatory currents (+20 mV) for spontaneous inhibitory postsynaptic currents (sIPSCs) recordings, with no series resistance (Rs) compensation.

sEPSCs and sIPSCs bursts durations were estimated by calculating the time between their onset (at the beginning of the inputs temporal summation over baseline) and the change of slope during the return of the current to the baseline level.

The mean excitatory and inhibitory synaptic conductances (G_e and G_i) in individual pyramidal cells during the recurrent network activity underlying the up-states were obtained by dividing the mean excitatory and inhibitory synaptic currents for the driving force (assuming a linear I-V relationship). The mean excitatory and inhibitory synaptic currents were obtained averaging the ratio of the synaptic charge (calculated from the baseline-adjusted voltage clamp recordings by integrating the current over time) of each sPSC over its duration.

A pharmacological approach with specific Ca^{2+} channel blockers was used to investigate the involvement of Ca^{2+} channels in spontaneous recurrent cortical activity. P/Q-type Ca^{2+} channel contribution was determined comparing the activity before and after the continuous application of saturating concentration of a specific blocker for this Ca^{2+} channel, ω-agatoxin IVA (400 nM), in the extracellular solution. The same approach was used to determine the role of N-type Ca^{2+} channels by applying saturating concentration of ω-conotoxin GVIA, a specific blocker for N-type Ca^{2+} channels.

8.4.6.2. Recordings and analysis of STC and K^+ currents from astrocytes

Only astrocytes with a -80 ± 5 mV resting potential and an access resistance below 25 MΩ (with less than 25% variation) were included in the analysis.

In voltage-clamp recordings, astrocytes were clamped at -80 mV. To record the STC, during whole-cell patch recordings from astrocytes in the layer 1 of somatosensory cortex slices, AMPA, NMDA, and $GABA_A$ receptors were blocked using specific antagonists (NBQX, D-AP5, MK-801 and bicuculline; Bergles and Jahr, 1997; Bernardinelli and Chatton, 2008). Under these conditions, stimulation of the fibers in layer 1 generates an inward current comprising fast and slow components. The transporter antagonist TFB-TBOA (15 µM) blocked the fast component, identifying it as the STC. The slower component mainly reflects a K^+ conductance caused by an increase in extracellular K^+ due to K^+ efflux through voltage-gated K^+ channels during the APs and through the NMDA receptors (Bergles and Jahr, 1997).

To isolate the STC of the single pulse, the response to single pulse in the presence of TFB-TBOA was subtracted to the response in control condition. To isolate the STC of the tenth pulse in a train of pulses delivered at 50 or 100 Hz, first the tenth pulse was isolate by subtracting a train of nine pulses from a train of ten pulses. Then, the current evoked in the presence of TFB-TBOA by a single stimulus was subtracted to this isolated response to the tenth pulses, in order to obtain the STC of the tenth pulse.

The STC decay was fitted with a single exponential function ($y = A * \exp(-x/\tau) + y0$, where A is the amplitude, y0 is the value at steady state, τ is the time constant, x is the time at which the decay starts) and the time constant (τ) was obtained, providing a measure of the rate of glutamate clearance.

The K^+ current was recorded in separated experiments, delivering single and train stimulation in the absence of synaptic receptors blockers (NBQX, D-AP5, MK-801 and bicuculline; Bergles and Jahr, 1997; Bernardinelli and Chatton, 2008). The K^+ current decay was fitted with a single exponential function ($y = A*\exp(-x/\tau) +y0$) and τ was obtained, providing a measure of the rate of K^+ clearance.

In both cases, for each different type of stimulation, at least six traces were mediated.

8.5. Experimental CSD

Brain slices were perfused with mACSF solution at a flowing rate of 3-6 mL/min, and pressure pulses of 3 M KCl (at 0.5 bar) of increasing duration (at 5 min intervals in 20 ms steps) were applied through a glass micropipette (resistance ranging from 0.19 to 0.25 MΩ) onto the slice surface on layer 2/3, using a PDES-02DX pneumatic drug ejection system (Npi Electronic), until a CSD was elicited.

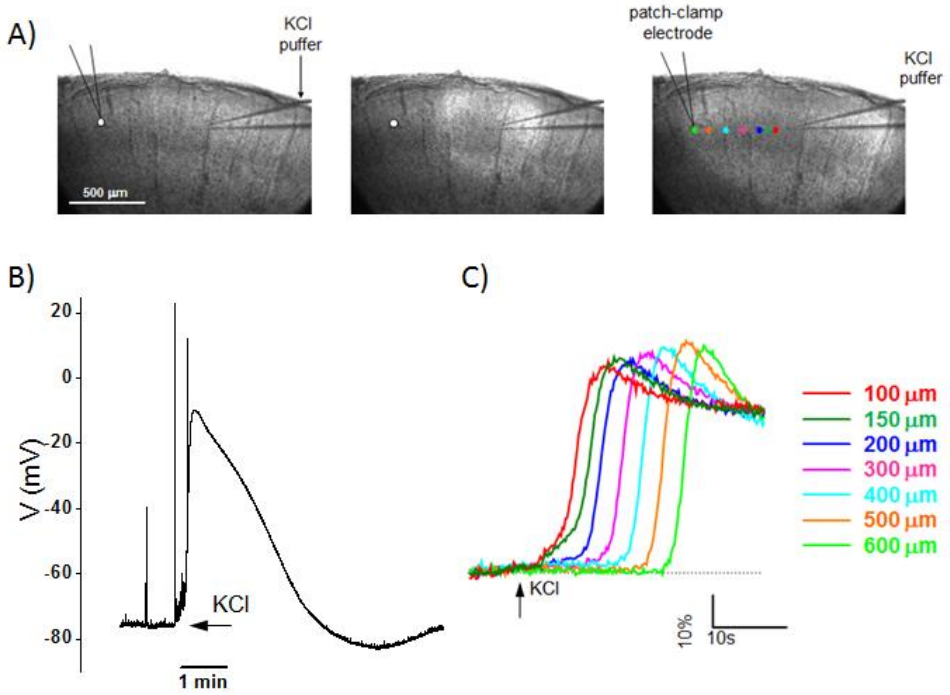

Figure 8.3. Experimental CSD induction by high KCl pressure pulses.
A) Three different frames from a CCD acquisition showing a representative slice before (first frame) and after CSD induction (second and third frame). Note the patch clamp pipette (on the left side of the slice), located at 600 µm from the KCl-injecting pipette (on the right side of the slice). In the third frame are indicate with different colours the distances from the puffer pipette at which the IOS was measured.
B) Typical current clamp recording of CSD depolarization in a layer 2/3 pyramidal cells of somatosensory cortex, located at 600 µm from the KCl-injecting pipette.
C) Typical IOS traces measured at increasing distances from the puffer pipette.

CSD was detected by the change in intrinsic optical signal (IOS) and/or recording in current clamp the membrane potential of a pyramidal cell at 600 µm from the pressure-ejection pipette tip (Fig. 8.3). The duration of the first pulse eliciting a CSD was taken as CSD threshold; CSD velocity was measured as the rate of the horizontal spread of the change in IOS produced by the CSD itself. MBF ImageJ software was used for the off line analysis of the digitalized images.

To test the effect of CPA, CSD threshold and velocity were measured in control condition and in different experiments during the perfusion with mACSF solution plus CPA.

8.6. Measurements of Ca^{2+} transients in astrocytic primary cultures

The Ca^{2+} transients were measured in cortical astrocytes primary cultures at 7-10 DIV, obtained from P7-8 old WT and FHM2 KI mice; brain cortex was treated following the procedure of Levi *et al.*, 1984 and then the cells were cultured under conditions promoting astrocytes growth.

For the Ca^{2+} transient recordings, cells, plated on coverslips, were loaded with fura-2 by incubation with 3 μM fura-2/AM at RT for 30 minutes and then at 37°C for another 30 minutes in modified Krebs-Ringer Buffer (mKRB, in mM: 140 NaCl, 2.8 KCl, 2 $MgCl_2$, 1 $CaCl_2$, 10 HEPES, 11 glucose, pH 7.4, at 37°C) containing 0.04% pluronic acid. To prevent fura-2 leakage and sequestration, 250 μM sulfinpyrazone was present throughout the loading procedure and the Ca^{2+} measurement. The coverslips were washed with mKRB, mounted on a thermostated chamber, placed on the stage of an inverted microscope (Zeiss, Axiovert 100 TV) equipped for single cell fluorescence measurements and imaging analysis (TILL Photonics, Martinsried, Germany). The sample was alternatively illuminated (t = 10 ms) by monochromatic light (at 340 and 380 nm) every second through a 20X objective. The emitted fluorescence passed through a dichroic beamsplitter, filtered at 505-530 nm and captured by a cooled CCD camera. The ratios (F340/F380) were offline normalized to the resting value measured within the first minute of the experiment.

The Ca^{2+} concentrations, expressed as the ratio F340/F380, were obtained from single WT and FHM2 KI astrocytes loaded with Fura-2, in an experiment in which EGTA (1.5 mM) and ionomycin (1 μM) were added. The area under the Ca^{2+} transient curve of individual astrocytes was calculated to obtain an indirect measure of the Ca^{2+} content in the stores and the values from individual cells were averaged to obtain the mean values in WT and FHM2 KI mice.

8.7. Statistical analysis

All averages were calculated with Microsoft Excel. Graphs, exponential fitting and statistical comparison were obtained with the Origin software (Microcal Software, Inc.). Data are given as mean ± standard error of the mean (SEM); stars indicate a statistically significant difference from control assessed by the Student's t test (* $p < 0.05$, ** $p < 0.01$ and *** $p < 0.001$).

ABBREVIATIONS

AMPA: (RS)-α-amino-3-hydroxy-5-methyl-4-isoxadepropionate
AP: action potential
ATP: adenosine-5'-triphosphate
BOLD: blood oxygenation level-dependent
Ca^{2+}: calcium ion
Ca_V: voltage-gated Ca^{2+} channels
Cd^{2+}: cadmium ion
Cl^-: chloride ion
CPA: cyclopiazonic acid
CSD: cortical spreading depression
D-AP5: D(-)-2-amino-5-phosphonopentanoic acid
DIV: day *in vitro*
EGTA: ethylene glycolbis (b-aminoethyl ether) N,N,N',N'-tetraacetic acid
EPSC: excitatory postsynaptic current
EPSP: excitatory postsynaptic potential
FHM1: familial hemiplegic migraine type 1
FHM2: familial hemiplegic migraine type 2
FS: fast-spiking
GABA: γ-aminobutyric acid
GAT: GABA transporters
GCS: gluconate cutting solution
G_e: excitatory synaptic conductance
G_i: inhibitory synaptic conductance
GTP: guanosine-5'-triphosphate
H^+: hydrogen ion
HEPES: N-2-hydroethylpiperazine-N'-2-ehanesulfonic acid
IOS: intrinsic optic signal
IPSC: inhibitory postsynaptic current
IPSP: inhibitory postsynaptic potential
IR: infrared
K^+: potassium ion
KI: knock-in
KO: knock-out
LJP: liquid junction potential
MA: migraine with aura
MO: migraine without aura
mACSF: modified artificial cerebrospinal fluid
MCS: mannitol cutting solution

NBQX: 2,3-Dioxo-6-nitro-1,2,3,4-tetrahydrobenzo[f]quinoxaline-7-sulfonamide
NMDA: N-methyl-D-aspartate
P: postnatal day
PSC: postsynaptic current
RT: room temperature
sACSF: standard artificial cerebrospinal fluid
STC: synaptically-activated glutamate transporter-mediated current
WT: wild-type
ω-AgaIVA: ω-agatoxin IVA
ω-CgTxGVIA: ω-conotoxin GVIA

REFERENCES

Ali AB, Nelson C. Distinct Ca^{2+} channels mediate transmitter release at excitatory synapses displaying different dynamic properties in rat neocortex. *Cereb Cortex* 2006;16:386-393.

Amaral DG. Chapter 17: The Anatomical Organization of the Central Nervous System. Principles of Neural Science, Kandel ER, Schwartz JS, Jessell TM. *McGraw-Hill* 2000.

Anderson CM, Swanson RA. Astrocyte glutamate transport: review of properties, regulation, and physiological functions. *Glia* 2000;32(1):1-14.

Araque A, Parpura V, Sanzgiri RP, Haydon PG. Tripartite synapses: glia, the unacknowledged partner. *Trends Neurosci* 1999;22(5):208-15.

Araque A, Carmignoto G, Haydon PG, Oliet SH, Robitaille R, Volterra A. Gliotransmitters travel in time and space. *Neuron* 2014;81(4):728-39.

Armbruster M, Hampton D, Yang Y, Dulla CG. Laser-scanning astrocyte mapping reveals increased glutamate-responsive domain size and disrupted maturation of glutamate uptake following neonatal cortical freeze-lesion. *Front Cell Neurosci* 2014;8:277.

Ayata C, Shimizu-Sasamata M, Lo EH, Noebels JL, Moskowitz MA. Impaired neurotransmitter release and elevated threshold for cortical spreading depression in mice with mutations in the alpha1A subunit of P/Q type calcium channels. *Neuroscience* 2000;95(3):639-45.

Ayata C, Jin H, Kudo C, Dalkara T, Moskowitz MA. Suppression of cortical spreading depression in migraine prophylaxis. *Ann. Neurol.* 2006;59:652-661.

Bazhenov M, Timofeev I, Steriade M, Sejnowski TJ. Model of thalamocortical slow-wave sleep oscillations and transitions to activated States. *J Neurosci* 2002;22(19):8691-704.

Beaulieu C. Numerical data on neocortical neurons in adult rats, with special reference to the GABA population. *Brain Res* 1993;609:284-292.

Beltramo R, D'Urso G, Dal Maschio M, Farisello P, Bovetti S, Clovis Y, Lassi G, Tucci V, De Pietri Tonelli D, Fellin T. Layer-specific excitatory circuits differentially control recurrent network dynamics in the neocortex. *Nat Neurosci* 2013;16(2):227-34.

Benediktsson AM, Marrs GS, Tu JC, Worley PF, Rothstein JD, Bergles DE, Dailey ME. Neuronal activity regulates glutamate transporter dynamics in developing astrocytes. *Glia* 2012;60(2):175-88.

Bergles DE, Jahr CE. Synaptic activation of glutamate transporters in hippocampal astrocytes. *Neuron* 1997;19(6):1297-308.

Bernardinelli Y, Chatton JY. Differential effects of glutamate transporter inhibitors on the global electrophysiological response of astrocytes to neuronal stimulation. *Brain Res* 2008;1240, 47-53.

Binzegger T, Douglas RJ, Martin KA. A quantitative map of the circuit of cat primary visual cortex. *J Neurosci* 2004;24:8441–8453.

Blanco G. Na,K-ATPase subunit heterogeneity as a mechanism for tissue-specific ion regulation. *Semin Nephrol* 2005;25(5):292-303.

Bolay, H., Reuter, U., Dunn, A.K., Huang, Z., Boas, D.A., and Moskowitz, M.A. Intrinsic brain activity triggers trigeminal meningeal afferents in a migraine model. *Nat Med* 2002;8, 136-142.

Buzsaki G. Neural syntax: cell assemblies, synapsembles, and readers. *Neuron* 2010;68:362–385.

CatterallWA, Kalume F, Oakley JC. NaV1.1 channels and epilepsy. *J Physiol* 2010;588, 1849–1859

Cestèle S, Schiavon E, Rusconi R, Franceschetti S, Mantegazza M. Nonfunctional NaV1.1 familial hemiplegic migraine mutant transformed into gain of function by partial rescue of folding defects. *Proc Natl Acad Sci USA* 2013;110(43):17546-51.

Charles A, Brennan K. Cortical spreading depression-new insights and persistent questions. *Cephalalgia* 2009, 29(10):1115-24.

Chauvette S, Volgushev M, Timofeev I. Origin of active states in local neocortical networks during slow sleep oscillation. *Cerebral Cortex* 2010;20:2660-2674.

Chauvette S, Seigneur J, Timofeev I. Sleep oscillations in the thalamocortical system induce long-term neuronal plasticity. *Neuron* 2012;75(6):1105-13.

Cholet N, Pellerin L, Magistretti PJ, Hamel E. Similar perisynaptic glial localization for the Na^+,K^+ ATPase alpha 2 subunit and the glutamate transporters GLAST and GLT-1 in the rat somatosensory cortex. *Cereb Cortex* 2002;12(5):515-25.

Cossart R, Aronov D, Yuste R. Attractor dynamics of network UP states in the neocortex. *Nature* 2003;423:283–288.

Constantinople CM, Bruno RM. Deep cortical layers are activated directly by thalamus. *Science* 2013;340(6140):1591-4.

Crunelli V, Hughes SW. The slow (<1 Hz) rhythm of non-REM sleep: a dialogue between three cardinal oscillators. *Nat Neurosci* 2010;13(1):9-17.

Crunelli V, David F, Lőrincz ML, Hughes SW. The thalamocortical network as a single slow wave-generating unit. *Curr Opin Neurobiol* 2015;31C:72-80.

Dallérac G, Chever O, Rouach N. How do astrocytes shape synaptic transmission? Insights from electrophysiology. *Front Cell Neurosci* 2013;7:159.

Danbolt NC. Glutamate uptake. *Prog Neurobiol* 2001;65(1):1-105.

David F, Schmiedt JT, Taylor HL, Orban G, Di Giovanni G, Uebele VN, Renger JJ, Lambert RC, Leresche N, Crunelli V. Essential thalamic contribution to slow waves of natural sleep. *J Neurosci* 2013;33(50):19599-610.

D'Ambrosio R, Gordon DS, Winn HR. Differential role of KIR channel and Na^+/K^+-pump in the regulation of extracellular K^+ in rat hippocampus. *J Neurophysiol* 2002;87(1):87-102.

Diamond JS, Jahr CE. Synaptically released glutamate does not overwhelm transporters on hippocampal astrocytes during high-frequency stimulation. *J Neurophysiol* 2000*;* 83, 2835-2843.

Diamond, J.S. Deriving the glutamate clearance time course from transporter currents in CA1 hippocampal astrocytes: transmitter uptake gets faster during development. *J Neurosci* 2005*;*25, 2906-16.

Dichgans M, Freilinger T, Eckstein G, Babini E, Lorenz-Depiereux B, Biskup S, Ferrari MD, Herzog J, van den Maagdenberg AM, Pusch M, Strom TM. Mutation in the neuronal voltage-gated sodium channel SCN1A in familial hemiplegic migraine. *Lancet* 2005;366(9483):371-7.

De Fusco M, Marconi R, Silvestri L, Atorino L, Rampoldi L, Morgante L, Ballabio A, Aridon P, Casari G. Haploinsufficiency of ATP1A2 encoding the Na^+/K^+ pump alpha2 subunit associated with familial hemiplegic migraine type 2. *Nat Genet* 2003;33(2):192-6.

de Kock CP, Bruno RM, Spors H, Sakmann B. Layer- and cell-type-specific suprathreshold stimulus representation in rat primary somatosensory cortex. *J Physiol* 2007;15;581:139-54.

Dodick DW. Examining the essence of migraine--is it the blood vessel or the brain? A debate. *Headache* 2008;48:661–67.

Doğanli C, Oxvig C, Lykke-Hartmann K. Zebrafish as a novel model to assess Na^+/K^+-ATPase-related neurological disorders. *Neurosci Biobehav Rev* 2013;37(10 Pt 2):2774-87.

Dugué GP, Dumoulin A, Triller A, Dieudonne S. Target-dependent use of co-released inhibitory transmitters at central synapses. *J Neurosci* 2005;25:6490-6498.

Eikermann-Haerter K, Dileköz E, Kudo C, Savitz SI, Waeber C, Baum MJ, Ferrari MD, van den Maagdenberg AM, Moskowitz MA, Ayata C. Genetic and hormonal factors modulate spreading depression and transient hemiparesis in mouse models of familial hemiplegic migraine type 1. *J Clin Invest* 2009;119(1):99-109.

Eikermann-Haerter K, Ayata C. Cortical spreading depression and migraine. *Curr Neurol Neurosci Rep* 2010;10(3):167-73.

Eikermann-Haerter K, Yuzawa I, Qin T, Wang Y, Baek K, Kim YR, Hoffmann U, Dilekoz E, Waeber C, Ferrari MD, van den Maagdenberg AM, Moskowitz MA, Ayata C. Enhanced subcortical spreading depression in familial hemiplegic migraine type 1 mutant mice. *J Neurosci* 2011;31:5755–5763.

Fanselow EE, Connors BW. The roles of somatostatin-expressing (GIN) and fast-spiking inhibitory interneurons in UP-DOWN states of mouse neocortex. *J Neurophysiol* 2010;104(2):596-606.

Favero M, Castro-Alamancos MA. Synaptic cooperativity regulates persistent network activity in neocortex. *J Neurosci* 2013;33(7):3151-63.

Fellin T, Halassa MM, Terunuma M, Succol F, Takano H, Frank M, Moss SJ, Haydon PG. Endogenous nonneuronal modulators of synaptic transmission control cortical slow oscillations *in vivo*. *Proc Natl Acad Sci USA* 2009;106(35):15037-42.

Ferrari MD vdMA, Frants RR, Goadsby PJ Migraine as a cerebral ionopathy with impaired central sensory processing. *In: Waxman SG (ed) Molecular neurology. Elsevier,Amsterdam.* 2007:439-61.

Fink D, Knapp PE, Mata M. Differential expression of Na,K-ATPase isoforms in oligodendrocytes and astrocytes. *Dev Neurosci* 1996;18(4):319-26.

Fino E, Packer AM, Yuste R. The logic of inhibitory connectivity in the neocortex. *Neuroscientist* 2013;19:228-37.

Fishell G, Rudy B. Mechanisms of inhibition within the telencephalon: 'Where the wild things are'. *Annu Rev Neurosci* 2011;34:535–567.

Furuta A, Rothstein JD, Martin LJ. Glutamate transporter protein subtypes are expressed differentially during rat CNS development. *J Neurosci* 1997;17(21):8363-75.

Gabernet L, Jadhav SP, Feldman DE, Carandini M, Scanziani M. Somatosensory integration controlled by dynamic thalamocortical feed-forward inhibition. *Neuron* 2005;48:315–327.

Giaume C, McCarthy KD. Control of gap-junctional communication in astrocytic networks. *Trends Neurosci* 1996;19(8):319-25.

Golovina VA, Song H, James PF, Lingrel JB, Blaustein MP. Na^+ pump alpha 2-subunit expression modulates Ca^{2+} signaling. *Am J Physiol Cell Physiol* 2003;284(2):C475-86.

Haglund MM, Schwartzkroin PA. Role of Na-K pump potassium regulation and IPSPs in seizures and spreading depression in immature rabbit hippocampal slices. *J Neurophysiol* 1990;63(2):225-39.

Haider B, Duque A, Hasenstaub AR, McCormick DA. Neocortical network activity *in vivo* is generated through a dynamic balance of excitation and inhibition. *J Neurosci* 2006;26:4535-4545.

Haider B, McCormick DA. Rapid neocortical dynamics: cellular and network mechanisms. *Neuron* 2009;62(2):171–189.

Hájos N, Ellender TJ, Zemankovics R, Mann EO, Exley R, Cragg SJ, Freund TF, Paulsen O. Maintaining network activity in submerged hippocampal slices: importance of oxygen supply. *Eur J Neurosci* 2009 Jan;29(2):319-27.

Halassa MM, Fellin T, Takano H, Dong JH, Haydon PG. Synaptic islands defined by the territory of a single astrocyte. *J Neurosci* 2007;27(24):6473-7.

Higashi K, Fujita A, Inanobe A, Tanemoto M, Doi K, Kubo T, Kurachi Y. An inwardly rectifying K^+ channel, Kir4.1, expressed in astrocytes surrounds synapses and blood vessels in brain. *Am J Physiol Cell Physiol* 2001;281(3):C922-31.

Hoffman KL, Battaglia FP, Harris K, MacLean JN, Marshall L, Mehta MR. The upshot of up states in the neocortex: from slow oscillations to memory formation. *J Neurosci* 2007;27(44):11838-41.

Ikeda K, Onimaru H, Yamada J, Inoue K, Ueno S, Onaka T, et al. Malfunction of respiratory-related neuronal activity in Na^+,K^+-ATPase alpha2 subunit-deficient mice is attributable to abnormal Cl^- homeostasis in brainstem neurons. *J Neurosci* 2004;24(47):10693-701.

Isaacson JS, Scanziani M. How inhibition shapes cortical activity. *Neuron* 2011;72:231-243.

Jurkat-Rott K, Freilinger T, Dreier JP, Herzog J, Gobel H, Petzold GC, Montagna P, Gasser T, Lehmann-Horn F, Dichgans M. Variability of familial hemiplegic migraine with novel A1A2 Na^+/K^+-ATPase variants. *Neurology* 2004;62(10):1857-61.

Kandel ER, Siegelbaum SA. Chapter 12: Synaptic Integration. Chapter 14: Transmitter Release. Principles of Neural Science, Kandel ER, Schwartz JS, Jessell TM. *McGraw-Hill* 2000.

Kapfer C, Glickfeld LL, Atallah BV, Scanziani M. Supralinear increase of recurrent inhibition during sparse activity in the somatosensory cortex. *Nat Neurosci* 2007;10:743–753.

Kinney GA, Spain WA. Synaptically evoked GABA transporter currents in neocortical glia. *J Neurophysiol* 2002;88:2899–2908.

Kofuji P, Newman EA. Potassium buffering in the central nervous system. *Neuroscience* 2004;129(4):1045-56.

Lashley K. Patterns of cerebral integration indicated by the scotomas of migraine. *Arch Neurol Psychiatry* 1941; 46:331-39.

Leão AAP, Morison RS. Propagation of spreading cortical depression. *J Neurophysiol.* 1945; 8:33-45.

Lehre KP, Danbolt NC. The number of glutamate transporter subtype molecules at glutamatergic synapses: chemical and stereological quantification in young adult rat brain. *J Neurosci* 1998;18(21):8751-7.

Lencesova L, O'Neill A, Resneck WG, Bloch RJ, Blaustein MP. Plasma membrane-cytoskeleton-endoplasmic reticulum complexes in neurons and astrocytes. *J Biol Chem* 2004;279(4):2885-93.

Leo L, Gherardini L, Barone V, De Fusco M, Pietrobon D, Pizzorusso T, Casari G. Increased susceptibility to cortical spreading depression in the mouse model of familial hemiplegic migraine type 2. *PLoS Genet* 2011;7(6):e1002129.

Lemieux M, Chen JY, Lonjers P, Bazhenov M, Timofeev I. The impact of cortical deafferentation on the neocortical slow oscillation. *J Neurosci* 2014;34(16):5689-703.

Levi G, Aloisi F, Ciotti MT, Gallo V. Autoradiographic localization and depolarization-induced release of acidic amino acids in differentiating cerebellar granule cell cultures. *Brain Res* 1984;290(1):77-86.

Levy D, Moskowitz MA, Noseda R, Burstein R. Activation of the migraine pain pathway by cortical spreading depression: do we need more evidence? *Cephalalgia* 2012;32(7):581-2.

Lübke J, Feldmeyer D. Excitatory signal flow and connectivity in a cortical column: focus on barrel cortex. *Brain Struct Funct* 2007;212:3–17.

Mann EO, Kohl MM, Paulsen O. Distinct roles of $GABA_A$ and $GABA_B$ receptors in balancing and terminating persistent cortical activity. *J Neurosci* 2009;29:7513-7518.

Markram H, Toledo-Rodriguez M, Wang Y, Gupta A, Silberberg G, Wu C. Interneurons of the neocortical inhibitory system. *Nat Rev Neurosci* 2004;5:793–807.

Matthias K, Kirchhoff F, Seifert G, Hüttmann K, Matyash M, Kettenmann H, Steinhäuser C. Segregated expression of AMPA-type glutamate receptors and glutamate transporters defines distinct astrocyte populations in the mouse hippocampus. *J Neurosci* 2003;23(5):1750-8.

McDermott JP, Sánchez G, Chennathukuzhi V, Blanco G. Green fluorescence protein driven by the Na,K-ATPase α4 isoform promoter is expressed only in male germ cells of mouse testis. *J Assist Reprod Genet* 2012;29(12):1313-25.

Meeks, J.P., Mennerick, S. Astrocyte membrane responses and potassium accumulation during neuronal activity. *Hippocampus* 2007*;* 17, 1100-8.

Melone M, Bellesi M, Conti F. Synaptic localization of GLT-1a in the rat somatic sensory cortex. *Glia* 2009;57:108–117

Milner PM. Note on a possible correspondence between the scotomas of migraine and spreading depression of Leao. *Electroencephalogr Clin Neurophysiol* 1958;10(4):705.

Minelli A, DeBiasi S, Brecha NC, Zuccarello LV, Conti F. GAT-3, a high-affinity GABA plasma membrane transporter, is localized to astrocytic processes, and it is not confined to the vicinity of GABAergic synapses in the cerebral cortex. *J Neurosci* 1996;16:6255–6264.

Mishima T, Hirase H. *In vivo* intracellular recording suggests that grey matter astrocytes in mature cerebral cortex and hippocampus are electrophysiologically homogeneous. *J Neurosci* 2010;30(8):3093-100.

Mölle M, Born J. Slow oscillations orchestrating fast oscillations and memory consolidation. *Prog Brain Res* 2011;193:93-110.

Molleman A. (2003). Patch Clamping: an introductory guide to patch clamp electrophysiology. *John Wiley & Sons, Ltd* 2003.

Morth JP, Pedersen BP, Toustrup-Jensen MS, Sørensen TL, Petersen J, Andersen JP, Vilsen B, Nissen P. Crystal structure of the sodium-potassium pump. *Nature* 2007;450(7172):1043-9.

Moseley AE, Lieske SP, Wetzel RK, James PF, He S, Shelly DA, et al. The Na,K-ATPase alpha 2 isoform is expressed in neurons, and its absence disrupts neuronal activity in newborn mice. *J Biol Chem* 2003;278(7):5317-24.

Navarrete M, Araque A. The Cajal school and the physiological role of astrocytes: a way of thinking. *Front Neuroanat* 2014;8:33.

Neher E. Correction for liquid junction potentials in patch clamp experiments. *Methods Enzymol* 1992;*207:*123-131.

Noseda R, Burstein R. Migraine pathophysiology: anatomy of the trigeminovascular pathway and associated neurological symptoms, cortical spreading depression, sensitization, and modulation of pain. *Pain* 2013;154 Suppl 1:S44-53.

Okun M, Lampl I. Instantaneous correlation of excitation and inhibition during ongoing and sensory-evoked activities. *Nat Neurosci* 2008;11(5):535-7.

Ophoff RA, Terwindt GM, Vergouwe MN, van Eijk R, Oefner PJ, Hoffman SM, Lamerdin JE, Mohrenweiser HW, Bulman DE, Ferrari M, Haan J, Lindhout D, van Ommen GJ, Hofker MH, Ferrari MD, Frants RR. Familial hemiplegic migraine and episodic ataxia type-2 are caused by mutations in the Ca^{2+} channel gene CACNL1A4. *Cell* 1996;87(3):543-52.

Pannasch U, Vargová L, Reingruber J, Ezan P, Holcman D, Giaume C, Syková E, Rouach N. Astroglial networks scale synaptic activity and plasticity. *Proc Natl Acad Sci USA* 2011;108(20):8467-72.

Parga N, Abbott LF. Network model of spontaneous activity exhibiting synchronous transitions between up and down States. *Front Neurosci* 2007;1(1):57-66.

Pellerin L, Magistretti PJ. Glutamate uptake stimulates Na^+,K^+-ATPase activity in astrocytes via activation of a distinct subunit highly sensitive to ouabain. *J Neurochem* 1997;69(5):2132-7.

Perea G, Navarrete M, Araque A. Tripartite synapses: astrocytes process and control synaptic information. *Trends Neurosci* 2009;32(8):421-31.

Perea G, Araque A. GLIA modulates synaptic transmission. *Brain Res Rev* 2010;63(1-2):93-102.

Perea G, Sur M, Araque A. Neuron-glia networks: integral gear of brain function. *Front Cell Neurosci* 2014;8:378.

Petersen CC, Sakmann B. The excitatory neuronal network of rat layer 4 barrel cortex. *J Neurosci* 2000;20(20):7579-86.

Petersen CC, Hahn TT, Mehta M, Grinvald A, Sakmann B. Interaction of sensory responses with spontaneous depolarization in layer 2/3 barrel cortex. *Proc Natl Acad Sci USA*, 2003;100(23):13638-43.

Petersen CC. The functional organization of the barrel cortex. *Neuron* 2007;56(2):339-55.

Pietrobon D, Striessnig J. Neurobiology of migraine. *Nat Rev Neurosci* 2003;4(5):386-98.

Pietrobon D. Function and dysfunction of synaptic calcium channels: insights from mouse models. *Curr Opin Neurobiol* 2005; 15:257-265

Pietrobon D. Familial hemiplegic migraine. *Neurotherapeutics* 2007;4(2):274-84.

Pietrobon, D. $Ca_V2.1$ channelopathies. *Pflugers Arch* 2010;460, 375-393.

Pietrobon D, Moskowitz MA. Pathophysiology of migraine. *Annu Rev Physiol* 2013;75:365-91.

Pietrobon D, Moskowitz MA. Chaos and commotion in the wake of cortical spreading depression and spreading depolarizations. *Nat Rev Neurosci* 2014;15(6):379-93.

Poduri A, Lowenstein D. Epilepsy genetics - past, present, and future. *Curr Opin Genet Dev* 2011;21:325-32.

Poolos NP, Mauk MD, Kocsis JD. Activity-evoked increases in extracellular potassium modulate presynaptic excitability in the CA1 region of the hippocampus. *J Neurophysiol* 1987 Aug;58(2):404-16.

Poskanzer KE, Yuste R. Astrocytic regulation of cortical UP states. *Proc Natl Acad Sci USA* 2011;108(45):18453-8.

Poulet JF, Petersen CC. Internal brain state regulates membrane potential synchrony in barrel cortex behaving mice. *Nature* 2008;454(7206):881-5.

Rajakulendran S, Graves TD, Labrum RW, Kotzadimitriou D, Eunson L, Davis MB, Davies R, Wood NW, Kullmann DM, Hanna MG, Schorge S. Genetic and functional characterisation of the P/Q calcium channel in episodic ataxia with epilepsy. *J Physiol* 2010;588:1905–1913.

Ransom CB, Ransom BR, Sontheimer H. Activity-dependent extracellular K^+ accumulation in rat optic nerve: the role of glial and axonal Na^+ pumps. *J Physiol* 2000;522 Pt 3:427-42.

Reig R, Mattia M, Compte A, Belmonte C, Sanchez-Vives MV. Temperature modulation of slow and fast cortical rhythms. *J Neurophysiol* 2010;103:1253–1261, 2010.

Reyes A, Lujan R, Rozov A, Burnashev N, Somogyi P, Sakmann B. Target-cell-specific facilitation and depression in neocortical circuits. Nat. Neurosci. 1998;*1*:279-285.

Riant F, De Fusco M, Aridon P, Ducros A, Ploton C, Marchelli F, et al. ATP1A2 mutations in 11 families with familial hemiplegic migraine. *Hum Mutat* 2005;26(3):281.

Rigas P, Castro-Alamancos MA. Thalamocortical up states: differential effects of intrinsic and extrinsic cortical inputs on persistent activity. *The Journal of Neuroscience* 2007;27(16):4261-4272.

Rose EM, Koo JC, Antflick JE, Ahmed SM, Angers S, Hampson DR. Glutamate transporter coupling to Na,K-ATPase. *J Neurosci* 2009;29(25):8143-55.

Rossignol E, Kruglikov I, van den Maagdenberg AM, Rudy B, Fishell G. $Ca_V2.1$ ablation in cortical interneurons selectively impairs fast-spiking basket cells and causes generalized seizures. *Ann Neurol* 2013;74(2):209-22.

Rozov A, Burnashev N, Sakmann B, Neher E. Transmitter release modulation by intracellular Ca^{2+} buffers in facilitating and depressing nerve terminals of pyramidal cells in layer 2/3 of the rat neocortex indicates a target cell-specific difference in presynaptic calcium dynamics. *J Physiol* 2001;531:807-826.

Rudy B, Fishell G, Lee S, Hjerling-Leffler J. Three groups of interneurons account for nearly 100% of neocortical GABAergic neurons. *Dev Neurobiol* 2011;71, 45–61.

Russell MB, Ducros A. Sporadic and familial hemiplegic migraine: pathophysiological mechanisms, clinical characteristics, diagnosis, and management. *Lancet Neurol* 2011;10(5):457-70.

Sanchez-Vives MV, McCormick DA. Cellular and network mechanisms of rhythmic recurrent activity in neocortex. *Nat Neurosci* 2000;3:1027–1034.

Schreiner AE, Durry S, Aida T, Stock MC, Rüther U, Tanaka K, Rose CR, Kafitz KW. Laminar and subcellular heterogeneity of GLAST and GLT-1 immunoreactivity in the developing postnatal mouse hippocampus. *J Comp Neurol* 2014;522(1):204-24.

Seamans JK, Nogueira L, Lavin A. Synaptic basis of persistent activity in prefrontal cortex *in vivo* and in organotypic cultures. *Cereb Cortex* 2003;13(11):1242-50.

Shih PY, Savtchenko LP, Kamasawa N, Dembitskaya Y, McHugh TJ, Rusakov DA, Shigemoto R, Semyanov A. Retrograde synaptic signaling mediated by K^+ efflux through postsynaptic NMDA receptors. *Cell Rep* 2013;5(4):941-51.

Sibille J, Pannasch U, Rouach N. Astroglial potassium clearance contributes to short-term plasticity of synaptically evoked currents at the tripartite synapse. *J Physiol* 2014;592, 87–102.

Shu Y, Hasenstaub A, McCormick DA. Turning on and off recurrent balanced cortical activity. *Nature* 2003;423:288–93.

Steriade M, Nuñez A, Amzica F. A novel slow (< 1 Hz) oscillation of neocortical neurons *in vivo*: depolarizing and hyperpolarizing components. *J Neurosci* 1993;13(8):3252-65.

Steriade M, Timofeev I, Grenier F. Natural waking and sleep states: a view from inside neocortical neurons. *J Neurophysiol* 2001;85(5):1969-85.

Syková E, Nicholson C. Diffusion in brain extracellular space. *Physiol Rev* 2008;88(4):1277-340.

Tahvildari B, Wölfel M, Duque A, McCormick DA. Selective functional interactions between excitatory and inhibitory cortical neurons and differential contribution to persistent activity of the slow oscillation. *J Neurosci* 2012;32(35):12165-79.

Takano T, Tian GF, Peng W, Lou N, Lovatt D, Hansen AJ, Kasischke KA, Nedergaard M. Cortical spreading depression causes and coincides with tissue hypoxia. *Nat Neurosci* 2007;10(6):754-62.

Theis M, Jauch R, Zhuo L, Speidel D, Wallraff A, Döring B, Frisch C, Söhl G, Teubner B, Euwens C, Huston J, Steinhäuser C, Messing A, Heinemann U, Willecke K. Accelerated hippocampal spreading depression and enhanced locomotory activity in mice with astrocyte-directed inactivation of connexin43. *J Neurosci* 2003;23, 766–776.

Thomas CG, Tian H, Diamond JS. The relative roles of diffusion and uptake in clearing synaptically released glutamate change during early postnatal development. *J Neurosci* 2011;31(12):4743-54.

Thomsen LL, Eriksen MK, Roemer SF, Andersen I, Olesen J, Russell MB. A population-based study of familial hemiplegic migraine suggests revised diagnostic criteria. *Brain* 2002;125(Pt 6):1379-91.

Timofeev I, Grenier F, Bazhenov M, Sejnowski TJ, Steriade M. Origin of slow cortical oscillations in deafferented cortical slabs. *Cereb Cortex* 2000;10:1185–1199.

Timofeev I, Chauvette S. Thalamocortical oscillations: local control of EEG slow waves. *Curr Top Med Chem* 2011;11(19):2457-71.

Tottene A, Conti R, Fabbro A, Vecchia D, Shapovalova M, Santello M, et al. Enhanced excitatory transmission at cortical synapses as the basis for facilitated spreading depression in $Ca_V2.1$ knockin migraine mice. *Neuron* 2009;61(5):762-73.

Tottene A, Urbani A, Pietrobon D. Role of different voltage-gated Ca^{2+} channels in cortical spreading depression: specific requirement of P/Q-type Ca^{2+} channels. *Channels (Austin)* 2011; 5:110-114

Tzingounis AV, Wadiche JI. Glutamate transporters: confining runaway excitation by shaping synaptic transmission. *Nat Rev Neurosci* 2007;8(12):935-47.

Vahedi K, Depienne C, Le Fort D, Riant F, Chaine P, Trouillard O, Gaudric A, Morris MA, Leguern E, Tournier-Lasserve E, Bousser MG. Elicited repetitive daily blindness: a new phenotype associated with hemiplegic migraine and SCN1A mutations. *Neurology* 2009;72(13):1178-83.

van den Maagdenberg AM, Pietrobon D, Pizzorusso T, Kaja S, Broos LA, Cesetti T, van de Ven RC, Tottene A, van der Kaa J, Plomp JJ, Frants RR, Ferrari MD. A Cacna1a knockin migraine mouse model with increased susceptibility to cortical spreading depression. *Neuron* 2004;41, 701-710.

van den Maagdenberg AM, Pizzorusso T, Kaja S, Terpolilli N, Shapovalova M, Hoebeek FE, Barrett CF, Gherardini L, van de Ven RC, Todorov B, Broos LA, Tottene A, Gao Z, Fodor M, De Zeeuw CI, Frants RR, Plesnila N, Plomp JJ, Pietrobon D, Ferrari MD. High cortical spreading depression susceptibility and migraine-associated symptoms in $Ca_V2.1$ S218L mice. *Ann Neurol* 2010;67(1):85-98.

Vecchia D, Pietrobon D. Migraine: a disorder of brain excitatory-inhibitory balance? *Trends Neurosci* 2012;35(8):507-20.

Vecchia D, Tottene A, van den Maagdenberg AM, Pietrobon D. Mechanism underlying unaltered cortical inhibitory synaptic transmission in contrast with enhanced excitatory transmission in $Ca_V2.1$ knockin migraine mice. *Neurobiol Dis* 2014;69:225-34.

Vecchia D, Angelita Tottene A, van den Maagdenberg AM, Pietrobon D. Cortical synaptic transmission in $Ca_V2.1$ knockin mice with the S218L missense mutation which causes a severe familial hemiplegic migraine syndrome in humans. *Front Cell Neurosci* 2015

Volterra A, Meldolesi J. Astrocytes, from brain glue to communication elements: the revolution continues. *Nat Rev Neurosci* 2005;6(8):626-40.

Wadiche JI, Kavanaugh MP. Macroscopic and microscopic properties of a cloned glutamate transporter/chloride channel. *J Neurosci* 1998;18:7650–7661.

Westenbroek RE, Sakurai T, Elliott EM, Hell JW, Starr TV, Snutch TP, et al. Immunochemical identification and subcellular distribution of the alpha 1A subunits of brain calcium channels. *J Neurosci* 1995;15(10):6403-18.

Wester JC, Contreras D. Columnar interactions determine horizontal propagation of recurrent network activity in neocortex. *J Neurosci* 2012;32(16):5454-71.

Wilson C. Up and down states. *Scholarpedia Journal* 2008;3(6):1410.

Zaitsev AV, Povysheva NV, Lewis DA, Krimer LS. P/Q-type, but not N-type, calcium channels mediate GABA release from fast-spiking interneurons to pyramidal cells in rat prefrontal cortex. *J Neurophysiol* 2007;97:3567-3573.

Zhang X, Levy D, Noseda R, Kainz V, Jakubowski M, Burstein R. Activation of meningeal nociceptors by cortical spreading depression: implications for migraine with aura. *J Neurosci* 2010;30(26):8807-14.

Zhang X, Levy D, Kainz V, Noseda R, Jakubowski M, Burstein R. Activation of central trigeminovascular neurons by cortical spreading depression. *Ann Neurol* 2011;69(5):855-65.

Zonta M, Angulo MC, Gobbo S, Rosengarten B, Hossmann KA, Pozzan T, Carmignoto G. Neuron-to-astrocyte signaling is central to the dynamic control of brain microcirculation. *Nat Neurosci* 2003;6(1):43-50.